12-2013

Optimization of Porous Pavement Mixtures Based on Aggregate Structure

Andrew Neptune
Clemson University, aneptun@g.clemson.edu

OPTIMIZATION OF POROUS PAVEMENT MIXTURES BASED ON AGGREGATE STRUCTURE

A Dissertation
Presented to
the Graduate School of
Clemson University

In Partial Fulfillment
of the Requirements for the Degree
Doctor of Philosophy
Civil Engineering

---

by
Andrew Isaac Neptune
December 2013

Accepted by:
Dr. Bradley J. Putman, Committee Chair
Dr. Prasada Rao Rangaraju
Dr. Amir Poursaee
Dr. Calvin Sawyer

ABSTRACT

Porous pavements are sustainable features that are used to help manage the quantity and quality of stormwater runoff. These pavements may include porous asphalt, permeable interlocking concrete pavers and pervious concrete. Since pavements that are purposefully designed to drain water through their matrix are relatively new, contractors and engineers are faced with various challenges such as improper design and installation, poor workability, and excessive finishing which may lead to clogged pores. Therefore, this study on porous pavements examined pervious concrete mixtures to evaluate an optimization process for the preparation of porous pavement mixtures based on aggregate structure to meet desired performance criteria.

Pervious concrete mixtures typically consist of aggregate, cement, water, little to no fines and admixtures. Since aggregate makes up a large portion of the pervious concrete mix, aggregate properties and proportioning were the main focus of this study. Two aggregate sources (L and C) were used in the preparation of pervious concrete mixtures. From these sources, three single-sized aggregate fractions were used in making blends, the #8 (2.36 mm), the #4 (4.75 mm) and the ⅜ in. (9.5 mm). Aggregate properties such as uniformity coefficient were calculated and others were measured including specific gravity, absorption, density (dry rodded and dry Proctor), void content, percent flat and elongated, shape and surface texture (particle index), California Bearing Ratio penetration stress, and compaction indices. From source L, fifteen (15) sample groups of twelve (12) 6 in. × 6 in. cylindrical specimens were made and from source C,

fourteen (14) sample groups were made similar to source L. The fresh pervious concrete had a water-cement ratio of 0.25, with a cement-aggregate ratio of 0.23 for source L and 0.25 for source C, and the unit weights (ASTM C1688 and an alternative method) and gravimetric air content were determined. Each sample group was divided into 4 subgroups of three specimens that had permeability values that were not statistically different from each other. Other tests conducted on the different subgroups included effective porosity, compressive strength, split tensile strength, and abrasion loss.

The aggregate test results showed that source L, had higher specific gravities, percent absorption, and densities than source C, but lower void contents, percent flat and elongated, particle index, and California Bearing Ratio penetration stress at 0.2 inches. The approach taken in evaluating an optimization process was to use regression analysis in combination with the simplex-centroid design of the three aggregate sizes. Relationships were analyzed within and across aggregate properties and pervious concrete properties.

The augmented simplex-centroid design with the polynomial special quartic model was used to predict the aggregate proportions that best fit the desired aggregate property or pervious concrete property. This design of experiment tool is a triangle with an elevated response surface on which contour lines present the predicted parameter values. For this study, the simplex triangle consisted of ten design points representing the aggregate proportions associated with the predicted parameters. The design points were located at the vertices, at the halfway point along the edges, and at the centroid, and three additional points within the triangle around the centroid on imaginary lines that run perpendicularly from the midpoint of an axis to the opposite vertex. The lack-of-fit test with $\alpha = 0.01$ was used to check the adequacy of the model based on all the data points and also on only the validation points. Based on the lack-of-tests, the special quartic model was over 50% adequate for source L mixtures and over 80% adequate for source C. The optimization process included two options: Option 1 − A regression analysis is done to predict an aggregate property that relates well to a pervious concrete property. The contour line on the simplex response surface that represents the predicted aggregate property is then used to predict aggregate proportions that meet the desired aggregate property. Option 2 − The contour line for the desired pervious concrete property could be located on the simplex response surface and used to predict the aggregate proportions that meet the desired pervious concrete property.

DEDICATION

I wish to dedicate this dissertation to my wife, Carmie Kim Neptune and my daughter, Jubilee Candace Neptune. Kim was tremendously involved in this study, from performing tests, to assisting with the mixing process (even when Jubilee was on the way), data compilation and the shuttling of meals when work hours were extended. She is worthy of this degree, because of the way she lovingly and sacrificially supported me. Her prayers, words of encouragement, advice and support in general, have given me the privilege of achieving this goal. Because of both their support and care, and coming home to their warm welcomes, I was able stay focused on the tasks before me. I praise my God for them, His continuous working in me to persevere and for giving me this privilege to serve Him in completing this degree.

ACKNOWLEDGMENTS

I would like to acknowledge those who have assisted with my dissertation research in some way or the other. First of all, I am forever grateful to my committee chair, Dr. Brad Putman, for his guidance, dedication, and wisdom he displayed over the years. His patience, encouragement and positive spirit has been greatly appreciated. The other members of my committee, Dr. Prasad Rangaraju, Dr. Amir Poursaee and Dr. Calvin Sawyer have played key roles in supporting my research and in giving profitable advice that made my dissertation complete. I am truly grateful.

I would like to thank the technical staff in the Glenn Department of Civil Engineering, Danny Metz, Scott Black, and their student workers who willingly assisted with the construction of some of the equipment for this research and making the "Old Ford" available for local trips. I thank Keith and Roger at the Vulcan Materials quarry in Liberty, SC who has been generous with providing aggregate and physical assistance. To all the faculty, staff and students at the Asphalt Rubber Technology Service (ARTS), especially Trent Dellinger and Katelyn Love, who have willingly allowed me to use the equipment and aggregate, I am truly grateful. And the faculty and staff of the Glenn Department of Civil Engineering have always been ready to assist me when asked, thank you.

I would like to acknowledge one of my colleagues who were very instrumental in my research, Dr. Sujay Math. His approach to his research prompted the thought for me to use the simplex-centroid design and allowed us to assist each other with how best to use this tool. Thank you Don Singer for your thoughtfulness and for easing some of my work load with data that was applicable for my study. Dr. Will Martin, I appreciate your assistance with projects and the opportunities for us to learn from each other. Special thanks to all the students who assisted me in the lab, John Primm, Jamie Sherer, and Melissa Gende. Without your assistance, life would have been extremely difficult.

I would like to acknowledge my parents, Wilmus and Voltina Neptune, who have shown their love by their faithful prayers and encouragement. My brother Philip and my sisters Wilene and Jill and their families have been very supportive caring, thank you.

Special thanks to my wife Kim, who helped me prepare samples, tested aggregate, prayed and encouraged me. And to our bundle of joy, Jubilee, thank you.

Finally, thanks to my Saviour and my Lord Jesus Christ for He is the reason for all my successes.

TABLE OF CONTENTS

Page

LIST OF TABLES

Page

LIST OF FIGURES

CHAPTER 1 : INTRODUCTION

The implementation of sustainable features in construction has motivated owners, engineers, and general contractors to think beyond the norm. Material compositions that may have previously been avoided are now reconsidered and suited for properly diagnosed applications. Many applications for these sustainable features involve sites that were once vegetated, allowing the natural infiltration of stormwater, but have since undergone development. These developments incorporated buildings, and pavements with impervious surfaces that intercept the stormwater routing the unfiltered runoff to surface water bodies. In the United States, approximately 46% of the identified estuarine water quality impairment cases were attributable to stormwater runoff (USEPA, 1996). In 2000, stormwater runoff was among the top three carriers of pollution to lakes, ponds, reservoirs and estuaries (USEPA, 2000). One means of restoring the vertical flow of stormwater into the soil is to implement porous surfaces such as pervious concrete, porous asphalt or permeable interlocking concrete pavers. Because of the interconnected pores, runoff can infiltrate these pavements and some debris and contaminants can be filtered out and broken down on and within the porous structure (Schaefer et al, 2006). Although efforts should be made to keep these contaminants away from porous pavements, sometimes it is unavoidable and clogging can occur. It is, therefore, critical to be aware of the type of surrounding materials that can access the porous pavements, so it is designed with pores that are not susceptible to clogging.

The size of these pores is affected by the aggregate gradation, the physical properties of the aggregate in the mixture (shape, size and surface roughness), the paste content (cementitious material, water, chemical admixtures and aggregate fines), and compaction energy. Because a large portion of a pervious concrete mixture is aggregate, it is essential to understand the relationships that exist between the aggregate properties and the pervious concrete properties. But to develop a mixture that performs adequately under known site conditions would require multiple trials which can be time consuming, and encouraging decisions based on assumptions from insufficient data. To reduce the extent to which assumptions are the basis for decisions, an analytical and statistical approach that measures the properties of a mixture as a function of the mixture composition could be utilized to make predictions from a more economically adequate number of trials (Cornell, 2002).

Problem Statement

The growing demand for sustainable construction has boosted the installation of performance based construction features such as porous pavements. But the idea of designing a pavement that allows water to pass through its matrix is still relatively new; therefore designers and contractors are met with various challenges (Deo et al., 2010). Some of these challenges include minimal knowledge of proper design and installation to meet site conditions, installation cost, and poor workability of mixtures (Chopra et al., 2007). In some cases, that lack of knowledge has led to poor pavement performance because of sealed surfaces due to over finishing or high paste mixes, clogging caused by the access of surrounding material, and raveling.

Along with these challenges is the limited number of specifications and guidelines presently available, since porous pavements have only recently been accepted as a stormwater Best Management Practice (Tennis et al., 2004). Therefore, more research is needed to develop methods that measure and control quality and provide an understanding of how the individual components affect the performance properties of porous pavements, such as permeability and strength. Hence the reason for this study to investigate a methodology of making porous mixtures suitably functional from a proper understanding of the effects of mixture components namely aggregates, through correlations between aggregate proportions and aggregate and porous mixture properties.

Objective

The primary objective of this study was to evaluate an optimization process for the preparation of porous pavement mixtures based on aggregate structure to meet desired performance criteria. The design of experiment simplex-centroid design (SCD) was the primary statistical tool used to accomplish this objective. Pervious concrete mixtures were used in this study, but the methodology can potentially be applied to porous asphalt mixtures.

Research Scope

This research study was conducted on pervious concrete mixtures prepared from two (2) aggregate sources. Tests and analyses were conducted on both aggregate and pervious concrete mixtures in accordance with the following steps which describe the three (3) research phases:

1. Phase I: Aggregate Characterization
    a. Measuring the specific gravities (BSG, BSG_{SSD}, and ASG), and percent absorption of the single-sized aggregate fractions, #8 (2.36 mm), #4 (4.75 mm), and ⅜ in. (9.5 mm) according to ASTM C127 and C128 procedures,
    b. Measuring the density and void content of the different aggregate blends according to ASTM C29 and an alternative density procedure developed for this study (dry rodded and dry Proctor, respectively),
    c. Calculating the uniformity coefficient of the blends, and measuring the percent flat and elongated particles of the coarse single-sized aggregate fractions according to ASTM D4791,
    d. Measuring the shape and surface texture index of the single-sized aggregate fractions according to ASTM D3398 and the California Bearing Ratio penetration stress based on ASTM D1883,
    e. Measuring the compaction indices of the aggregate blends based on the loose and compacted unit weights using the standard Proctor hammer.
2. Phase II: Pervious Concrete Mix Testing

a. Measuring the unit weight and the gravimetric air content of the pervious concrete mixtures according to ASTM C1688 and an alternative method, and ASTM C138, respectively,
b. Measuring the compaction indices of the pervious concrete mixtures,
c. Measuring the permeability and effective porosity of the pervious concrete mixtures,
d. Measuring the compressive strength, split tensile strength, and abrasion loss according the ASTM C39, ASTM C496 and based on the Cantabro method, respectively.

3. Phase III: Statistical Analysis and SCD Modeling
   a. Performing statistical analysis on the data to determine the significant differences between the aggregate properties and pervious concrete mixture properties,
   b. Performing regression analyses to determine correlations between aggregate and pervious concrete mixture properties,
   c. Developing a simplex-centroid model to optimize the selection of aggregate gradation to meet desired specifications.

Research Product

The final product of this study combines regression analysis plots and the design of experiment simplex-centroid design. The regression plots were used to determine how the porous pavement performance properties correlated to the aggregate properties.

These performance properties included unit weight, permeability, effective porosity, compressive strength, splitting tensile strength, and abrasion loss. Combined with the regression analysis, the simplex-centroid design was used to predict aggregate proportions based on desired aggregate properties. The simplex-centroid was also used to predict aggregate proportions associated with desired pervious concrete properties. The aggregate properties included surface texture index (roughness), uniformity coefficient, unit weight, void content, CBR and aggregate compaction indices. The possibility of predicting the performance property of a porous pavement mixture from testing the aggregate was the ultimate goal of the product.

Potential Benefits

Aggregate properties, classification and gradation were explored in this study and their influence was traced to pervious concrete mix performance properties. Optimizing porous paving mixtures from the perspective of aggregate structure seems promising. The information related to aggregate properties is more readily available, making this approach viable for the construction industry. The proportions of the materials used in typical pervious concrete mixtures are approximately 76% for aggregate, 18% cement and 6% water by weight (Neptune, 2008). This shows that aggregate properties would most likely influence the porous mixture to a high degree. The sensitivity of the aggregate structure to compaction was also assessed to aid in optimizing the aggregate selection.

Organization of Dissertation

Chapter I is the introduction to the optimization of porous pavement mixtures based on aggregate structure. Chapter II presents a literature review of work done in the classifying of aggregate characteristics and its effects on porous mixtures. Also, methods of estimating porous mixture performance are summarized. Chapter III is a description of the materials and the methods implemented for this research study. Chapter IV is the presentation and discussion of empirical results in the examination of aggregate structure and porous pavement performance. Chapter V is the description and validation of the statistical method, simplex-centroid design that was used to predict both the volumetric properties of the aggregate gradation and the performance parameters of porous mixtures. Finally Chapter VI provides a summary of the research, presents the conclusions, and details recommendations based on the results of this study.

CHAPTER 2 : LITERATURE REVIEW

This chapter focuses on previous work done to understand the effects that aggregate properties have on the physical and performance properties of pervious concrete mixtures. In keeping with the objective of the study, a suitable definition of optimization is necessary. According to the American Heritage College dictionary, optimization is "the procedure used to make a system or design most effective or functional." The goal is to enhance the effectiveness of porous pavement mixtures to function at their best with the available materials for the proper management of stormwater at any given site. One material that is believed to have a major impact on pervious concrete is aggregate. In this study the aggregate structure was used as the basis by which porous pavement mixtures could be optimized. In many ways, aggregate particles bear similar characteristics to soil and share some test methods. Das defined soil structure as the geometric arrangement of soil particles with respect to each other, and the same can be expressed for aggregate structure. Some of the factors that affect the structure of aggregate and soil alike are the shape, size and mineralogical compositions (Das, 2006).

The ongoing development of naturally vegetated areas with impermeable surfaces has increased the volume and rate of stormwater runoff, leading to reduced time lags between peak rainfall and peak runoff. This has increased the risks of flooding and the transporting of pollutants into rivers and lakes. In an effort to manage these increased volumes of runoff, many municipalities have adopted sustainable stormwater remediation processes to help maintain the quantity and quality of runoff as close as possible to that of the original undeveloped site and have put restrictions on the percentage of impervious surfaces present on a developed property (Schokker, 2010). So what options are there for reaching this goal of minimizing the hydrological disturbance in local communities and how are these options well suited for the available materials and designed for the site conditions?

An optimized porous pavement mixture has the potential of minimizing the hydrological disturbance caused by development. Among the porous paving options, there is porous asphalt, pervious concrete and permeable interlocking concrete pavers, but the focus of this study is on pervious concrete. Pervious concrete pavement mixtures are typically comprised of aggregate, cementitious material, water, chemical admixtures and sometimes fines. Because the aggregate makes up such a large portion of a porous pavement matrix, an understanding of its effects on the performance properties of pervious concrete mixtures is necessary.

Physical Properties of Aggregate

Void Content

The volume of a specific aggregate gradation required to fill a known volume varies with each trial. The irregularity in aggregate shape influences the arrangement of the particles or the mode of packing, consequently controlling the void content of the mixture (Hardiman, 2004). Kosmatka et al. observed that the void content was constant between one aggregate sample of uniform size and shape to another aggregate sample of the same volume but smaller particles of uniform size and shape. But when the two samples were combined, the void content decreased (Kosmatka et al., 2002).

Larrard's, study on packing density of particles (2009), defined it as the volume of solids to the total volume to be filled and how it depends on the placement of the particles. He expressed that packing density was essential in determining another parameter referred to as the compaction index *K*. This compaction index expresses the closeness between the actual packing density and the virtual packing density and is calculated by equation 2.1:

$$K = \sum_{i=1}^{n} K_i = \sum_{i=1}^{n} \frac{\Phi_i / \Phi_i^*}{1 - \Phi_i / \Phi_i^*} \qquad 2.1$$

where K_i represents all the partial compaction indices for the ith aggregate fraction in the mixture, Φ_i is the actual aggregate volume of the ith aggregate fraction and Φ_i^* is the virtual aggregate volume, which is associated with the virtual packing density. The virtual packing density is derived from placing the aggregate one at a time without changing its shape. Such a packing process will allow additional aggregate to fit the actual volume but when the aggregate is used collectively to fill the actual volume, a greater space is occupied resulting in the virtual volume Φ_i^* (Larrard, 2009).

Other major factors that affect void content or porosity are aggregate size and shape distribution (gradation) and level of compaction. The size of the aggregate particles is inversely proportional to the void content, so an increase in aggregate size results in a decrease in void content or porosity due to weak attractive van der Waal forces (Latham, 2002). Studies by Youd found that aggregate roundness increased with increased aggregate sizes and can lead to a reduction in void content (Youd, 1973). Other studies on dry aggregate mixtures found that the lowest porosity of an aggregate blend was always lower than the porosity of a single-size fraction. Also, the porosity of aggregate blends with a maximum size of 10 mm had marginally higher porosity as compared to blends with 14 mm as the maximum size (Hardiman, 2004).

Aggregate Surface Area

Besides cement paste composition, another important factor that affects the cement paste film thickness coating the aggregates in the mixture is the aggregate surface area. A unit volume of finer aggregate has a higher surface area compared with the same unit volume of larger aggregate. Because of this, smaller aggregates require more cement paste for an adequate film thickness as compared to larger aggregate. Roberts et al. stated that the aggregate gradation was a common way of estimating the surface area of aggregate by multiplying the surface area factor by the percent (decimal form) passing each sieve used. These surface area factors can be determined by the specific gravity and assuming all particles are rounded or cubic in shape (Roberts et al. 1996). Table 2.1 lists the surface area factors for the various sieve sizes. From the list, it shows that the two (2) single-sized fractions (No. 4 and ⅜ in.) used in this study have the same surface area factor of 2 and No. 8 has a SA factor of 4, but for verification purposes, a surface area factor of 2 was used for the No. 8 aggregate to observe whether a higher SA factor was necessary.

Table 2.1 Surface Area Factors (Roberts et al., 1996)

Sieve Size	Surface Area Factors
Percent Passing Maximum Sieve Size	2
Percent Passing No. 4	2
Percent Passing No. 8	4
Percent Passing No. 16	8
Percent Passing No. 30	14
Percent Passing No. 50	30
Percent Passing No. 100	60
Percent Passing No. 200	160

Aggregate Shape and Surface Texture

The shape and texture of aggregate particles influence the permeability and strength of a pervious concrete mixture. Regarding aggregate shape, it is typically categorized as flat or elongated, or both or neither. The texture of the particle describes the roughness of the aggregate (ACI Committee E-701, 2007). ASTM D3398 is the "Index of Aggregate Particle Shape and Texture" test that is typically used to quantify the shape, angularity, and surface texture of particles (National Stone Association, 1993). As the particle index increases, the smoothness and roundness of the aggregates decreases giving evidence of rougher and more angular particles.

Jain et al. (2011) studied the effects of aggregate shape and size on the permeability of pervious concrete. The aggregates were separated into single-sized fractions and categorized as flaky, angular, and irregular. Flaky aggregate was described as "materials having small thickness relative to the other two dimensions." Angular aggregate was described as "possessing well defined edges formed at the intersection of roughly planar faces." And irregular aggregate was described as "partly shaped by attrition and having rounded edges." Working with a sequence of (1) flaky, (2) angular, and (3) irregular, it was found that angularity number, Los Angeles abrasion loss, average water absorption and voids decreased following that order. The unit weight of the aggregate increased when following that sequence. It was observed that mixtures made from aggregate with high angularity numbers or flaky aggregate, had higher permeability than mixtures with lower angularity numbers. For all types of aggregates studied, it was found that smaller aggregate produced lower permeability in comparison to larger aggregates even when smaller aggregate mixtures had higher porosity values. Also, the rate of reduction in permeability with increasing w/c ratio was higher in pervious concrete mixtures made from more angular or flaky aggregate (Jain et al., 2011).

Pervious Concrete Performance Properties

Permeability and Porosity

Materials used in pervious concrete and the placing techniques have a significant effect on permeability. Permeability is a measure of the rate by which a fluid flows through a porous medium (Bedient, 2002). Permeability, also referred to as hydraulic conductivity, is impacted by the aggregate gradation, and pore size and distribution within the matrix (Neithalath et al., 2006). The intrinsic permeability which is directly proportional to permeability and considered as the frictional resistance to flow through the porous matrix, is dependent on porosity, pore size and distribution, roughness, and constrictions, connectivity, and tortuosity (Garboczi, 1990). Neithalath et al. observed that a pervious concrete specimen with the highest permeability did not have the highest porosity nor the greatest average pore size. By this, they realized that the pore connectivity can also significantly affect permeability. This is possibly due to porosity being a volumetric property and permeability a flow property (Neithalath et al. 2006). "Typical flow rates for water through pervious concrete are 3 gal/ft²/min (288 in./hr, 120 L/m²/min, or 0.2 cm/s) to 8 gal/ft²/min (770 in./hr, 320 L/m²/min, or 0.54 cm/s)" (Tennis et al, 2004). Laboratory apparatus used for testing permeability typically consist of a falling head permeability set-up. This type of set-up typically includes placing a specimen in a membrane to prevent water from flowing out of the sides of the specimen. Different levels of head have been tested depending on the amount of rainfall that the pervious concrete system is being designed to handle (Schaefer et al, 2006; Yang and Jiang, 2003; Neithalath et al, 2006).

Compressive Strength

Although the typical compressive strength of pervious concrete is approximately 2500 psi, the range of values of its strength falls within 500 to 4000 psi (Tennis et al, 2004). Drilled cores are the best means found for measuring pavement strengths in the field. However, cast cylinders have also provided adequate results in laboratory testing (Shaefer et al, 2006). The compressive strength is dependent on the size of the aggregate whereas the air voids depend on the gradation. As the size of the aggregate decreases, the area of contact increases and improves the strength (Ghafoori, 1995; Tennis et al, 2004). Pervious concretes produced from rounded aggregate tend to possess higher strength capacities than mixtures from angular aggregate.

Abrasion Resistance

Pervious concrete consists of a high level of voids that make it quite susceptible to moisture loss due to evaporation while it cures. This loss of moisture can reduce the strength of the cement paste that bonds the aggregate to each other and with the lower water-to-cement ratio of pervious concrete, moisture loss can have more detrimental effects (Kevern, 2009). Therefore, curing techniques are critical in preventing this loss and promoting strong bonding. With weakened cement paste, abrasion or raveling of aggregate particles from the matrix can be more extensive. ASTM C944 was the testing procedure used by Kevern et al. 2009, to verify the surface abrasion mass loss of pervious concrete samples experiencing different curing techniques. It involved the use of a “rotary cutter dresser wheel” with a constantly applied load of 98 N (22 lb) for 2 minutes (Kevern, 2009). An abrasion index was determined from the average mass loss of the sample group to the average mass loss of the controlled mixture and it was used to compare the different curing techniques for field mixtures. These curing techniques comprised of air, 7 days plastic covering, 28 days plastic covering, soybean oil, white pigment coating and non-film evaporation retardant. The curing technique that showed the least abrasion loss was the plastic covering, followed by the soybean oil, then white pigment and the non-film evaporation retardant (Kevern, 2009).

Permeability Prediction Technique

One of the major parameters of a porous pavement is permeability. Continuous efforts have been made to determine the factors that best predict permeability. The correlation between porosity and permeability has been considered as a good starting point for predictions but there are limitations to porosity fully explaining the variability in permeability, because a pervious concrete sample may have a lower porosity but a higher permeability as compared with other samples (Neithalath et al., 2006). Porosity measures the volume of the accessible voids in the medium to the total volume of the medium, whereas permeability measures the flow rate of a fluid through a porous medium (Bedient, 2002). Other factors such as pore size, geometry and void connectivity influence the permeability of pervious concrete which has been investigated by measuring the electrical conductivity of specimens and using image analysis (Neithalath et al., 2006; Neithalath et al., 2010). The Kozeny-Carman equation was modified to incorporate the electrical conductivity and to derive a new parameter, "hydraulic connectivity" which better describes the pore structure producing a stronger correlation and better estimate of permeability (Neithalath et al., 2006).

To determine the conductivity of the specimen, Neithalath et al. (2006) measured porosity, permeability and the bulk resistance (R_b) using Electrical Impedance Spectroscopy with a Soartron 1260^{TM} Impedance/Gain-Phase analyzer and sodium chloride electrolyte. The bulk resistance was obtained from the Nyquist plot at the point where the imaginary component was at a minimum. The electrical conductivity (σ_{eff}) was calculated from equation 2.2

$$\sigma_{eff} = \frac{l}{R_b A} \qquad 2.2$$

where l is the length and A is the cross sectional area of the specimen. The coefficient of permeability or hydraulic conductivity (K) is related to the intrinsic permeability (k), the latter being a property of the porous medium only, independent of the fluid, and measures the ability of the porous medium to transmit a fluid. They are related by equation 2.3

$$k = \frac{K\mu}{\rho g} \qquad 2.3$$

where μ is the dynamic viscosity of the fluid, ρ is the fluid density and g is the gravitational constant (Bedient, 2002). Another equation that is used to define the intrinsic permeability is the Kozeny-Carman equation given as

$$k = \frac{\phi^3}{F_s \tau^2 S_0^2 (1-\phi)^2} \qquad 2.4$$

where ϕ is the porosity, F_s is the generalized factor accounting for different pore shapes (2 for circular tubes), τ is the tortuosity and S_0^2 is the specific surface area of the pores (Neithalath et al., 2010). Neithalath et al. observed that the sample with the highest permeability did not always have the highest porosity or pore size and so confirmed that permeability was strongly influenced by the pore distribution and connectivity.

A parallel mixed model is used to express the effective electrical conductivity (σ_{eff}) based on the arithmetic mean of conductivities for the pore liquid σ_p (sodium chloride) and solid phase σ_s (concrete) weighted by their volume fractions for pores ϕ_p and solid ϕ_s (Glover, 2000; Neithalath, 2006). This model was modified to include the connectivity factors (β_p *and* β_s) for both the pore and solid network, respectively as given in equation 2.5 (Garboczi, 1990).

$$\sigma_{eff} = \sigma_p \phi_p \beta_p + \sigma_s \phi_s \beta_s \qquad 2.5$$

The pervious concrete pore structure was measured by "modified normalized conductivity" σ^*_{norm}, and was defined as the product of porosity ϕ_p and the pore phase connectivity, β_p (Neithalath et al., 2006). Because of the relationship between porosity and intrinsic permeability in the Kozeny-Carman equation, it was determined that pore tortuosity, τ, was the inverse of pore phase connectivity. The substitution of σ^*_{norm}, which is equivalent to $\beta_p\varphi_p$, and $\tau = 1/\beta_p$ into the Kozeny-Carman equation for the term $\left(\frac{\phi_p}{\tau}\right)^2$ resulted in equation 2.6

$$k = \underbrace{\left(\frac{\left[\sigma^*_{norm}\right]^2}{F_s S_0^2}\right)}_{\beta_H} \left(\frac{\phi_p}{(1-\phi_p)^2}\right)$$

2.6

where the intrinsic permeability k is related to a constant β_H referred to as the hydraulic connectivity factor, a function that expresses the volume fraction of the pores. It was recorded that the samples with similar connectivity factors, $\beta_{H,}$ had similar permeability values. The mixtures that had lower β_H values were those with smaller sized aggregate, 100% #8, which had smaller inter-connected pore sizes and those prepared from the boundary aggregate, for example 50% #8 and 50% ⅜", which had their voids filled in to some degree by the smaller aggregate. In contrast to the above mentioned, the mixtures that had higher β_H values were those with larger sized aggregate, 100% ⅜ in., which had larger inter-connected pore sizes, along with those mixtures that promoted a highly continuous channel network such as 75% #4 and 25% #8. A stronger relationship existed between the intrinsic permeability and the hydraulic connectivity factor as compared to the porosity (Neithalath et al., 2006).

The Simplex-Centroid Design

The simplex-centroid design is a statistical tool that has been used in the design of mixture experiments for optimization purposes. Cornell, in *Experiments with Mixtures* (2002), defines the design of mixture experiments as the measurement of responses that depends on varying proportions of components in a mixture and not the amount of the mixture (Scfeffé, 1958; Cornell, 2002). Another approach he discusses is the factorial experiment where the measured responses are generated by varying two or more factors while the others are held constant. But for this study, the focus is on the design of mixture experiment using the simplex-centroid design. Simon et al. stated that the advantage and disadvantage of the mixture experiments is that the experimental region being examined is more easily defined, but it involves a more complicated analysis. However, with the factorial design, while it follows a more standard approach, its experimental region can be more challenging to define because it changes based on how components are reduced to independent variables (Simon, 1997). Overall, the mixture design regards each variable as a dependent component whereas the factorial design regards each variable as an independent factor (Yeh, 2008).

The simplex-centroid design is used in different industries including food, petroleum, textile, chemical, rubber and others, for performance optimization of blended ingredients (Cornell, 2002). Little attention has been given to it in the concrete industry (Simon, 1997). This method of optimization reduces the number of mixes necessary to accurately analyze the relationships between component proportions and the tested parameters (Yeh, 2008). The design involves an equilateral triangle or tetrahedral, depending on the number of ingredients that makes up the mixture, 3 or 4, respectively. Each vertex of the triangle is designated a pure or single component. At the midpoints along the edges are the binary blends (two equal components) and at the centroid is a ternary blend (three equal proportions). The sum of the proportions, x_i, at each point equals 1 or unity (Cornell, 2002). Figure 2.1 is a layout of the simplex-centroid triangle for a 3 component mixture design made up of three (3) axes which represent the proportion of the component that comes before it going in a clockwise direction.

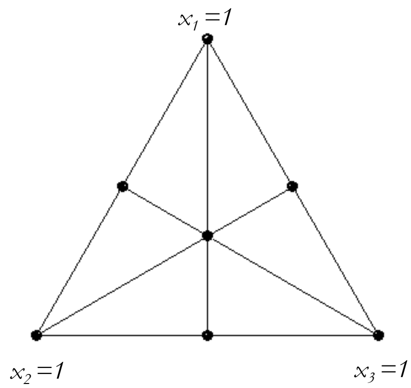

Figure 2.1 Layout of the simplex-centroid triangle for a 3 component mixture.

The response surface over the triangle or simplex factor space is typically modeled with a polynomial equation that best fits the data collected to obtain the best predictions. The different polynomials, referred to as {*q*, *m*} or "canonical" polynomials where the mixture has *q* components and a polynomial of degree *m*, can be first-degree, second-degree, full cubic, special cubic and special quartic and are listed in Table 2.2 for three component mixtures (Cornell, 2002).

Table 2.2 Polynomials to model Mixture Experiments

First-degree	$y_u = \beta_1 x_1 + \beta_2 x_2 + \beta_3 x_3$
Second-degree	$y_u = \beta_1 x_1 + \beta_2 x_2 + \beta_3 x_3 + \beta_{12} x_1 x_2 + \beta_{13} x_1 x_3 + \beta_{23} x_2 x_3$
Full Cubic	$y_u = \beta_1 x_1 + \beta_2 x_2 + \beta_3 x_3 + \beta_{12} x_1 x_2 + \beta_{13} x_1 x_3 + \beta_{23} x_2 x_3 + \delta_{12} x_1 x_2 (x_1 - x_2) + \delta_{13} x_1 x_3 (x_1 - x_3) + \delta_{23} x_2 x_3 (x_2 - x_3) + \beta_{123} x_1 x_2 x_3$
Special Cubic	$y_u = \beta_1 x_1 + \beta_2 x_2 + \beta_3 x_3 + \beta_{12} x_1 x_2 + \beta_{13} x_1 x_3 + \beta_{23} x_2 x_3 + \beta_{123} x_1 x_2 x_3$
Special Quartic	$y_u = \beta_1 x_1 + \beta_2 x_2 + \beta_3 x_3 + \beta_{12} x_1 x_2 + \beta_{13} x_1 x_3 + \beta_{23} x_2 x_3 + \beta_{1123} x_1^2 x_2 x_3 + \beta_{1223} x_1 x_2^2 x_3 + \beta_{1233} x_1 x_2 x_3^2$

Definition of the terms in the above equations can be found in Chapter 5 (Cornell, 2002).

The simplex-centroid design has been used in the optimization of high-performance concrete mixtures (Simon, 1997; Yeh, 2008). With regard to its use in pervious concrete mixtures, little to no use has been noted. Simon et al. did an experimental design for a six-component high-performance concrete mixture. The six (6) components were water, cement, microsilica, HRWRA, coarse and fine aggregate. There were constraints on the simplex, since it was not feasible to make concrete mixtures solely from some of the components. In deciding on a suitable experimental design, the following three criteria were considered: A basic model of the design must be attainable; repeatability of results estimated; and a reliable process for checking the adequacy of the fitted model was important. The appropriate model for the simplex-centroid design was chosen by trial from the linear model upward, until the coefficients or β terms did not significantly differ in value represented by a p-value greater than 0.05. The adequacy of the model was approved when the residual standard deviation was close to the replicate standard deviation and the residual plots that were random and without structure. Several contour plots were used to show the component proportions that gave maximum and minimum responses. It was concluded that the optimum mixture was the one that minimized cost but met the specifications (Simon et al., 1997).

The studies discussed in this chapter have examined various parameters that impact the volumetric and performance properties of pervious concrete mixtures. But the question remains, is there a process that potentially allows the examination of pervious concrete properties for all possible aggregate gradations? It would be beneficial to evaluate such a process that may satisfy site conditions. This research was designed to examine this possibility. An approach was taken that regards the variables as dependent components and not independent where one factor is changed at a time (Yeh, 2008). The simplex-centroid design takes this approach with a triangular coordinate system where vertices represent the proportion of single-sized aggregate components with additional points along the edge and within the triangle.

CHAPTER 3 : MATERIALS AND EXPERIMENTAL PROCEDURES

In this chapter, the components of the pervious concrete mixtures, the experimental methods, and modeling and analysis processes are described. A pervious concrete mix consists largely of aggregate, for this study approximately 78% by mass or 54 % by volume. To achieve the optimum mix design based on the given material for any given application, the approach was to understand the effects of aggregate structure, both its individual and group properties, on the performance of the pervious concrete mixtures. This research was divided into three phases that consist of (1) the characterization of aggregate structure, (2) the determination of the pervious concrete mixture performance properties and (3) the modeling and analysis (simplex-centroid design) of the data for aggregate proportioning and performance predictions. Flowcharts of these phases of the investigation are shown in Figures 3.1, 3.2 and 3.3, respectively.

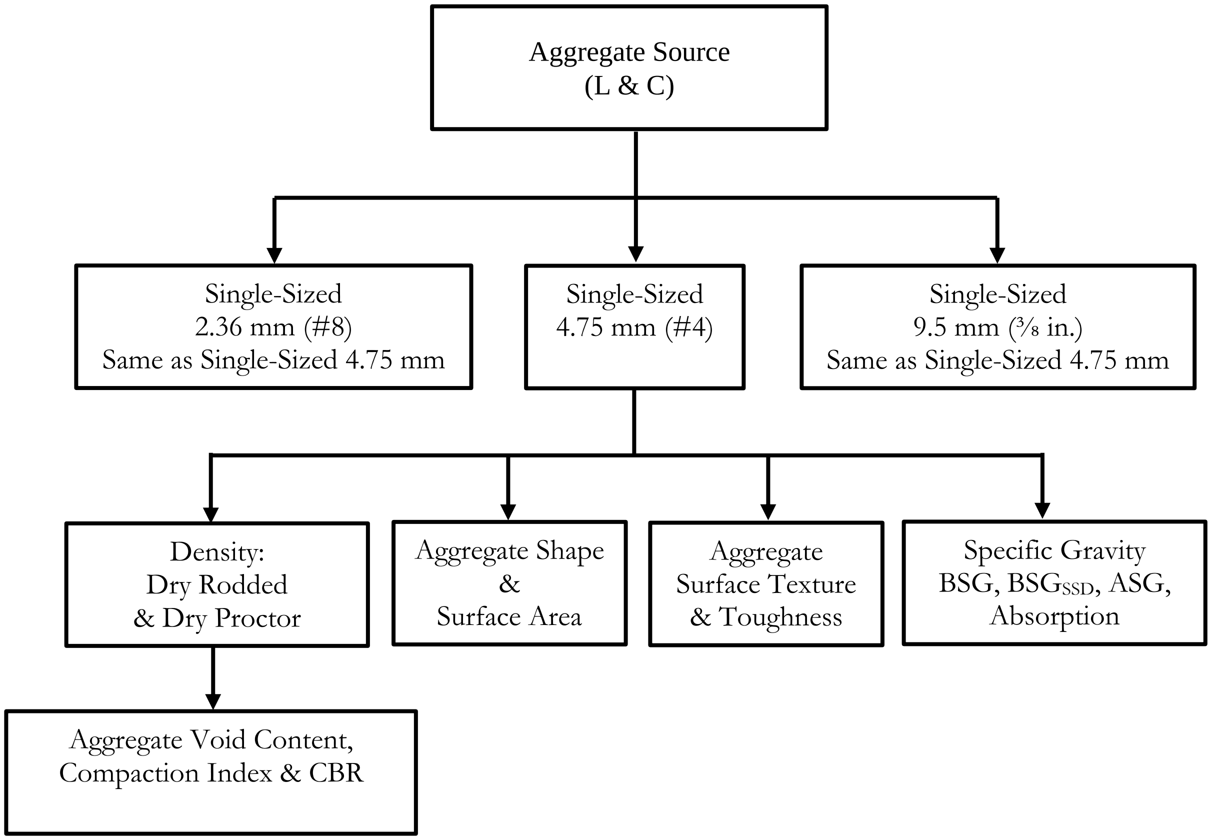

Figure 3.1 Phase 1, the experimental design to classify aggregate structure.

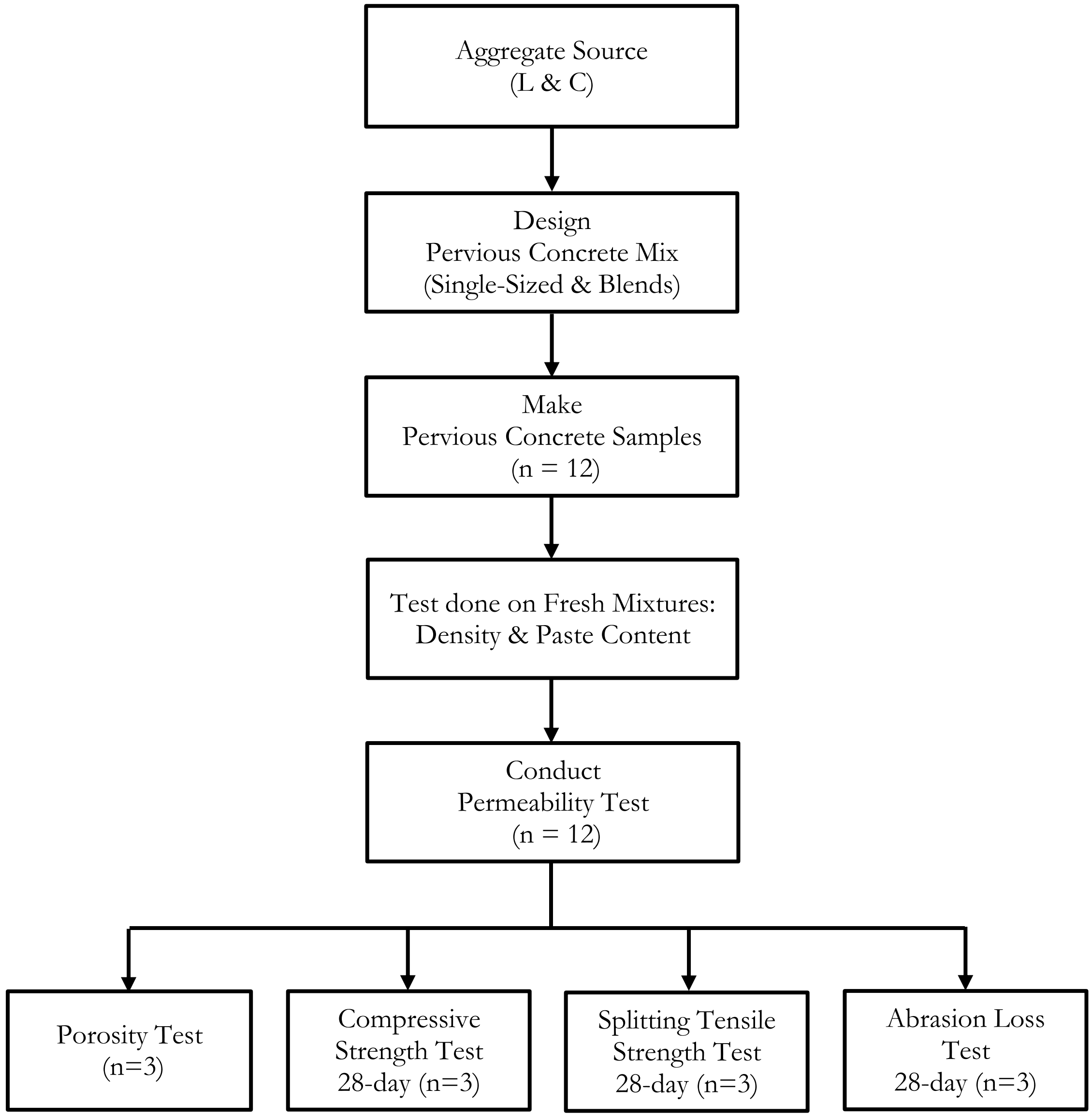

Figure 3.2 Phase 2, the experimental design to determine performance properties of the pervious concrete mixtures.

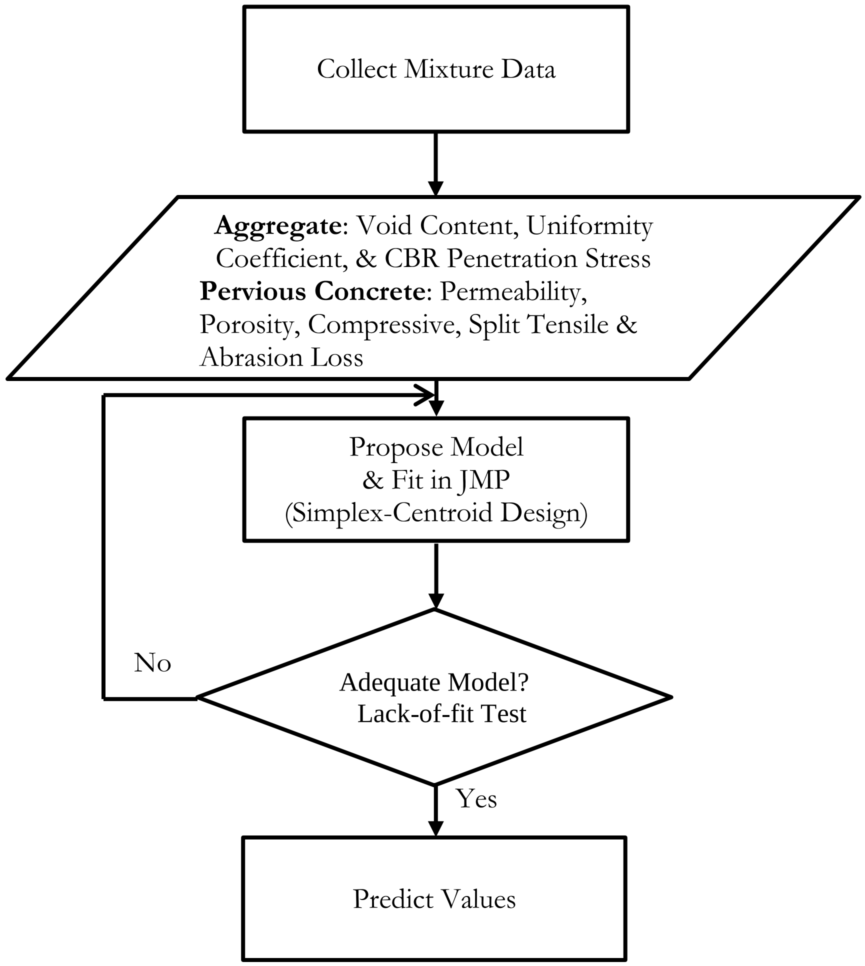

Figure 3.3 Phase 3, the modeling and analysis of aggregate and pervious concrete mixture data for performance predictions.

Materials

Aggregate

The aggregate types considered for this study were representative of the aggregate types sourced from South Carolina quarries. The aggregate types studied were micaceous blue granite, classified as aggregate L (Figure 3.4) and the other granite, classified as aggregate C (Figure 3.5). Aggregates were prepared by oven drying at 110°C (230°F), before being separated with a mechanical shaker into single-sized fractions of #8 (2.36 mm), #4 (4.75 mm), and ⅜ in. (9.5 mm) with an upper limit of ½ in. (12.5 mm). To facilitate the analysis process, the aggregates finer than the #8 was excluded from the mixture gradation.

Figure 3.4 Aggregate L, from left to right: #8, #4, and ⅜ in.

Figure 3.5 Aggregate C, from left to right: #8, #4, and ⅜ in.

Table 3.1 presents the specific gravities and absorption values of each aggregate fraction determined according to ASTM C 127 or C 128. The absorption values were used to determine suitable absorption water quantities for the different aggregate fractions incorporated in the pervious concrete mixtures. As expected, it was observed that as the aggregate size fraction decreased, the absorption levels increased, showing the effects of an increase in surface area. The LA abrasion loss values for aggregates L and C are very different from each other, approximately 55% and 27%, respectively, showing C as a much tougher aggregate as compared to L.

Table 3.1 Specific gravities and absorption of individual size fractions for aggregates L and C.

Sieve Size	ASTM Designation	Aggregate Properties							
		Bulk Specific Gravity		SSD Specific Gravity		Apparent Specific Gravity		Absorption (%)	
		L	C	L	C	L	C	L	C
#8	C 128	2.634	2.602	2.656	2.618	2.694	2.644	0.85	0.62
#4	C 127	2.631	2.608	2.650	2.622	2.683	2.644	0.73	0.52
⅜ in.	C 127	2.639	2.614	2.654	2.625	2.680	2.642	0.58	0.41

Cement

A general purpose Type I/II Portland cement was used for the preparation of the pervious concrete mixtures. This cement was manufactured to meet the requirements of ASTM C150. Typical chemical and oxide composition of the cement used for all of the pervious concrete samples are given in Table 3.2.

Table 3.2 Chemical and oxide composition of the Type I/II Portland cement used (Cemex, 2008).

Chemical Composition		**Oxide Composition**	
Chemical	**Weight Percent**	**Oxide**	**Weight Percent**
C_3S	60.0	CaO	62.5
C_2S	10.0	SiO_2	19.4
C_3A	8.0	Al_2O_3	5.3
C_4AF	11.0	Fe_2O_3	3.6
Insoluble Residue	0.42	MgO	2.7
Loss on Ignition	1.5	SO_3	3.0
		Na_2O eq.	0.48

Methods

Mix Design

The pervious concrete batches were designed to make twelve (12) 6 in. × 6 in. cylindrical specimens. Each mix consisted of aggregate, cement, water and superplasticizer. The independent variables (fixed) were the water-cement ratio of 0.25 (excluding aggregate absorption water), the cement-aggregate ratio of 0.23 for mixes with aggregate L and 0.25 for mixes with aggregate C and the quantity of superplasticizer (Glenium 7500) was 4.5 fl oz/cwt. The water-cement and cement-aggregate ratios were determined from work done on cement paste and pervious concrete mixtures by Singer as shown in Table 3.3 and illustrated in Figure 3.6 (Singer, 2012). The pervious concrete mixtures were prepared from aggregates L and C based on a No.89M gradation (SCDOT 2007). The dependent variables (random) were the aggregate proportions in the mixtures, consisting of the three (3) fractions (#8, #4 and ⅜ in.). The volumetric values and masses of the batch components for pervious concrete mixtures prepared from aggregates L and C are presented in Table 3.4 and 3.5, respectively.

Table 3.3 Relationship of compressive strength to water-cement ratio of cement paste and relationship of permeability and compressive strength to cement-aggregate ratio of pervious concrete mixtures made from aggregate L and C (Singer, 2012).

Water/Cement Ratio	Compressive Strength (psi)	Cement/Aggregate Ratio	Permeability (in./hr.)		Compressive Strength (psi)	
			L	C	L	C
0.250	9696					
0.275	9147	0.200	2297	2378	647	610
0.300	8693	0.225	1656	2078	1049	667
0.325	8033	0.250	1623	1761	1083	754
0.350	7125	0.275	1231	1211	1271	1025

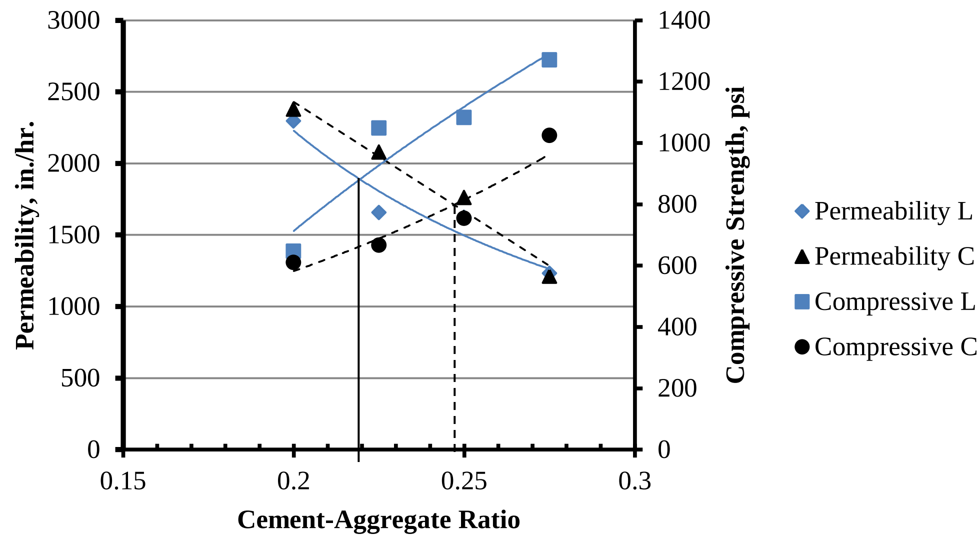

Figure 3.6 Cement–aggregate ratios based on permeability and compressive strength interactions for pervious concrete mixtures made from aggregate L and C (Singer, 2012).

Table 3.4 Volumetric values and masses of the pervious concrete components prepared from aggregate L for one batch.

Pervious Concrete Components	Volume		Weight	
	yd^3	Percentage	lb	Percentage
Air	6.45×10^{-3}	26.9	0	0
Water	1.96×10^{-3}	8.2	3.303	4.43
Superplasticizer	2.34×10^{-5}	0.1	0.042	0.06
Cement	2.51×10^{-3}	10.5	13.311	17.9
Aggregate	0.0131	54.6	57.876	77.7
Total	2.4×10^{-3}	100.0	74.5	100.0

Table 3.5 Volumetric values and masses of the pervious concrete components prepared from aggregate C for one batch.

Pervious Concrete Components	Volume		Weight	
	yd^3	Percentage	lb	Percentage
Air	6.31×10^{-3}	26.3	0	0
Water	2.09×10^{-3}	8.71	3.522	4.73
Superplasticizer	2.45×10^{-5}	0.1	0.044	0.06
Cement	2.68×10^{-3}	11.2	14.193	19.0
Aggregate	0.013	53.8	56.773	76.2
Total	2.4×10^{-2}	100.0	74.5	100.0

Aggregate Proportioning

The aggregates used to prepare the pervious concrete mixtures were of sieve designations #8, #4 and ⅜ inch. The aggregate proportions corresponded with the seven (7) points of a simplex-centroid design. The simplex-centroid design is a statistical analysis tool used in mixture experiments. Mixture experiments are experiments where it is assumed that the response depends solely on the proportions of the mix components (Cornell, 2002). Since there are three (3) aggregate components, the simplex is an equilateral triangle with the three (3) single-sized (pure) fractions at the vertices, the binary or two component blends at the halfway points along the edges and the ternary or three component blend at the centroid as shown in Figure 3.7a. In addition to these seven

(7) points, the power of the simplex may be increased by incorporating more points within the triangle making the simplex an augmented triangle as shown in Figure 3.7b.

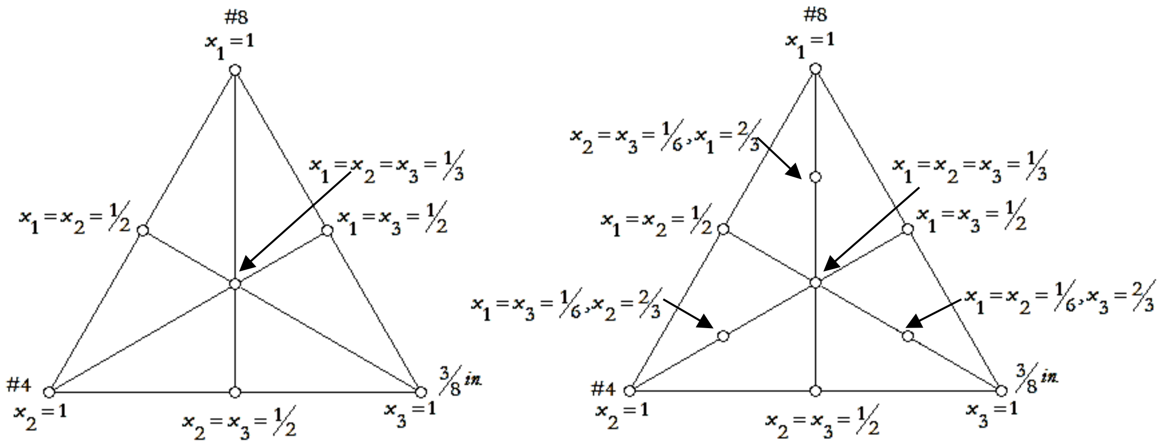

(a) (b)

Figure 3.7 (a) A simplex-centroid design and (b) an augmented simplex-centroid design **(Cornell, 2002)**

The responses associated with the ten (10) design points or blends on the augmented simplex triangle were the density, void content, and uniformity coefficient of the dry aggregate. Beside these design points, there were additional points to be used as validation points for aggregate L and C, comparing the measured values with the predicted. The statistical prediction and analysis of the simplex-centroid design was first conducted on the dry aggregate to better understand the predictions of the performance parameters of the pervious concrete mixtures. The aggregate proportions for both the dry aggregate tests and the pervious concrete mixtures are presented in Table 3.6.

Table 3.6 Aggregate blends and proportions used in dry aggregate tests and in pervious concrete mixtures.

No.	Aggregate Gradation	Blend ID	Aggregate Proportions #8 (2.36 mm)	#4 (4.75 mm)	⅜ in. (9.5 mm)
1	#8*	8	1	0	0
2	#4*	4	0	1	0
3	⅜*	38	0	0	1
4	¾·8,¼·4	8884	0.75	0.25	0
5	½(8,4)*	84	0.5	0.5	0
6	¼·8,¾·4	8444	0.25	0.75	0
7	¾·4,¼·⅜	4443	0	0.75	0.25
8	½(4,⅜)*	43	0	0.5	0.5
9	¼·4,¾·⅜	4333	0	0.25	0.75
10	¼·8,¾·⅜	8333	0.25	0	0.75
11	½(8,⅜)*	83	0.5	0	0.5
12	¾·8,¼·⅜	8883	0.75	0	0.25
13	⅓(8,4,⅜)*	843	0.333	0.333	0.333
14	⅔·8,⅙(4,⅜)*	8843	0.667	0.167	0.167
15	⅔·4,⅙(8,⅜)*	8443	0.167	0.667	0.167
16	⅔·⅜,⅙(8,4)*	8433	0.167	0.167	0.667
17	#89*	89	0.26	0.737	0.003
18	#789*	789	0.248	0.693	0.059
19	(60,10,30)*	613	0.60	0.10	0.30
20	(39,45,16)*	341	0.39	0.45	0.16
21	(15,32,53)*	135	0.15	0.32	0.53

* Blends used to prepare pervious concrete mixtures.

The aggregate gradations were given a blend ID that matched the aggregate size and proportion in the blend (Table 3.6). The identification numbers for standard aggregate gradations were kept, such as #8, #4, #89, and #789. The ⅜ in. aggregate was referred to as 38 because those numbers are associated with its size in inches. With the exception of the three (3) random gradations 613, 341, and 135, the binary and ternary blends were given numbers that were ordered from the smallest aggregate size (8) to the largest (38) where the ‘8’ in 38 was dropped to maintain a reasonable length for numbers. The numbers for the single-sized fractions making up the binary and ternary blend ID’s were repeated to indicate higher proportions in the blends, for example ⅔·4,⅙(8,⅜) would be 844443 but would be too long therefore, it was reduced to 8443. For the three random blends, the first number of each proportion was used.

Mixing and Curing Techniques

The pervious concrete mixtures were mixed and cured according to ASTM C 192 with the exception of adding approximately 5% of the cement while the drum was rotating to the saturated surface dry (SSD) aggregates, which was allowed to rotate for approximately 1 minute to promote even cement coating of the aggregate (Schaefer et al, 2006). The aggregate was mixed in SSD conditions by adding the absorption water at the beginning while the mixing drum was rotating. Two batches of six (6) cylinders each were made for each sample group, due to the capacity of the mixer, giving a total of 12 specimens as shown in Figure 3.8 (a). The dimensions of these specimens were 6 × 6 inches (diameter × height). A total of 348 pervious concrete specimens were made for this study with constant paste content, CPC.

(a) (b)

Figure 3.8 Pervious concrete specimens (a) demolded and (b) in wet curing room.

Each mold was filled with one (1) lift of pervious concrete to approximately 1 inch beyond the top and the mix was retained by a detachable collar. A standard Proctor hammer (5.5 lb) was used to apply 25 blows in the one (1) level to consolidate the samples. The samples were allowed to set in the moisture curing room for 24 ± 8 hours before demolding and then cured for twenty-eight (28) days in the moisture room as shown in Figure 3.8 (b).

Aggregate Tests

Flat and Elongated Properties

The shape of coarse aggregate particles impacts the performance properties of pervious concrete mixtures. Therefore, the aggregates were closely examined in accordance with both testing methods ("A" and "B") documented in ASTM D4791. Aggregates that are flat and elongated tend to fail earlier than rounded or cubic shaped aggregate. For pervious concrete mixtures, higher strengths have been observed from more rounded aggregate particles (Tennis et al., 2004).

Density and Void Content

The density and void content of the aggregate fractions were measured to understand the correlations between the aggregate properties and related pervious concrete properties and the effects of aggregate gradation. The compaction process used in determining the density followed both ASTM C29 and the method used to compact the pervious concrete samples. Involved in the latter process was the determination of loose and compacted density. To determine the loose density, the molds were filled with dried aggregate, the excess aggregate was struck off, and the loose weight recorded. Then it was filled to approximately ⅝ in. beyond the rim of the mold and compacted with 25 blows from a standard Proctor hammer to measure the compacted density. The density and void content were calculated for both the loose and the compacted state to determine the sensitivity of the dry aggregate gradations to compaction, which was referred to as the aggregate compaction index (C_a). This density procedure was also referred to as the "dry Proctor" in this study. The optimum compaction level of 25 blows was determined from Figure 3.8 where changes in density and void content were observed with the increase in number of blows applied by a Proctor hammer. Compaction energies of 20 and 30 blows showed a possible compaction limit for larger size fractions, 4 and 38, this was deduced from the gentle slopes of the linear curves between the corresponding points (Figure 3.9). There was a possibility of aggregate breakdown at compaction levels greater than 30 blows based on the increased slope of connecting lines, therefore, 25 blows was chosen as an appropriate number of blows for compaction of the aggregate and the pervious concrete mixtures in this study.

The aggregate void content, which is the ratio of volume of voids to volume of the specimen, was calculated based on ASTM C29 and is given in equation 3.1:

$$Void\,Content = 100 \times \frac{\left[(BSG \times \rho_w) - UW\right]}{BSG \times \rho_w} \tag{3.1}$$

where *BSG* is the bulk specific gravity, ρ_w is density of water, 62.3 lb/ft^3 and *UW* is the aggregate density (lb/ft^3).

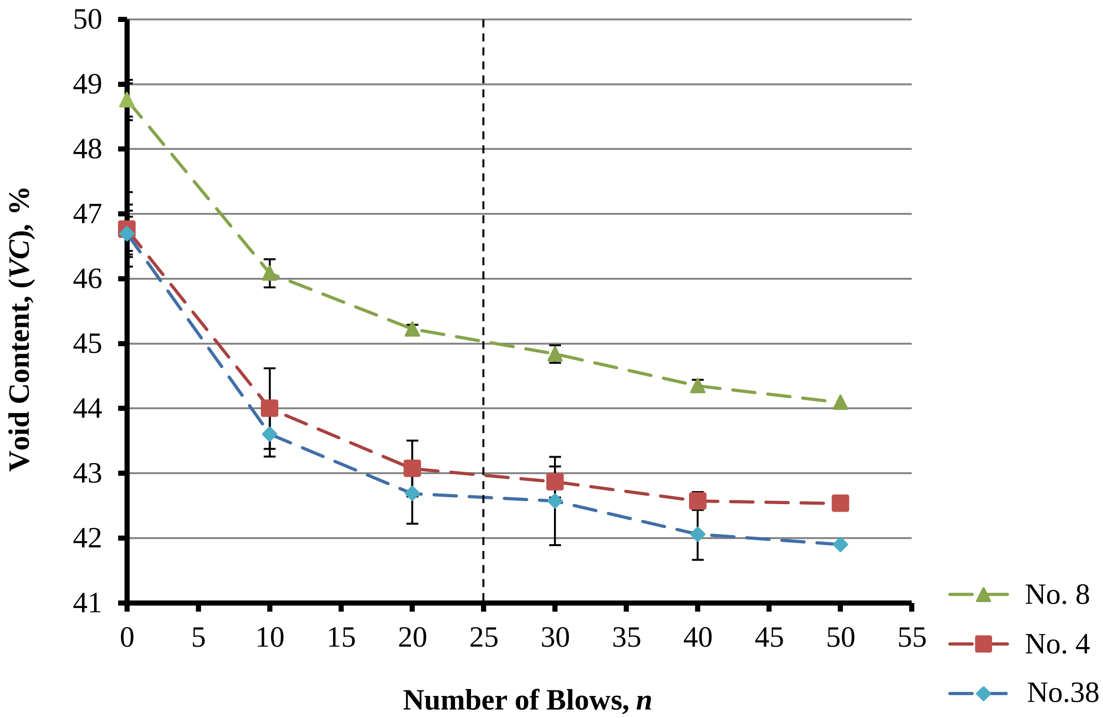

Figure 3.9 Relationship of single-sized aggregate void content to increasing compaction energies from a stand Proctor hammer.

Shape and Surface Texture Index and Uniformity Coefficient

Another factor that influences the performance of a pervious concrete pavement is the texture, roughness or smoothness, of the aggregate particles. The ASTM D3398 procedure was used to determine the particle index I_a, of the aggregates. This test gives a quantitative measure of the effects of aggregate shape and texture characteristics on percent voids. The tamping rod for smaller aggregate was lighter than the tamping rod for the larger aggregate so that the compaction process did not significantly breakdown or polish the aggregate surface. It was conducted on the single-sized fractions and it involved the volume of the voids at 10 and 50 tamps using the specified tamping rods to calculate the particle index using equation 3.2, (Figure 3.10),

$$I_a = 1.25V_{10} - 0.25V_{50} - 32.0 \qquad 3.2$$

where Ia is the particle index, V_{10} is voids in aggregate compacted at 10 drops per layer and V_{50} is voids in aggregate compacted at 50 drops per layer.

Figure 3.10 Shape and Surface Texture Index (Particle Index) test set-up.

The uniformity coefficient, C_u, is a measure of the degree of uniformity of an aggregate gradation − how similar the aggregate sizes are to each other. It is defined as the ratio of aggregate diameters corresponding to 60% finer and 10% finer based on the aggregate size distribution curve (Das, 2006).

California Bearing Ratio Penetration Stress

The California Bearing Ratio, CBR, penetration stress test conducted on the aggregate samples was based on ASTM D1883 but with some variations. The CBR penetration test is usually done to evaluate the potential strength or load-bearing capacity of a base material or subgrade for a pavement (ASTM D1883). A set-up of the CBR penetration stress test is shown in Figure 3.11. In this study, the aggregate samples were tested dry and the aggregate samples were placed in a 6 in. (152.4 mm) diameter metal mold with a height of 7 in. (177.8 mm) without the metal spacer disk at the bottom. The aggregate was tested in both the loose and compacted conditions. The compaction procedure involved 25 blows from the standard Proctor hammer in one level lift, which was when the mold was completely filled. After the excess aggregate was struck off, the extension collar was placed on the mold to keep the metal surcharge disks in place. The test was conducted by applying a load to a 2 in. (50.8 mm) diameter piston at a rate of 0.05 in/min (1.27 mm/min.). The penetration load was applied to the surface of the aggregate sample while the depth of penetration was recorded. The test was stopped when the aggregate would no longer allow a steady increase in load, which was a sign of potential aggregate breakdown.

Figure 3.11 CBR Penetration Stress test set-up.

Pervious Concrete Testing

Unit Weight

The unit weight of the pervious concrete mixtures was measured two (2) ways. One method was according to ASTM D1688 and the other followed the method of preparation and compaction used in making the pervious concrete cylinders. The reasoning behind the latter was based on field practice where a pervious concrete pavement having a thickness of approximately 6 in. is compacted only at the top surface, therefore it was deemed valid to have a unit weight procedure that was representative of the compaction process of the pervious concrete in the field.

The unit weight testing involved the measuring of both the loose and compacted mixture. The mold was filled with pervious concrete, the excess concrete was struck off and the weight recorded to determine the loose unit weight. The mold was filled again beyond the rim to approximately 1 inch and the concrete was kept from falling off the edges by a detachable collar. The pervious concrete compressed more than the dry aggregate, therefore a larger portion was added to approximately 1 inch above the rim as compared to ⅝ inch for the dry aggregate. It was then hit twenty-five (25) times with the standard Proctor hammer and concrete was added if the top surface went below the rim of the mold or removed if there was too much concrete to bring the surface flush with the rim. The specimens were leveled by first striking off excess concrete and then by rolling a ⅝ in. tamping rod across the top. The unit weights of both the loose and compacted pervious concrete mixtures were determined. From this, the sensitivity of the pervious concrete mixtures to the compaction of 25 blows was determined. This measure of sensitivity was the change in unit weight to the number of blows and was referred to as the pervious concrete compaction index C_c.

Paste Content

The paste content was considered as the portion of the pervious concrete mixture that passed the No. 30 (600 μm) sieve. In this procedure, the weight of two (2) samples with a volume of approximately 25 in.^{3} of pervious concrete was taken. The samples were washed over a No. 30 sieve and the aggregate retained on the sieve was dried in an oven at 110°C (230°F) and weighed. The paste content *(pc)* was calculated based on equation 3.3:

$$pc = \frac{C - (A + aw)}{C} \times 100 \qquad (3.3)$$

where *C* is the mass of the pervious concrete mixture specimen, *A* is the mass of the dried aggregate retained on the No. 30 sieve and *aw* is the absorption water. This test was conducted as a means of quality control, comparing the design paste content to the actual.

Effective Porosity

Effective porosity (*P*) is the ratio of volume of the accessible voids to total volume of the specimen (Das, 2006). The voids being considered were those accessible by water. Testing the effective porosity of the pervious concrete specimens was done according to the procedure outlined by Montes et al., 2005. The samples were dried for approximately 24 hours in an oven at 38 °C (100 °F) and then allowed to reach ambient temperature before testing. The height and diameter of the specimens were measured and the total volume calculated. The specimen was submerged in 25°C water for 30 minutes after which it was inverted and tapped five times on a neoprene pad at the bottom of the tank while submerged. The effective porosity was calculated using equation 3.4:

$$P(\%) = \left[1 - \frac{\frac{(W_{dry} - W_{sub})}{\rho_w}}{V_T} \right] \times 100 \qquad (3.4)$$

where W_{dry} and W_{sub} is the dry mass and submerged mass of the pervious concrete specimen, respectively. The density of the water (ρ_w) at 25 °C was 62.3 lb/ft^3 and the V_T represented the total volume of the specimen. The experimental setup for the porosity test is shown in Figure 3.12.

Figure 3.12 Effective porosity test setup.

Permeability

Permeability is an essential performance parameter considered in the construction of porous pavements. It is not only impacted by the porosity of the matrix but also by the pore size distribution and roughness, the tortuosity, and connectivity of the pores (Garboczi, 1990). To measure the permeability of the pervious concrete specimens, a falling-head apparatus was assembled as shown in Figure 3.13. The preparation of the specimens involved measuring the diameter and height of a specimen at three (3) representative locations, and wrapping the specimens tightly at the upper end with packaging tape, which was folded in a manner that allowed part of the adhesive surface to bond with the specimen and the remainder facing outwards. Plastic wrap was then tightly wrapped around the specimen and was adhered to the lower portion of the tape, leaving the upper portion to adhere to the inside of the standpipe after loading the specimen. This preparation of the specimen is shown in Figure 3.14.

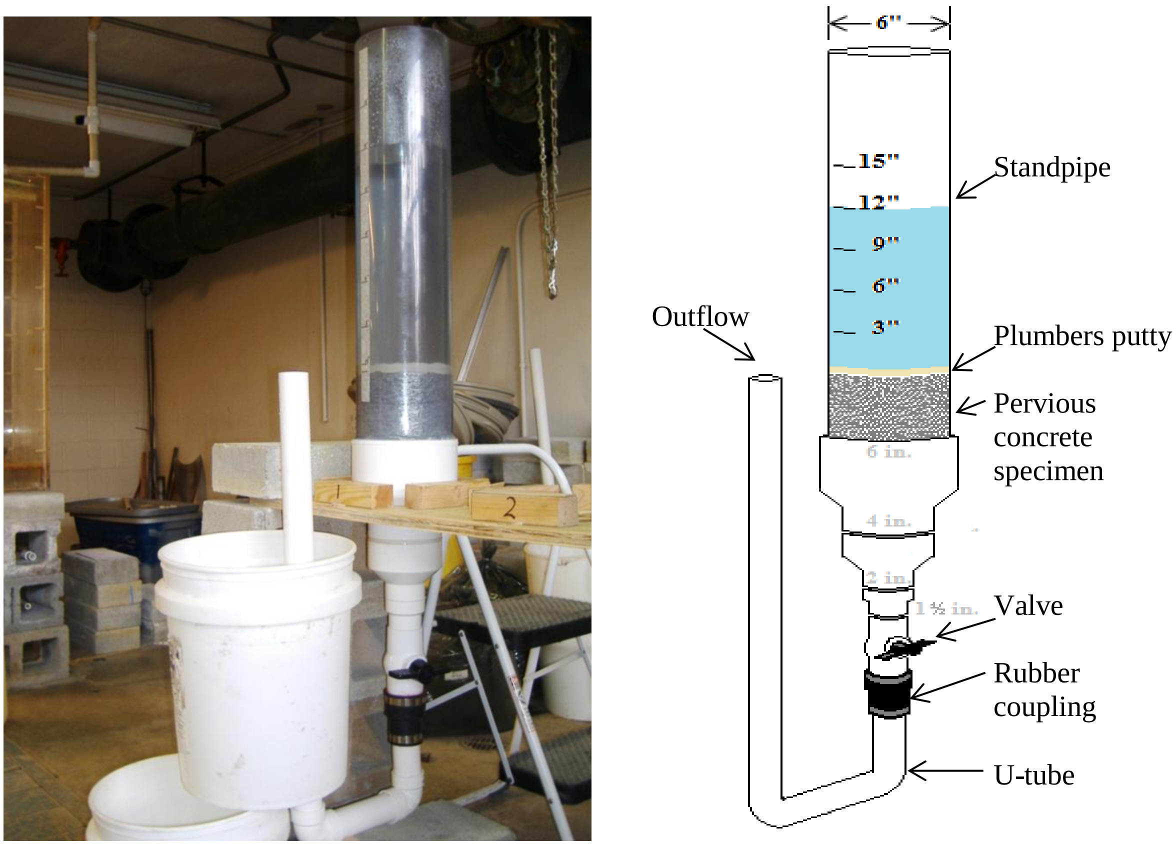

(a) (b)

Figure 3.13 Permeability of pervious concrete samples determined by falling-head apparatus: (a) the lab set-up; (b) schematic diagram

Figure 3.14 Stages in preparing pervious concrete specimens for the permeability test.

The standpipe was loaded with the specimen, and plumbers putty was used to seal the tape to the standpipe. The U-tube was connected with the end of the outflow leveled to the top of the specimen. Water was added from the bottom to eliminate any air pockets that may form below or within the specimen. When the water glazed over the surface of the specimen, the valve was closed and the standpipe was filled from the top. The valve was opened and the time, t (in seconds), taken for the water to fall from the initial head, h_1, of 12 in. (305 mm) above the specimen to the final head, h_2, of 3 in. (76 mm) above the specimen was measured. The permeability or hydraulic conductivity, k, of the specimen was calculated from equation 3.5:

$$k = \frac{aL}{At} \ln \frac{h_1}{h_2} \tag{3.5}$$

where a is the cross-sectional area of the standpipe, L is the length of the specimen and A is the cross-sectional area of the pervious concrete specimen. This process was done three (3) times to each specimen, and the average permeability was calculated. These values were used to categorize the twelve (12) specimens from each mixture into four (4) sample groups of three (3), so that each group had statistically similar permeability values based on a 95% level of confidence. Different tests were conducted on each sample group including porosity, compressive strength, split tensile strength and abrasion loss.

Compressive and Split Tensile Strength Tests

The strength tests used for the pervious concrete samples were the compressive strength test (ASTM C39), and the split tensile strength test (ASTM C496). To meet the standard specimen dimensions for testing, 3 in. diameter cores were drilled out of the samples. The ends of the samples were sawed off and made parrel to each other to achieve a height to diameter ratio of 1.8 to 2.2 in accordance with the standard (ASTM C 39). The new heights and diameters were measured, and then the two (2) sample groups of three (3) specimens were tested for compressive and split tensile strength.

Abrasion Loss

The abrasion loss procedure used in this study followed the Cantabro mass loss procedure for asphalt mixtures where 6 in. cylindrical specimens undergo abrasion in a rotating Los Angeles abrasion machine. This test measured the abrasion loss after 300 revolutions in the Los Angeles abrasion machine without the steel charge. Prior to testing, the pervious concrete samples were allowed to air dry for approximately an hour before the initial mass (A) was measured. The specimen was placed in the LA abrasion machine, and the mass (B) was measured after every 100 revolutions until it reached 300 revolutions (Figure 3.15). This was done for three (3) specimens and the percent loss (*AL*) was calculated from equation 3.5:

$$AL = \frac{A - B}{A} \times 100 \tag{3.5}$$

Figure 3.15 LA Abrasion machine used for abrasion loss test.

CHAPTER 4 : EXPERIMENTAL RESULTS AND DISCUSSION

The empirical results relating to the physical and volumetric properties of the aggregate and the volumetric and performance properties of the lab prepared Portland cement pervious concrete mixtures are presented in this chapter. Statistical analysis of the data was used to examine least significant differences amongst the results for each performance category with a 95% level of significance. Correlations between aggregate properties and pervious concrete properties were examined along with some properties within these categories.

Aggregate Properties

In this research study, different tests were conducted to determine properties of aggregate sources L and C to aid in the evaluation process of how aggregate influence pervious concrete mixtures. As indicated in Chapter 3, these tests included the determination of Flat and Elongated particles, Shape and Surface Texture Index, Density, Void Content, Uniformity Coefficient, Aggregate Compaction Index and the California Bearing Ratio Penetration Stress. One of the differences between aggregate L and C is that aggregate C is a much tougher rock compared to aggregate L based on the LA abrasion values of approximately 27 and 55, respectively. The following sections present more details about the results obtained from the tests conducted.

Flat and Elongated

The determination of the percentage flat and elongated aggregate particles was done in accordance with ASTM D4791. The percentages of flat and/or elongated particles are shown in Tables 4.1 and 4.2 for aggregate L and C. The results based on the 3:1 ratio were more distinct than those of the 5:1 ratio which depicted both sources as being almost 100% “neither flat nor elongated” for both methods A and B. From the 3:1 ratio, it was determined that aggregate C had a higher percentage of flat particles leading to an overall lower quantity of “neither flat nor elongated” particles (93%) as compared to aggregate L (99%) based on method A. For the same ratio, method B showed that with increasing aggregate size the “flat and elongated” percentages decreased, conveying that larger particles were more rounded or cubic in shape. It gave aggregate C a marginally lower percentage (69%) for “neither flat nor elongated” than aggregate L (71%). Based on the 3:1 ratio it was observed that aggregate L had more “neither flat nor elongated” aggregate particles compared to aggregate C.

Table 4.1 Flat and elongated percentages for aggregates L and C based on the 3:1 testing ratio.

3:1 Ratio							
Method	Aggregate Shape	Aggregate L			Aggregate C		
		#4 (%)	⅜" (%)	Total Percentage (%)	#4 (%)	⅜" (%)	Total Percentage (%)
A	Flat	0	2	1	8	6	7.0
	Elongated	0	0	0	1	0	1.0
	Flat and also Elongated	0	0	0	0	0	0.0
	Neither Flat nor Elongated	100	98	99	91	94	92
B	Flat and Elongated	34	24	29	40	23	31
	Neither Flat nor Elongated	66	76	71	60	77	69

Table 4.2 Flat and elongated percentages for aggregates L and C based on the 5:1 testing ratio.

5:1 Ratio							
Method	Aggregate Shape	Aggregate L			Aggregate C		
		#4 (%)	⅜" (%)	Total Percentage (%)	#4 (%)	⅜" (%)	Total Percentage (%)
A	Flat	0	0	0	0	0	0
	Elongated	0	0	0	0	0	0
	Flat and also Elongated	0	0	0	0	0	0
	Neither Flat nor Elongated	100	100	100	100	100	100
B	Flat and Elongated	1	0	1	0	2	1
	Neither Flat nor Elongated	99	100	99	100	98	99

Shape and Surface Texture Index

The shape and surface texture index (or particle index), I_a, test was done according to ASTM D3398. The particle index was found for the single-sized aggregate fractions namely the #8 (2.36 mm), #4 (4.75 mm) and ⅜ in. (9.5 mm). From these indices, the particle indices for other gradations were calculated, based on the percentages of single-sized fractions in the blends. These values are listed in Table 4.3.

Aggregate L had the lower particle indices between the two (2) sources. An aggregate matrix with a lower particle index can be described as smoother and more rounded; which would be the case for the source L aggregate as compared to source C. Some of the typical effects of a more rounded and smoother aggregate are its reduction in void content, abrasion loss, and absorption but it increases unit weight of the pervious concrete mixtures (Jain et al.,2011).

Table 4.3 Shape and Surface Texture Particle Index, for Aggregate L and C

Aggregate Blend ID		**L** Particle Index	**C** Particle Index
		(I_a)	(I_a)
Pure	8	12.4	14.3
	4	11.6	13.7
	38	11.0	14.2
Binary	84	12.0	14.0
	43	11.3	14.0
	83	11.7	14.3
Ternary	843	11.6	14.1
	8843	12.0	14.2
	8443	11.6	13.9
	8433	11.3	14.2
Binary	8884	12.2	14.2
	8444	11.8	13.9
	4443	11.4	13.9
	4333	11.1	14.1
	8333	11.3	14.2
	8883	12.0	14.3
Ternary	89	11.8	13.9
	789	11.7	13.9
	613	11.9	14.2
	341	11.8	14.0
	135	11.4	14.1

Density and Void Content

Dry Rodded Density

The dry rodded density procedure in this study followed ASTM C29. It was conducted on both aggregate sources to calculate both the density and void content. This procedure is used to calculate the ratio of the dry compacted aggregate mass to the volume of the measure or container. It was used for comparison purposes to the alternative density method or “dry Proctor density”, described in Chapter 3. Table 4.4 shows the aggregate density results of all the methods used for aggregate L and C gradations.

For the pure blends, it was observed that as the aggregate size increased, the density of the aggregate gradation increased. It was also observed that in most cases, aggregate L had slightly higher loose densities compared to aggregate C, which could be linked to source L aggregates having a slightly higher average bulk specific gravity (2.635 compared to 2.608). The gradations with the highest densities for aggregate L, before and after compaction, were those with at least one third of the blend being the 38 aggregate or the largest aggregate size evaluated in this study. Gradations with large portions of the smallest aggregate size, #8, resulted in lower densities. Aggregate C gradations showed similar results with larger aggregate sizes yielding higher densities and smaller sizes producing lower densities (Figure 4.1).

Within the aggregate sources, the dry rodding process resulted in an increase in density of 7% to 12% for source L and 5% to 9% for source C. This indicates that L is more sensitive to this form of compaction. One reason for this may be related to aggregate L having a lower particle index compared to aggregate C; therefore, L was smoother and generated less friction during compaction. The rodding process was able to compact the aggregate with little disturbance to aggregate surrounding the point of impact or no heave effect. Aggregate L had higher loose and compacted densities compared to C based on the dry rodding method.

Table 4.4 Loose, Dry Rodded, and Dry Proctor Density Values for Aggregate L and C

Aggregate Gradation ID		**L** Loose Density (ρ_l) lb/ft^3	**C** Loose Density (ρ_l) lb/ft^3	**L** Dry Rodded Density (ρ_r) lb/ft^3	**C** Dry Rodded Density (ρ_r) lb/ft^3	**L** Dry Proctor Density (ρ_p) lb/ft^3	**C** Dry Proctor Density (ρ_p) lb/ft^3
Pure	8	86	83	93	89	93	89
	4	90	86	97	93	96	93
	38	92	88	98	93	98	94
Binary	84	88	87	96	93	94	94
	43	89	88	98	94	95	96
	83	93	91	100	98	99	99
Ternary	843	91	90	100	98	98	97
	8843	89	90	97	94	95	95
	8443	89	88	97	95	96	96
	8433	90	91	99	97	98	98
Binary	8884	86		94		92	
	8444	87		96		94	
	4443	88	87	97	94	95	95
	4333	89		100		95	
	8333	93		100		99	
	8883	89		97		95	
Ternary	89	88	89	97	95	95	96
	789	89		98		95	
	613	90	89		96	97	97
	341	88	90		95	95	96
	135	90	90		97	98	98

*Darkened cells were additional aggregate blends that were not tested for source C.

Dry Proctor Density

As defined in Chapter 3, the standard Proctor hammer was used as an alternate method to compact the different aggregate gradations to determine density and void content of both aggregate L and C. This was done in an effort to simulate the compaction process used for the pervious concrete samples in the lab. The aggregate density was determined by placing the aggregate in a 6 $\times$ 6 in. cylindrical mold, to approximately ⅝ in. beyond the rim and compacting with 25 blows of the standard proctor hammer. The aggregate dry Proctor density values are included in Table 4.4. Except for the single-sized fractions where density increased with aggregate size, the dry Proctor densities for aggregate L and C in most cases were generally similar to each other as illustrated in Figure 4.1. This could have been linked to the blows from Proctor hammer causing the aggregate around the area of contact to heave, adversely affecting the compaction process. A disk placed on the aggregate may help to reduce this effect. The density increase between the loose and the dry Proctor aggregate ranged from 6% (blend 83) to 9% (blend 8433) for aggregate L. The same range was observed for aggregate C, but with different blends representing the boundaries (6% for blend 8843 and 9% for blends 4443 and 613). The comparison of aggregate L to C showed that the Proctor hammer caused an increase in density values as the size of the single-sized aggregate increased, but similar densities for most of the other blends.

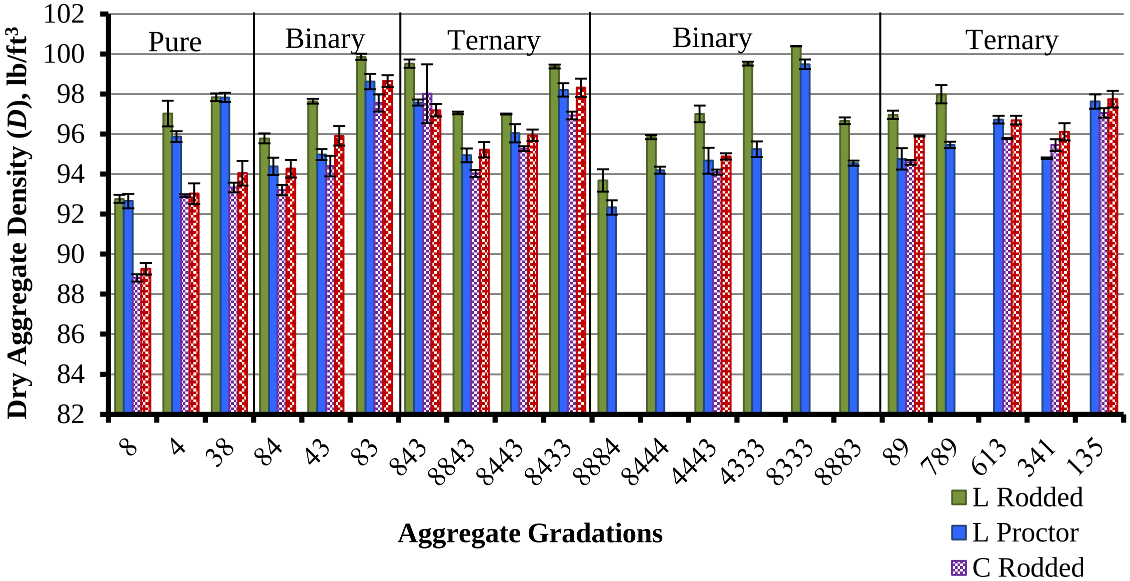

Figure 4.1 Comparison of dry rodded and Proctor density values for aggregates L and C. Missing columns were additional aggregate blends that were not tested for source C.

Void Content

The void content is a measure of the ratio of the volume of voids in the specimen to the volume of the entire specimen. Table 4.5 presents the void contents from the loose, dry rodded, and dry Proctor tests on aggregate sources L and C. In both loose and compacted states, the pure fractions for aggregate L had lower void contents compared to aggregate C. The void contents also decreased as the aggregate size increased. The dry rodded void contents for aggregate L remained lower than aggregate C, but for the dry Proctor, aggregate L was only slightly higher than aggregate C reflecting the heave effect mentioned previously with the dry Proctor density. The percentage reduction in void content after compaction by rodding ranged from 8% to 14% for aggregate L and 6% to 11% for aggregate C, averaging 11% and 8%, respectively. This showed that aggregate L was more sensitive to compaction by rodding than aggregate C, possibly due to the lower LA abrasion value of aggregate L which may have caused it to break down sooner than C under the impact of the Proctor hammer. It could also relate to aggregate L having lower particle indices compared with C, meaning that its smoother surface and more rounded edges led to less friction and tightly packed aggregate with less voids space. For the dry Proctor, aggregate L exhibited reductions in void content ranging from 8% to 11% with an average of 9% for aggregate L. Source C had the same reduction of void content from the loose to the compacted aggregate of 8% to 11%. The impact that the Proctor hammer had on the cohesionless aggregate material may be the reason for this similarity.

The effects of the dry rodded and the dry Proctor compaction methods on void content are illustrated in Figure 4.2. For the single-sized aggregate, the #8 aggregate had the lowest density and the highest void content, followed by the #4 and then the ⅜ in. with the highest density and lowest void content. Latham et al. observed similar trends for single-sized particles where the void content increased as the particle size decreased because of weak attractive van der Waals forces which form clumps of small aggregate that oppose the packing effect of gravitational compaction energies (Latham, 2002). It can be concluded that higher densities and lower void contents came from binary and ternary blends that had equal proportions of the boundary size aggregate (8 and 38) or higher distribution of the largest size aggregate (38).

The relationships between compacted aggregate densities and void contents are shown in Figure 4.3. The slope of the linear regression lines predicted that approximately 60% of the change in density was reflected in the change of the void content for both aggregate L and C and for both dry Proctor and rodding. This showed that the methods of compaction did not significantly affect the change in void content to change in density. For a given density, source L had the higher void content for both compaction methods. This indicated that because source C had a lower specific gravity compared to L, it took more of its aggregate to reach the given density therefore reducing its void content.

Table 4.5 Loose, Dry Rodded, and Dry Proctor Void Contents for Aggregate L and C

Aggregate Gradation ID		**L.** Loose Void Content	**C.** Loose Void Content	**L.** Dry Rodded Void Content	**C.** Dry Rodded Void Content	**L.** Dry Proctor Void Content	**C.** Dry Proctor Void Content
		(VC_l) %	(VC_l) %	(VC_r) %	(VC_r) %	(VC_p) %	(VC_p) %
Pure	8	47.8	48.8	43.4	45.2	43.5	44.9
	4	45.0	47.2	40.8	42.8	41.5	42.7
	38	44.1	45.8	40.5	42.7	40.5	42.2
Binary	84	46.1	46.1	41.6	42.5	42.4	41.9
	43	45.9	45.6	40.5	41.9	42.1	41.0
	83	43.6	43.9	39.2	39.9	39.9	39.3
Ternary	843	44.5	44.7	39.3	39.6	40.5	40.2
	8843	46.0	44.7	40.8	42.0	42.1	41.3
	8443	45.8	45.5	40.8	41.3	41.4	40.9
	8433	45.2	43.9	39.5	40.4	40.2	39.5
Binary	8884	47.8		42.9		43.7	
	8444	46.7		41.5		42.5	
	4443	46.3	46.2	40.8	42.1	42.3	41.6
	4333	46.0		39.4		42.0	
	8333	43.7		38.9		39.4	
	8883	45.9		41.1		42.4	
Ternary	89	46.1	45.1	40.8	41.7	42.2	40.9
	789	45.8		40.2		41.8	
	613	45.2	45.4		41.0	41.1	40.4
	341	46.5	44.7		41.2	42.2	40.8
	135	45.2	44.4		40.3	40.5	39.9

*Darkened cells were additional aggregate blends that were not tested for source C.

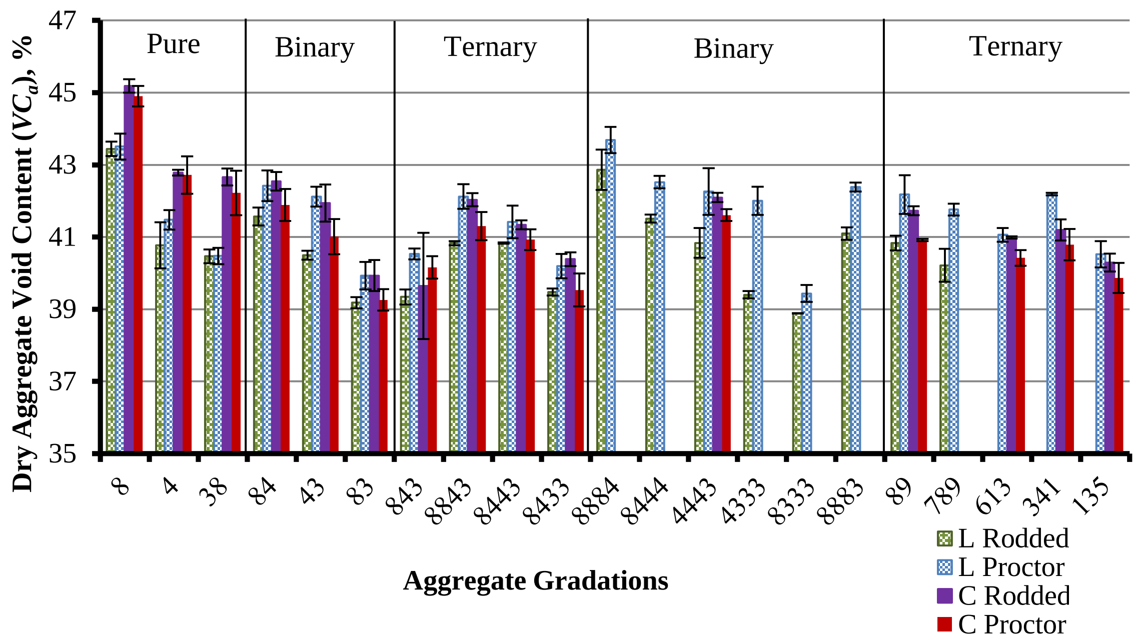

Figure 4.2 Comparison of dry Proctor and rodded void content for aggregate L and C. Missing columns were additional aggregate blends that were not tested for source C.

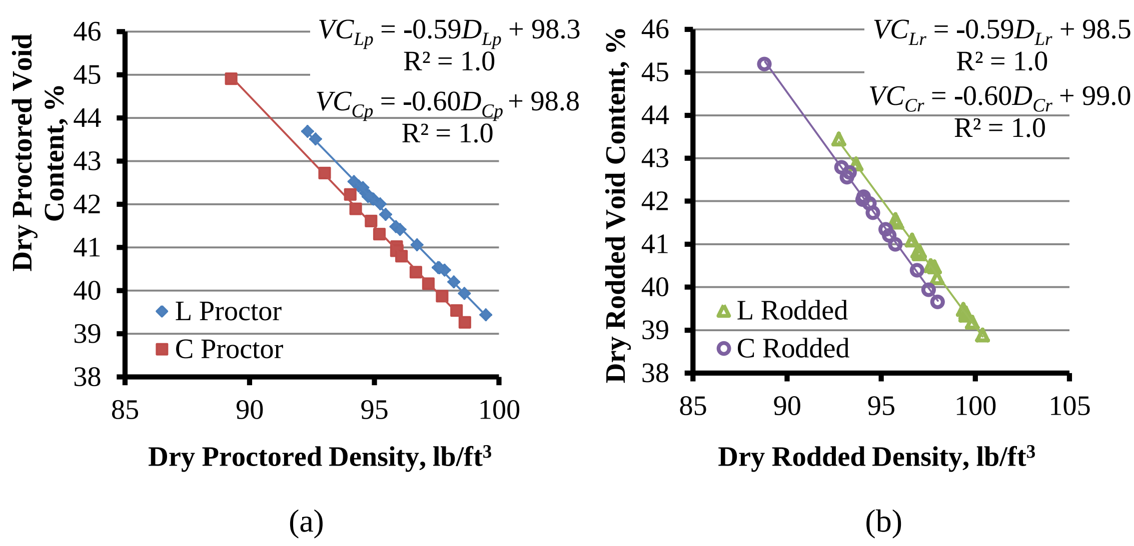

Figure 4.3 Relationships of (a) aggregate dry Proctor void content to density and (b) aggregate dry Rodded void content to density for both aggregate L and C.

Uniformity Coefficient

The uniformity coefficient, C_u, is a measure of the variation of the diameter of aggregate particles on the particle-size distribution curve corresponding to 60% finer (D_{60}) and 10% finer (D_{10}), and can be related to permeability (National Stone Association, 1993). It is the ratio of D_{60} to D_{10}. A gradation that has a C_u value lower than 4 is considered to be uniformly graded (National Stone Association, 1993). As shown in Table 4.6 all of gradations have C_u values lower than 4.

The relationship of dry rodded density and void content to uniformity coefficient of aggregate L and C is shown in Figure 4.4. The trend illustrated in the plot followed a general increase in density as C_u values increased. Aggregate C exhibited a stronger relationship between the C_u and the density and void content for the dry rodded method than aggregate L with R^2 values of 0.55 for density and 0.61 for void content. Based on the linear function, the uniformity coefficient can explain 55% of the variations in aggregate dry rodded density and 61% of the void content variation.

Figure 4.5 shows the relationship between dry Proctor density, D_p, and void content, VC_p, to uniformity coefficient, C_u. The relationship of D_p and VC_p for aggregate L compared with C_u did improve slightly with R^2 values of 0.46 as compared to 0.43. This is because the points for aggregate L are much closer to each other with fewer outliers and similar to values of aggregate C both for D_p and VC_p.

Table 4.6 Uniformity Coefficients

Aggregate Blend ID		Uniformity Coefficient (C_u)
Pure	8	1.42
Pure	4	1.41
Pure	38	1.15
Binary	84	2.01
Binary	43	1.84
Binary	83	3.70
Ternary	843	2.84
Ternary	8843	1.69
Ternary	8443	1.68
Ternary	8433	2.94
Binary	8884	1.59
Binary	8444	2.10
Binary	4443	1.59
Binary	4333	1.72
Binary	8333	3.46
Binary	8883	1.59
Ternary	89	2.12
Ternary	789	2.16
Ternary	613	1.72
Ternary	341	1.92
Ternary	135	2.59

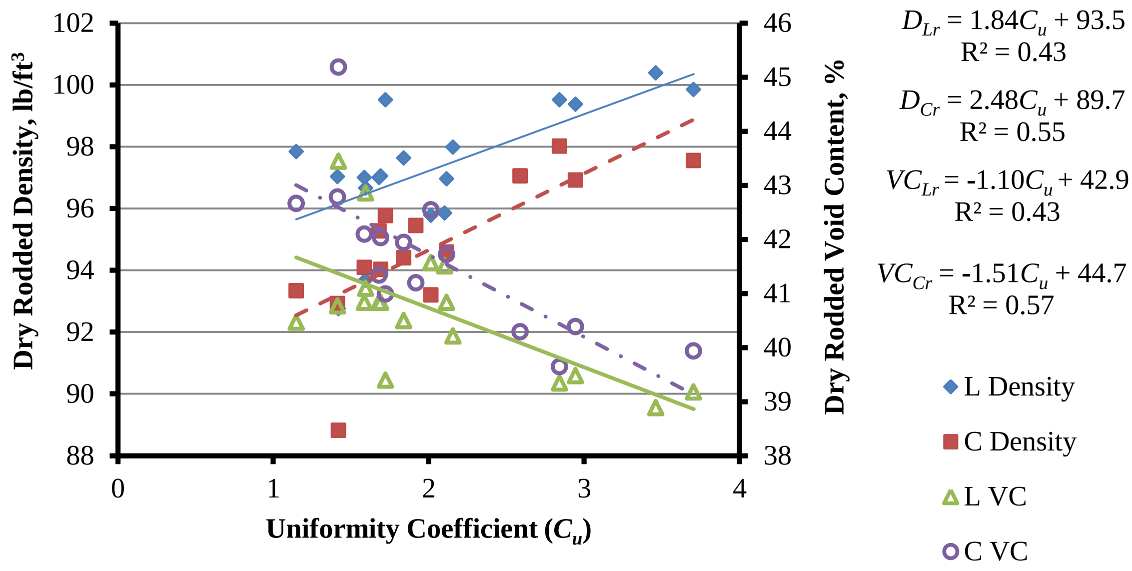

Figure 4.4 Relationship between the aggregate dry rodded density and void content to uniformity coefficient for L and C.

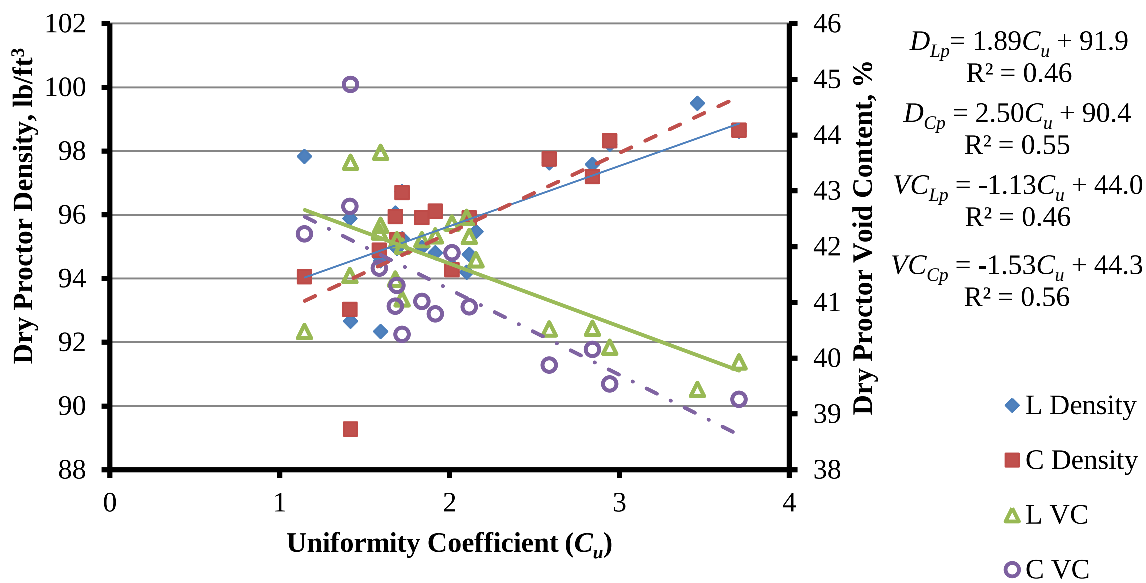

Figure 4.5 Relationship between the aggregate dry proctor density and void content to uniformity coefficient for L and C.

Aggregate Compaction Index (C_a)

To better understand the sensitivity of the different dry aggregate blends to compaction, both the loose and compacted densities were determined. The ratio of change in density to the number of blows applied was used to quantify the sensitivity of the aggregate gradation to compaction. Figure 4.6 illustrates an example comparing only single-sized aggregate densities at zero and 25 blows from a standard Proctor hammer. The linear curves for the other blends were not included in the plot for the sake of clarity. The slope of the linear curve between the two points of each aggregate blend was referred to as the compaction index. This aggregate compaction index (C_a), defines the change in density per blow from a standard Proctor hammer as expressed in equation 4.1:

$$C_a = \frac{\rho_n - \rho_0}{n} \qquad 4.1$$

where ρ_n and ρ_0 are the densities at n number of blows and zero blows, respectively. The reason for basing the compaction index equation off of the change in density instead of change in void content was because the density and void content is very closely related and density is easily obtained. The compaction indices for all the aggregate blends are presented in Table 4.7.

The pure fractions for aggregate L showed increasing sensitivity to compaction based on this order of #4, #38, and #8. For the pure blends, gradation 4 was more difficult to compact because of the wider range of aggregate sizes within the fraction as compared to other pure blends, (4.75 mm as compared to 2.39 mm for gradation 8 and 3 mm for 38). Gradation 8 for aggregate L had higher void content in the loose state;

therefore, it had more void spaces to fill, resulting in a higher compaction index. A different order was observed for aggregate C beginning with fraction 38, then 8 and finally 4. This higher compaction index for gradation 4 for aggregate C may be related to it having the lowest surface texture index (13.7), meaning less friction between the particles. There are also the effects of its flatter and more elongated shape and having a wider range of aggregate sizes that may allow the particles to reorient to fill gaps. For the binary blends made with aggregate L, the fifty-fifty blends had a lower C_a, compared to the seventy-five to twenty-five blends. The ternary blends for aggregate L had the highest C_a values when at least 60% of the mix was of larger aggregate fractions (4 or 38). The blends that exhibited higher loose densities but had lower compaction indices showed less susceptibility to compaction. For aggregate L, those blends were 83, 843 and 613 which had at least 30% of the blend being the boundary aggregate sizes. And for aggregate C, those blends were 341 and 8843 which appear to depend on the #8 fraction proportion being either 3 to 4 times the upper boundary fraction 38. Aggregate properties can have varying effects on the packing of aggregate gradations but the single-sized fraction behavior can be a useful guide.

Table 4.7 Compaction Index for Aggregate L and C

Aggregate Blend ID		**L** Compaction Index	**C** Compaction Index
		(C_a)	(C_a)
Pure	8	0.284	0.254
	4	0.234	0.289
	38	0.241	0.232
Binary	84	0.243	0.277
	43	0.248	0.299
	83	0.240	0.302
Ternary	843	0.258	0.298
	8843	0.252	0.223
	8443	0.287	0.299
	8433	0.328	0.282
Binary	8884	0.270	
	8444	0.275	
	4443	0.268	0.299
	4333	0.265	
	8333	0.280	
	8883	0.233	
Ternary	89	0.257	0.274
	789	0.262	
	613	0.269	0.324
	341	0.282	0.256
	135	0.307	0.294

*Darken cells were additional aggregate blends that were not tested for source C

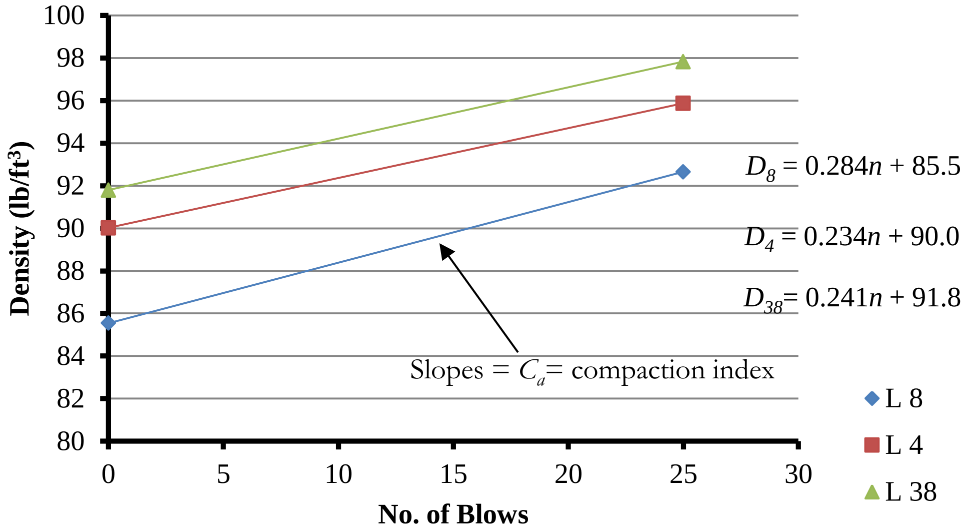

(a)

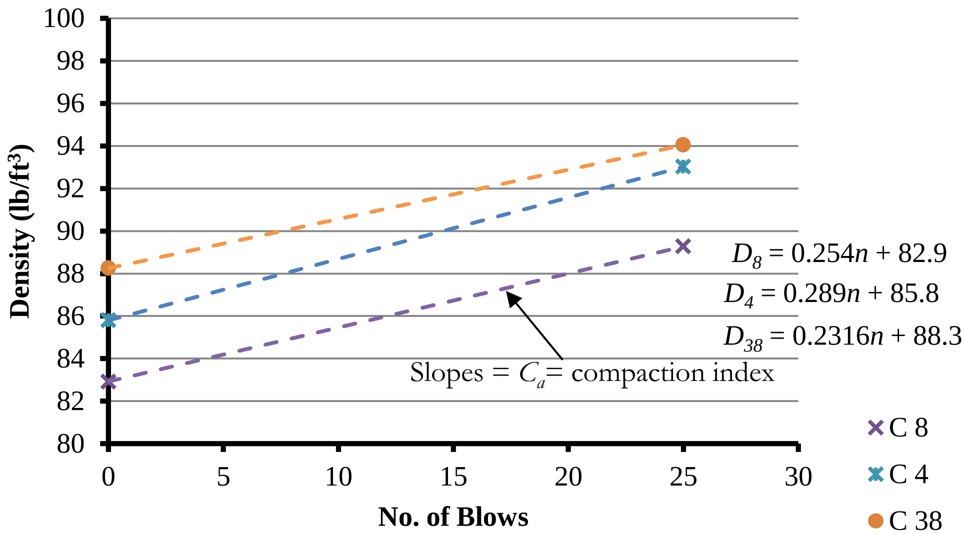

(b)

Figure 4.6 Example of aggregate compaction indices for (a) single-sized fractions of L and for (b) single-sized fractions of C. Equations follow the order of the legend.

California Bearing Ratio Penetration Stress

According to ASTM C1883, the CBR penetration stress test, *PS*, was used to determine the load-bearing capacity of a base material for pavements. It involved the penetration of a piston into the aggregate sample. Table 4.8 presents the penetration stresses at 0.2 in. into the aggregate samples along with the connecting letters report for the test for Least Significant Difference at a 95% level of significance comparing aggregate L and C.

Table 4.8 CBR Penetration Stress for Gradations of Aggregate L and C

Aggregate Gradation ID	**L** Penetration Stress		**C** Penetration Stress	
	psi	Significant Difference	psi	Significant Difference
8	98	i	201	efgh
4	160	ghi	264	cde
38	236	cdef	383	a
84	177	fgh	239	cdef
43	234	cdef	376	a
83	162	ghi	222	defg
843	159	ghi	251	cde
8843	153	hi	264	cde
8443	204	efgh	274	cd
8433	178	fgh	299	bc
4443			350	ab
89	177	fgh	227	defg
789	215	defgh		
613	162	ghi	214	defgh
341	215	defgh	258	cde
135	161	ghi	258	cdefgh

*Darkened cells were additional aggregate blends that were not tested for source C.

A comparison of the penetration stresses at 0.2 in. for aggregate L and C are illustrated in Figure 4.7. All gradations for aggregate C had higher penetration stresses compared to aggregate L. The highest penetration stress for aggregate L came from the 38 blend with blends 84, 8433 and 89 stresses being near to the average and the #8 blend having the lowest stress. The highest and lowest penetration stresses for aggregate C also came from the 38 and 8 blends, respectively but the 8443 blend generated the average stress (Table 4.8). For both aggregate sources, the penetration stress for the single-sized fractions increased as aggregate size increased. The binary and ternary blends of aggregate L had penetration stresses that typically increased as the proportion of mid-size aggregate (4) increased. For aggregate C, the penetration stress of the binary and ternary blends typically increased as the proportion of mid-size aggregate (4) in combination with larger aggregate sizes (38) increased. Greater variation was observed in the stress values for aggregate C than aggregate L gradations which could be linked to the difference in aggregate shape.

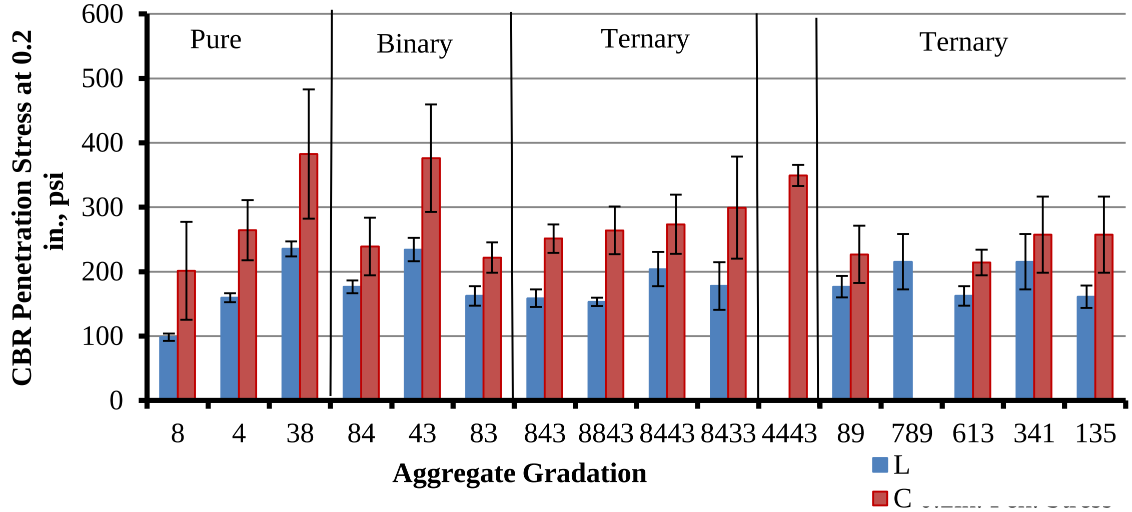

Figure 4.7 Comparison of the CBR Penetration Stresses at 0.2 in. for blends of aggregate L and C. Gradation 4443 is a binary blend.

<u>Pervious Concrete Properties</u>

This section examines the properties of the pervious concrete pavement mixtures prepared from aggregate sources L and C. The volumetric and performance parameters tested included Unit Weight, Compaction Index, Effective Porosity, Permeability, Compressive Strength, Split Tensile Strength and Abrasion Loss. From these parameters relationships were examined between the aggregate and pervious concrete properties.

Paste Content

As a means of quality control, the paste content in the Portland cement pervious concrete (PCPC) mixtures was verified to that of the designed paste content. This test involved a process of removing the paste from a sample of the pervious concrete mixture by washing. The paste contents of the different pervious concrete mixtures are shown in Table 4.9. Figure 4.8 illustrates a comparison of the measured paste content to the designed for source L and C. The designed paste content for the PCPC mixtures made with aggregate L was constant at 22.3% by mass and 23.8% for mixtures made from aggregate C. The measured values ranged from 20.2% (mix 4) to 21.8% (mix 8843) with an average value of 21.0% for aggregate L mixtures. PCPC mixtures made from aggregate C had paste contents that ranged from 22.2% (mix 43) to 23.7% (mixes 83 and 8433) with an average value of 23.2%. The maximum percentage difference from the designed paste content was approximately 9% for PCPC mixtures from aggregate L and for aggregate C mixtures about 7%. Based on the results, a likely tolerance level for quality control purposes could be ±10% by mass of the designed paste content.

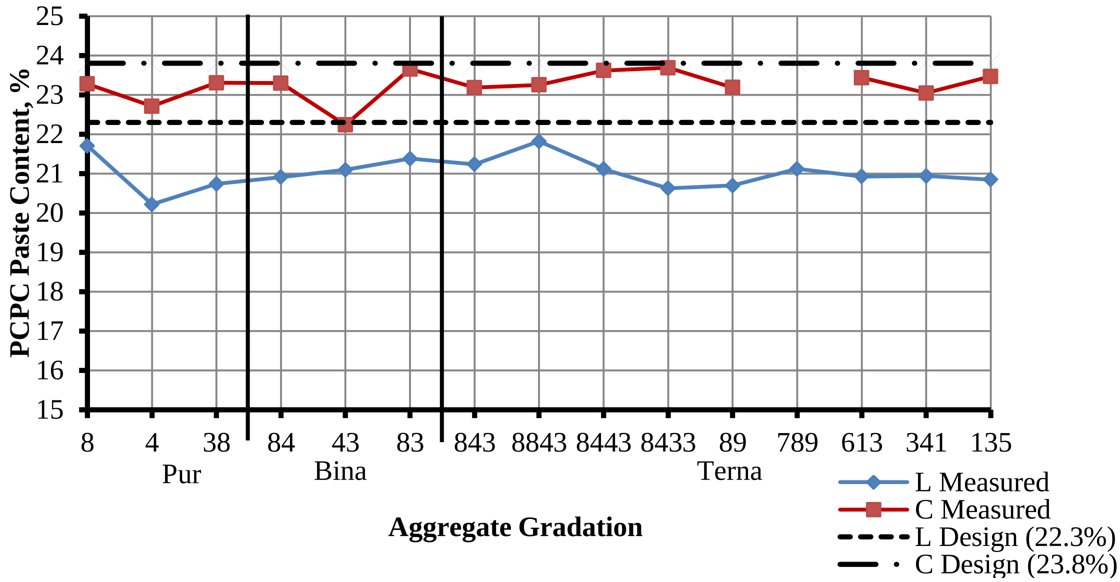

Figure 4.8 Comparison of the designed to the measured paste content of the pervious concrete mixtures for sources L and C. Missing points were additional aggregate blends that were not tested for source C.

Table 4.9 Paste Content for Source L and C

Aggregate Gradation ID		**L** Paste Content	**C** Paste Content
		(*pc*) %	(*pc*) %
Pure	8	21.7	23.3
	4	20.2	22.7
	38	20.7	23.3
Binary	84	20.9	23.3
	43	21.1	22.2
	83	21.4	23.7
Ternary	843	21.2	23.2
	8843	21.8	23.3
	8443	21.1	23.6
	8433	20.6	23.7
	89	20.7	23.2
	789	21.1	
	613	20.9	23.4
	341	20.9	23.0
	135	20.8	23.5

*Darkened cells were additional aggregate blends that were not tested for source C.

Unit Weight

The unit weight test is primarily used in the field as a quality control measure for pervious concrete. A good level of tolerance for density is ± 5% or ± 5 lb/ft^3 (80 kg/m^3) of the design density (Tennis et al, 2004). The standard test for unit weight of pervious concrete is ASTM C1688. Along with this test, was an alternative unit weight testing procedure (in Chapter 3) which followed the compaction process performed in making the pervious concrete samples. For the ASTM C1688 method, the specimen receives 20 blows of the Proctor hammer for each of two lifts, but for the alternative method, 25 blows were applied at one lift (height = 6 in.). Tables 4.10 and 4.11 present the pervious concrete mixture unit weights in the loose state, for the ASTM C1688 method, and for the alternative method, with the 95% level of significant differences denoted by a lettering system for aggregate L and C, respectively. Figure 4.9 shows a comparison of the ASTM C1688 unit weight test method with the alternative unit weight test method.

Table 4.10 Pervious Concrete Unit Weights Based on ASTM C1688, Loose State and Alternative Method for Aggregate L

Aggregate Gradation ID		L Loose Unit Weight	L ASTM C1688 Unit Weight	L Alternative Unit Weight (AUW)	L ASTM : AUW Significant Difference	
		lb/ft^3	lb/ft^3	lb/ft^3	ASTM	AUW
Pure	8	87	113	111	kl	lm
	4	88	114	110	jk	m
	38	87	116	112	ghij	lm
Binary	84	87	116	114	hij	jk
	43	86	117	115	fgh	ij
	83	89	121	120	bc	cd
Ternary	843	89	121	118	bc	def
	8843	94	118	117	def	fgh
	8443	97	119	117	cde	fgh
	8433	94	120	117	cde	fghi
	89	87	118	115	efg	hij
	789	88	118	116	def	ghij
	613	93	124	120	a	bcd
	341	96	122	118	abc	def
	135	94	122	118	ab	def

Gradations that did not share the same letters were significantly different.

The ASTM C1688 unit weight procedure gave higher density values compared with the alternative unit weight method (*AUW*) for both aggregate sources because more compaction energy was applied in the ASTM method. As anticipated, the single-sized fractions were on the lower end of the range of unit weights. For aggregate L, the ternary gradation 613 had the highest ASTM unit weight of 124 lb/ft^3 and gradations 83 and 613 had the highest alternative unit weight of 120 lb/ft^3. For aggregate C, gradation 83 had the highest ASTM unit weight value of 123 lb/ft^3 and gradation 8433 and 135 had the highest alternative unit weight value of 117 lb/ft^3.

For aggregate L, approximately 73% of the ASTM unit weight values were significantly different to the alternative unit weight. For aggregate C, all the ASTM unit weights were significantly different from the alternative method. A comparison of the alternative unit weight of the pervious concrete mixtures from source L with source C showed 43% of mixtures as not having significantly different unit weights even with the source C mixtures having a higher cement-aggregate (c/a) ratio of 0.25 as compared to the L mixtures with a c/a ratio of 0.23. The single-sized mixtures from source L tested by the alternative unit weight method did not have significantly different unit weights, but source C single-sized #8 mixture was significantly different from the 4 and 38 mixtures. The unit weight of the pervious concrete mixtures increased with gradations that had boundary aggregate sizes (#8 and #38). It is likely that the cement paste in the pervious concrete mixtures made changes in the arrangement of the aggregate particles as it filled in portions of the aggregate contact areas and the voids in the matrix, but the trend of unit weight increasing with increasing aggregate size was still evident. Aggregate C pervious concrete mixtures had lower unit weights compared to aggregate L, which was consistent with its lower aggregate densities, and suggested that it would require more compaction energy to overcome surface friction to reach the desired unit weight.

Table 4.11 Pervious Concrete Unit Weights Based on ASTM C1688, Loose State and Alternative Method for Aggregate C

Aggregate Gradation ID		**C** Loose Unit Weight	**C** ASTM C1688 Unit Weight	**C** Alternative Unit Weight (*AUW*)	**C** *ASTM* : *AUW* Significant Difference	
		lb/ft^3	lb/ft^3	lb/ft^3	ASTM	AUW
Pure	8	88	114	108	jkl	o
	4	87	114	110	ij	n
	38	88	115	111	hij	mn
Binary	84	88	117	112	def	kl
	43	93	119	115	cd	ghi
	83	90	123	116	a	fg
Ternary	843	89	120	115	b	hij
	8843	89	118	112	de	lm
	8443	88	118	114	de	ijk
	8433	90	122	117	ab	efg
	89	88	117	112	def	l
	789					
	613	91	120	116	bc	fgh
	341	88	118	114	de	hij
	135	90	121	117	b	def

Gradations that did not share the same letters were significantly different.
Darkened cells were additional aggregate blends that were not tested for source C.

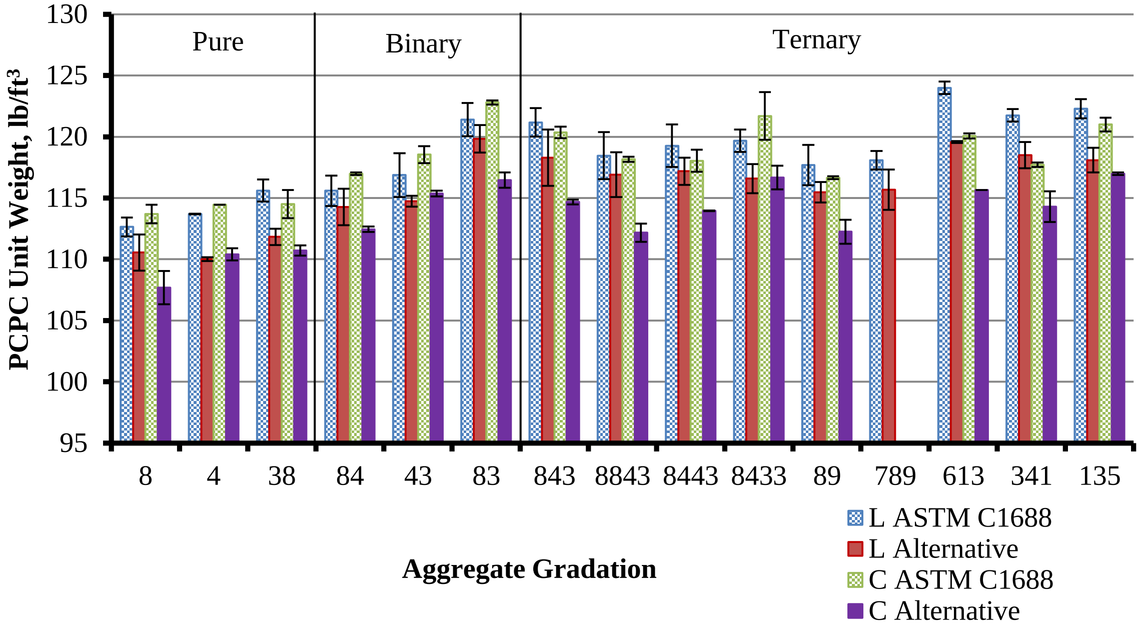

Figure 4.9 Comparison of the ASTM C1688 unit weights to the alternate unit weight method for aggregate sources L and C. Missing columns were additional aggregate blends that were not tested for source C.

Pervious Concrete Compaction Index (C_c)

Similar to the aggregate compaction index, C_a, the pervious concrete compaction index, C_c, was determined by measuring both the loose and compacted unit weights of the pervious concrete mixtures and calculated using equation 4.2.

$$C_c = \frac{\gamma_n - \gamma_0}{n}$$

4.2

where γ_n and γ_0 are the unit weights of the pervious concrete mixtures after n = 25 blows and the uncompacted condition, respectively. The compaction indices for the pervious concrete mixtures of source L and C are listed in Table 4.12. Figure 4.10 shows the comparisons between the aggregate compaction indices and the pervious concrete compaction indices.

When PC compaction indices, C_c, are compared with the aggregate compaction indices, C_a, similar patterns are observed for the pure gradations where mix 4 appears to be the least sensitive (lowest compaction index). A comparison of the compaction indices of the aggregate blends to that of the pervious concrete mixtures (Figure 4.10) showed that the addition of cement paste changed the responses of the binary and ternary mixtures. For binary mixtures, the dry aggregate blend 83 had the lowest C_a value, but then it had the second highest C_c value for source L pervious concrete mixtures. For aggregate C mixtures, the higher C_a values gave high C_c values, showing less paste effects. The pervious concrete mixtures with higher proportions of the largest aggregate or an equal blend of all three sizes had higher compaction indices for sources L and C. The cohesive properties of the cement paste restricted the loose pervious concrete mixtures from self-settling but acted as a lubricant under compaction allowing greater changes in compaction of the specimens. The compaction indices for the pervious concrete mixtures from source L ranged from 3 to 5 times greater than those of the dry aggregate blends and for C mixtures 3 to 4 times greater, showing source L as more sensitive to compaction. This is expected since aggregate L has a lower average particle index of 11.6 and aggregate C has an average particle index of 14.1 giving evidence of a rougher aggregate generating higher surface friction for aggregate C.

Table 4.12 Pervious Concrete Compaction Index and PCPC Compaction Index-to-Aggregate Compaction Index Ratio for Source L and C

Aggregate Gradation ID		**L** Pervious Concrete Compaction Index	**C** Pervious Concrete Compaction Index	**L** C_c:C_a Ratio	**C** C_c:C_a Ratio
		(C_c)	(C_c)		
Pure	8	0.929	0.872	3	3
	4	0.885	0.932	4	3
	38	1.01	0.900	4	4
Binary	84	1.08	0.984	4	4
	43	1.16	0.890	5	3
	83	1.25	1.08	5	4
Ternary	843	1.18	1.04	5	3
	8843	0.900	0.924	4	4
	8443	0.825	1.02	3	3
	8433	0.908	1.06	3	4
	89	1.12	0.973	4	4
	789	1.12		4	
	613	1.06	0.982	4	3
	341	0.918	1.06	3	4
	135	0.965	1.09	3	4

*Darkened cells were additional aggregate blends that were not tested for source C.

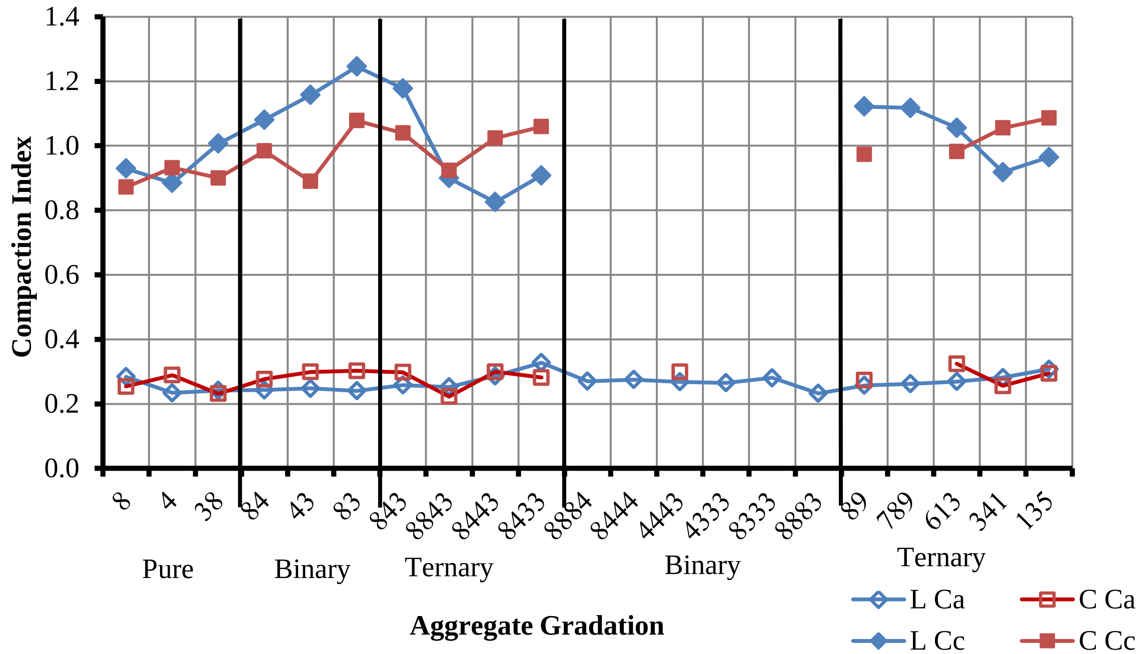

Figure 4.10 Comparison of pervious concrete compaction indices (C_c) to aggregate compaction indices (C_a) for sources L and C**.** Missing points were additional aggregate blends that were not tested for source C or used to make pervious concrete samples.

Permeability and Porosity

Source L Permeability and Effective Porosity

Permeability, *k*, and effective porosity, *P*, are two essential parameters that are typically closely related but are affected differently by mixture gradation. Table 4.13 and Figure 4.14 provide the permeability and porosity values for the pervious concrete mixtures for aggregate L, along with letters of significant differences within the categories. Since more of the pervious concrete samples had significantly different permeability values in contrast with the number of the significantly different porosity values, changes in mixture gradation are likely to have a greater influence on permeability than porosity. The single-sized mixture gradations along with mix 43 and mix 135 were in the upper range of permeability values while 83 and 843 which had higher compaction indices were in the lower range. Permeability increased as the proportion of larger aggregate size increased; this was observed with the pure and ternary blends. It was also observed that some gradations may have had a greater percentage of interconnected or larger pores resulting in higher permeability values but may have had a lower percentage of pores altogether, resulting in a similar porosity, (e.g., mix 4 as compared with mix 8). Blends that gave higher porosity values for source L mixtures were 43 and 89, partially matching with higher permeability, and blends with the lowest porosities were 613 and 341.

Table 4.13 Average Permeability and Porosity Results for Source L PCPC Mixtures

Aggregate Gradation ID		**L** Permeability		**L** Porosity		**L** Gravimetric Air Content (AC_G) %
		(k) in./hr.	Significant Difference	(P) %	Significant Difference	
Pure	8	1528	de	32.2	ab	30.2
	4	2047	b	31.9	bc	30.5
	38	2351	a	33.7	a	29.4
Binary	84	1400	fg	29.8	def	27.8
	43	1638	c	31.3	bcd	27.5
	83	957	k	27.1	gh	24.4
Ternary	843	948	k	28.4	fg	25.3
	8843	1199	ij	29.5	ef	26.2
	8443	1408	fg	29.0	ef	26.0
	8433	1468	ef	29.7	def	26.4
	89	1392	fg	30.4	cde	27.0
	789	1334	gh	29.3	ef	26.9
	613	1105	j	25.3	i	24.5
	341	1239	hi	25.5	hi	25.2
	135	1601	cd	28.4	fg	25.4

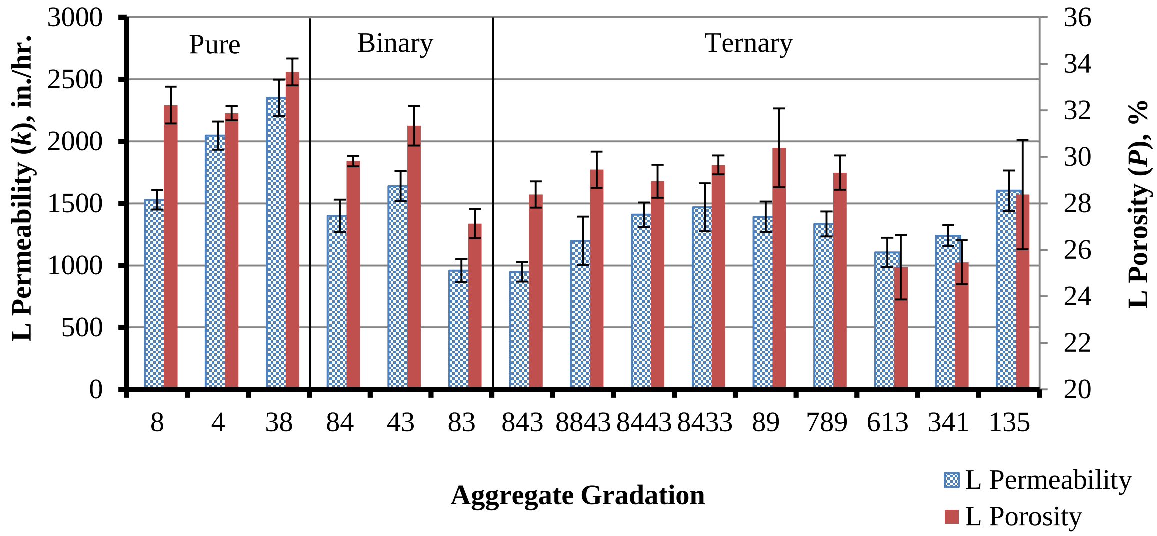

Figure 4.11 Permeability and porosity of aggregate L PCPC mixtures.

Source C Permeability and Porosity

The permeability and porosity values for the PCPC mixtures prepared from aggregate C, along with the lettering system for the 95% level of least significant differences are presented in Table 4.14. Similar to the source L mixture, the single-sized mixture gradations followed the trend of permeability increasing with the increase in aggregate size and porosity showing a slight drop at the central gradation or mix 4 (Figure 4.12). This drop was not sufficient to make the single-sized mixtures significantly different from each other which supports Kosmatka et al., 2002, who stated that uniform particles, no matter the size, has the same void content for a given volume and here the effect of uniform aggregate is observed on source C PCPC mixtures. The blends (binary and ternary) that had the highest permeability were mix 89 and 43 and the blend that had the lowest permeability was mix 83. The blends did not always follow the trend of increasing aggregate size resulting in increasing permeability. How well the smaller aggregate filled the spaces between the larger particles impacted the availability of interconnected pores. But porosity of the blends showed a pattern of decreasing as the proportion of smaller aggregate in the PCPC mixture decreased. On the other hand, the porosity did not necessarily increase with the increase of larger aggregate because, depending on the proportion of boundary aggregate size (8 and 38) in the mixture, the voids within fraction 38 were filled by fraction 8 leading to a lower porosity.

Table 4.14 Average Permeability and Porosity values for Source C PCPC Mixtures

Aggregate Gradation ID		**C** Permeability		**C** Porosity		**C** Gravimetric Air Content
		(k) in./hr.	Significant Difference	(P) %	Significant Difference	(AC_G)%
Pure	8	1385	ef	31.3	a	31.1
	4	1949	b	30.6	a	29.4
	38	2431	a	31.5	a	29.3
Binary	84	1339	efg	28.3	cde	28.1
	43	1613	c	27.5	de	26.3
	83	1052	i	27.1	e	25.6
Ternary	843	1300	fgh	27.6	de	26.7
	8843	1293	fgh	29.0	bc	28.3
	8443	1504	d	28.8	bcd	27.2
	8433	1279	gh	27.9	cde	25.5
	89	1669	c	30.1	ab	28.2
	789					
	613	1202	h	27.7	cde	26.1
	341	1413	de	28.4	cde	26.9
	135	1299	fgh	27.2	e	25.3

*Darkened cells were additional pervious concrete mixtures that were not tested for source C.

One method that was used to calculate the air content of the fresh pervious concrete mixtures is the gravimetric air content (ASTM C1688). Tables 4.13 and 4.14 present the theoretical air content of the PCPC mixtures. The specific gravities of each component in the mix are used in determining the air content. These air contents were lower than the hardened porosity for both L and C mixtures probably because of no account of water lost to evaporation or consumed in the hydration process, loss of paste to the mixer or loss of weakly attached pervious concrete particles.

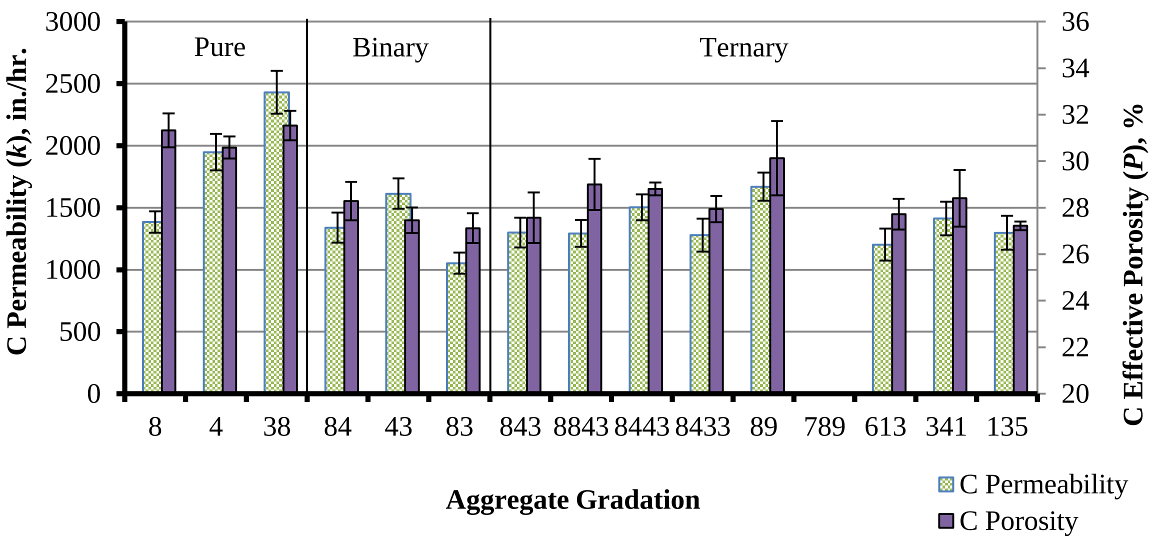

Figure 4.12 Comparison of permeability and porosity of aggregate C PCPC mixtures.

Compressive and Split Tensile Strength

Pervious concrete cores (3 in. × 6 in.), were tested for compressive strength and splitting tensile strength in accordance to ASTM C39 and ASTM C496, respectively (Figure 4.13). The values form these tests, compression and split tensile, are presented in Table 4.15 and 4.16 for PCPC mixtures L and C, respectively. A comparison of the average compressive and split tensile strengths is shown in Figure 4.14. Failure during compression testing for both mixtures L and C typically occurred in the lower portion of the specimens where there were larger voids. The method of compaction for this study was done to pattern certain aspects of field compaction, where compaction is typically done at the top surface of the pavement for a thickness of 6 in. (150 mm). For the compression test, the PCPC cores from source L with higher percentages of size 8 aggregate, showed more paste failure around the smaller aggregate, but more breakage of the larger aggregate which may have resulted because of higher surface area for the smaller aggregate and a need for a higher cement-aggregate ratio for proper coating. Source C cores under compression showed more breakage of the smaller aggregate that had a higher tendency to be either flat or elongated or both. Both sources L and C cores tested for split tensile strength showed little apparent differences in the way they failed.

Figure 4.13 Testing PCPC cores made from source C aggregate for compression strength (left) and split tensile strength (right).

From statistical analysis based on a 95% level of significant difference, most of the compressive strengths were not significantly different and the same applied to the split tensile results. The pure fractions PC mixtures gave lower compressive and split tensile strengths for both source L and C but not necessarily the lowest. The ternary blends typically were in the higher compressive and split tensile strength zone for source L. But for source C mixtures, the binary blends had higher compressive and split tensile strength than most ternary blends.

Table 4.15 Average Compressive and Split Tensile strengths of the PCPC Mixture from Aggregate L

Aggregate Gradation ID		**L** Compressive Strength		**L** Split Tensile Strength	
		(f'_c) psi	Significant Difference	(f'_c) psi	Significant Difference
Pure	8	705	d	149	d
	4	762	cd	178	cd
	38	701	d	162	d
Binary	84	825	cd	150	d
	43	887	bcd	221	bc
	83	986	abcd	246	ab
Ternary	843	924	bcd	237	ab
	8843	1122	ab	256	ab
	8443	1142	ab	288	a
	8433	852	bcd	254	ab
	89	877	bcd	245	ab
	789	853	bcd	245	ab
	613	1134	ab	253	ab
	341	1244	a	249	ab
	135	1021	abc	256	ab

Although source L mixture 341 had the highest average compressive strength of 1244 psi (9 MPa), it did not have the highest split tensile strength, it was mix 8843 with 288 psi (2 MPa). But for source C mixtures, blend 43 had both the highest compressive and split tensile strength. The binary blends increased in strength with the increase of the average aggregate size for L mixtures. Ternary blends increased with increased proportions of the lower and mid-range aggregate sizes for the L mixtures. Mixture C pervious concrete samples increased in compressive strength with the increase in the proportion of the mid-size and the largest aggregate but then dropped off when the mid-size aggregate quantity was very low or absent. In most cases even with a higher cement-aggregate (c/a) ratio of 0.25 compared to the source L c/a of 0.23, the L pervious concrete mixtures had higher compressive and split tensile strengths. This is most likely a result of source C having a higher particle index, being rougher and more angular, and so would require more compaction energy to reach densities that were typical of aggregate L which was smoother and more rounded. During testing, failure of the source C specimens was observed in areas where there were higher levels of size 8 aggregate which were more likely to be "flat and elongated" as compared to the other sizes and also size 8 aggregate had the highest particle index which increased in blends that had higher levels of size 8 aggregate. This could be another likely reason for failure, higher frictional resistance.

Table 4.16 Average Compressive and Split Tensile strengths of the PCPC Mixture from Aggregate C

Aggregate Gradation ID		**C** Compressive Strength		**C** Split Tensile Strength	
		(f'_c) psi	Significant Difference	(f'_c) psi	Significant Difference
Pure	8	546	e	145	ef
	4	644	cde	179	bcdef
	38	633	cde	118	f
Binary	84	880	bc	218	abcd
	43	1131	a	255	a
	83	736	bcde	166	def
Ternary	843	785	bcde	215	abcd
	8843	735	bcde	171	cdef
	8443	842	bc	235	abc
	8433	704	bcde	243	ab
	89	903	ab	187	bcdef
	789				
	613	580	de	182	bcdef
	341	768	bcde	204	abcde
	135	820	bcd	226	abcd

*Darkened cells were additional pervious concrete mixtures that were not tested for source C.

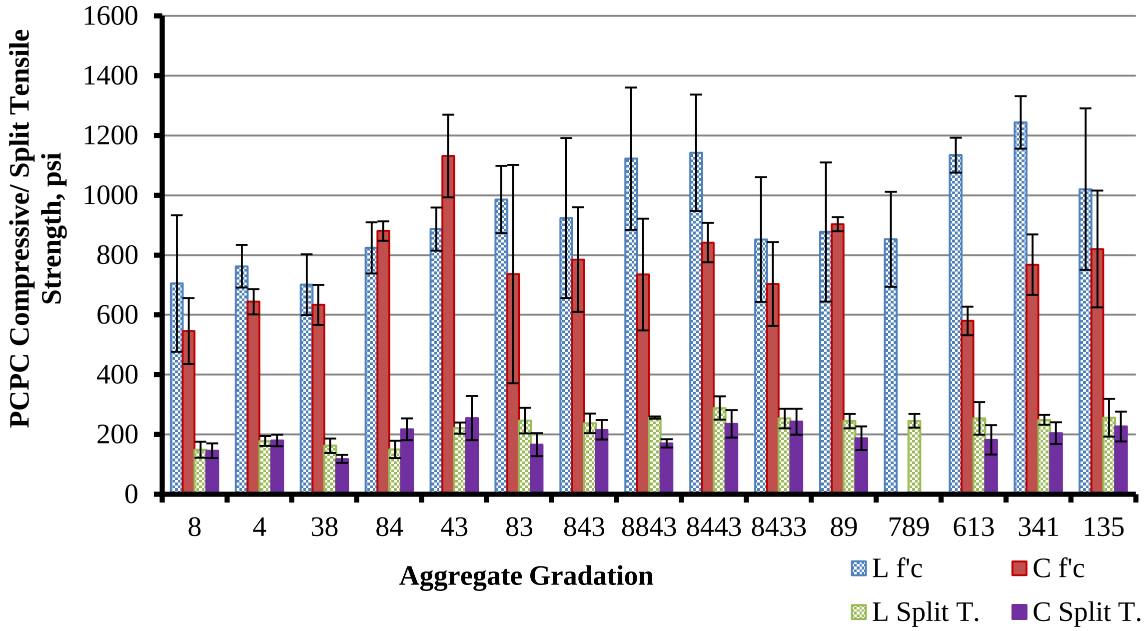

Figure 4.14 Comparison of average compressive and split tensile strengths for PCPC mixtures made from aggregate L and C. Missing columns were additional pervious concrete mixtures that were not tested for source C.

Abrasion Loss

The abrasion loss (*AL*) of the pervious concrete samples for source L and C are presented in Table 4.17. The comparison of abrasion loss for PCPC mixtures made from aggregate L and C are illustrated in Figure 4.15. The abrasion loss values of the single-size gradations were not significantly different from each other for source L samples but were significantly different for source C samples. The test results for source L mixtures showed that the highest abrasion loss occurred with blend 8 at 46% and the lowest occurred with blend 341 at 25%. Consequently, the higher the percentages of smaller aggregate in the mix, the higher the abrasion loss for source L. The reason for this may be linked to insufficient cement paste coating fraction 8 in the mixtures. Generally, source L pervious concrete mixtures decreased in abrasion loss as the blends moved from pure into ternary blends. Figure 4.16 displays from the top to the bottom, the PCPC specimens for aggregate L followed by specimens from aggregate C, all stacked in increasing size within gradation categories after the abrasion loss test.

The pervious concrete (PC) mixture from source C had higher abrasion loss in all cases except for blend 43 when compared with source L. The highest abrasion loss for the C mixtures occurred with pure fraction 38 at 72% and the lowest was blend 43 at 30%. For source C mixtures, the pure blends increased in abrasion loss as aggregate size increased but binary and ternary blends decreased in abrasion loss as the proportion of blend 8 decreased. For the pure blends, the voids in the PC samples with larger aggregate were likely larger than the voids in the smaller aggregate samples. Therefore, more support of neighboring aggregate led to lower abrasion loss for samples with smaller aggregate. But for the binary and ternary blends, the voids were likely reduced in size, so aggregate shape became critical. With the likelihood of “flat and elongated” properties of the aggregate increasing for source C as the aggregate size reduced, there is potentially a greater possibility of the aggregate 8 fraction being flatter since that was the pattern between the 4 and 38 aggregate blends. This may have caused earlier failure in the smaller aggregate than failure caused by void size.

Table 4.17 Abrasion loss of pervious concrete samples prepared from aggregate L and C.

Aggregate Gradation ID		**L** Abrasion Loss		**C** Abrasion Loss	
		(*AL*) %	Significant Difference	(*AL*) %	Significant Difference
Pure	8	45.6	a	46.7	c
	4	41.1	ab	56.6	b
	38	40.8	ab	71.9	a
Binary	84	37.6	bc	48.0	c
	43	33.3	cd	30.1	d
	83	33.9	cd	55.2	b
Ternary	843	30.2	def	47.1	c
	8843	30.3	def	42.2	c
	8443	32.5	cde	32.3	d
	8433	26.3	f	45.7	c
	89	29.6	def	46.5	c
	789	32.5	cde		
	613	30.7	def	45.4	c
	341	25.3	f	47.6	c
	135	27.1	ef	45.5	c

*Darkened cells were additional pervious concrete mixtures that were not tested for source C.

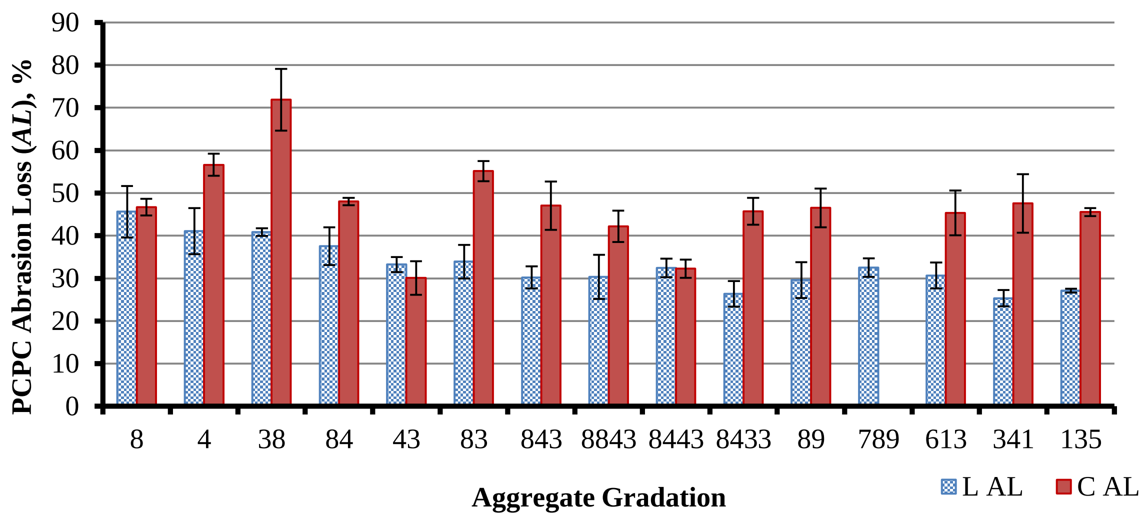

Figure 4.15 Comparison of abrasion resistance for pervious concrete sample from aggregate L.

Figure 4.16 PCPC specimens after the abrasion mass loss test for aggregate L and C.

Dry Aggregate and Pervious Concrete Relationships

One of the goals of this study was to develop a methodology that links the aggregate and gradation properties to the volumetric and performance properties of the pervious concrete mixtures for prediction and optimization purposes. To reach this goal, the void content of the different aggregate blends was correlated to unit weight, permeability, porosity, and strength parameters of the pervious concrete mixtures.

Dry Aggregate Void Content

Aggregate Void Content to PCPC Unit Weight

Figure 4.17 shows the linear relationships of the pervious concrete unit weight to the void content of the aggregate matrix compacted by proctor and rodding and with equations listed in the same order as the legend. Since the aggregate void content and density is strongly related, void content was chosen as a property that would eliminate the effects of properties such as bulk specific gravity that impacts unit weight.

The decrease in pervious concrete unit weight to the increase in aggregate void content is clearly shown in Figure 4.17. The strength of the relationships between the PCPC unit weight and the aggregate void content was much stronger for aggregate C than for aggregate L. The higher friction between source C aggregate particles may have kept the aggregate matrix in place more while being compacted. The dry proctor void content relationship for aggregate L was not as strong as the other relationships obtained. This may be linked to lower aggregate friction levels causing excessive movement of the aggregate during compaction. From the linear regression, the slope indicates that for every 1% increase in aggregate void content, the pervious concrete unit weight decreased by 1.5 to 2 lb/ft^3. The equations in Figure 4.17 represent the relationships of PCPC unit weights to aggregate void content, where γ_C, γ_L, VC_p, and VC_r are the unit weights of PC mixtures made from source C and L and the aggregate void content compacted by proctor and rodding, respectively.

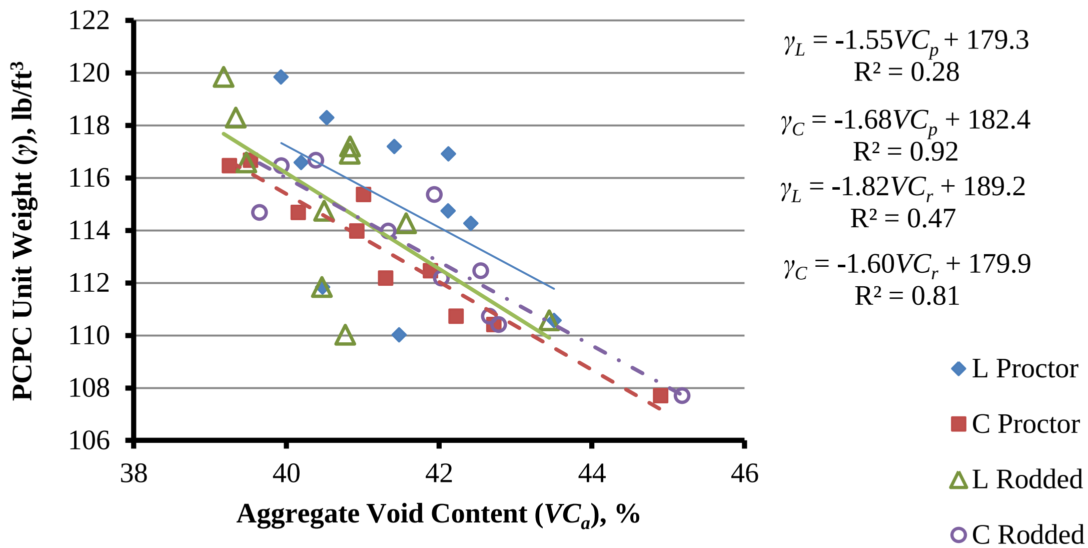

Figure 4.17 Relationship between PCPC unit weight and dry aggregate void content compacted by proctor and rodding from aggregate L and C.

Aggregate Void Content to PCPC Gravimetric Air Content, Porosity, and Permeability

The pervious concrete gravimetric air content as a function of the aggregate void content showed stronger correlations for both aggregate sources and compaction methods (Figure 4.18). As expected, the pervious concrete air content increased as aggregate void content increased. The equations in Figure 4.18 represent the relationships of PCPC gravimetric air content to aggregate void content, where AC_C and AC_L are the gravimetric air content for mixtures prepared with aggregate C and L, respectively.

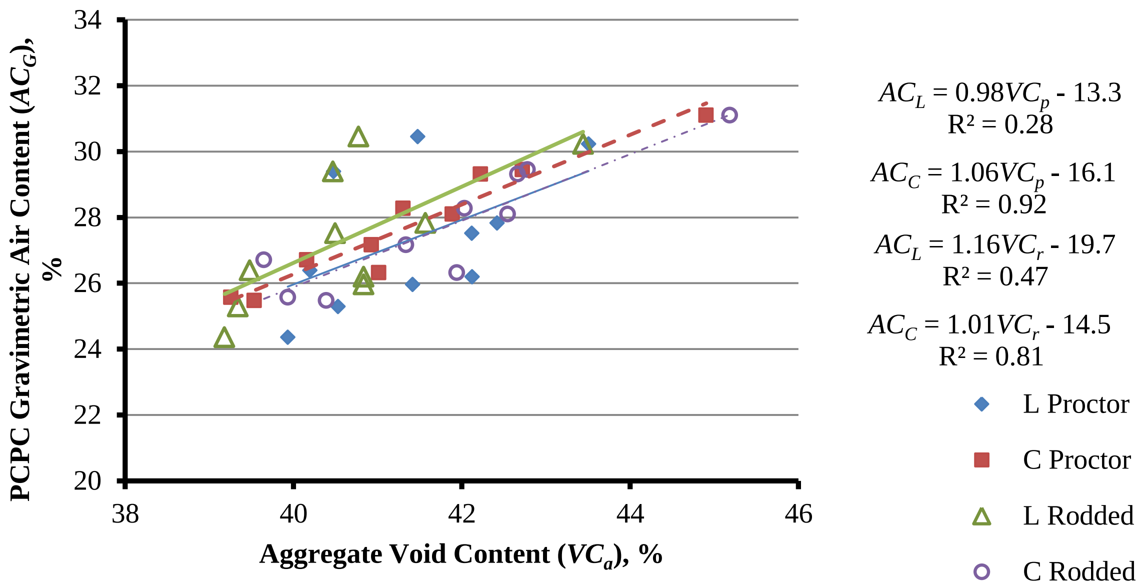

Figure 4.18 Relationship between PCPC gravimetric air content and the dry aggregate void content of aggregate L and C.

The relationship between the average porosity of the pervious concrete mixtures to the corresponding dry aggregate void content is shown in Figure 4.19. Increasing aggregate void content showed an increase in effective porosity of the mixtures. The equations for the relationships between PCPC effective porosity and the aggregate void content was shown in Figure 4.19, where P_C was the average effective porosity of the pervious concrete mixtures from source C. The functions showed trends that gave different predictions for the effective porosity values but source C came closer to what should theoretically happen, both methods, Proctor and rodding, should give the similar predictions since only one method of compaction was done on the PCPC mixtures.

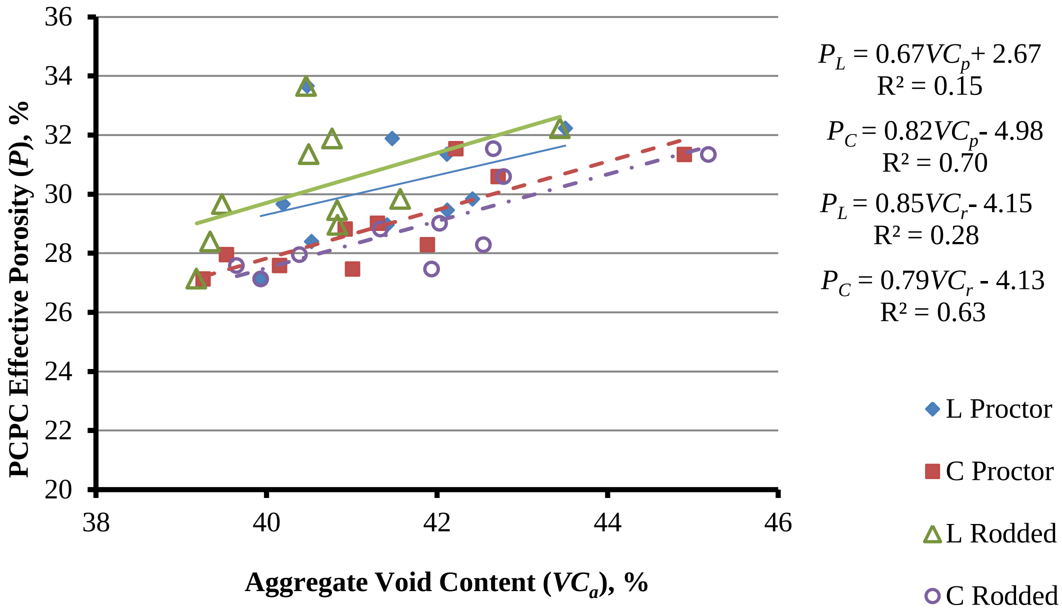

Figure 4.19 Relationship between PCPC effective porosity and the dry aggregate void content of aggregate L and C.

The relationships between the PC permeability and the aggregate void content compacted by Proctor or rodding are presented in Figure 4.20. The expected trend of increasing permeability with increasing aggregate void content was observed. But the permeability and aggregate void content relationships were not strong. Figure 4.20 shows the equations for the relationships between PCPC permeability and aggregate void content.

.

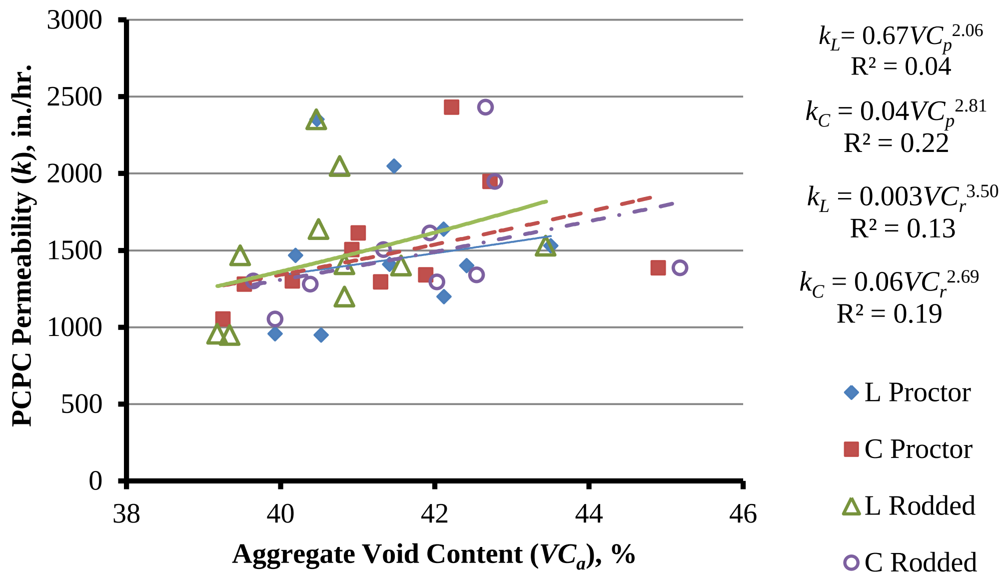

Figure 4.20 Relationship between dry aggregate void content and the permeability of pervious concrete mixtures for aggregate L and C.

Aggregate Void Content to PCPC Compressive Strength and Split Tensile Strength

The relationships between the pervious concrete compressive and split tensile strength to aggregate void content are presented in Figures 4.21 and 4.22. Stronger correlations were observed for the split tensile strength test as compared to the compressive strength relationships, but the functions generally did not adequately explain variations between the strength and the void content. Figure 4.21 shows the equations for the relationships between compressive strength and aggregate void content. Figure 4.22 shows the equations for the relationships between the split tensile strength and aggregate void content. Both the compressive and split tensile strengths showed a decrease in strength as the aggrgegate void content increased. The split tensile as a function of aggregate void content produced a steep slope compared to the compressive strength relationship, showing void content as having greater effect on split tensile strength.

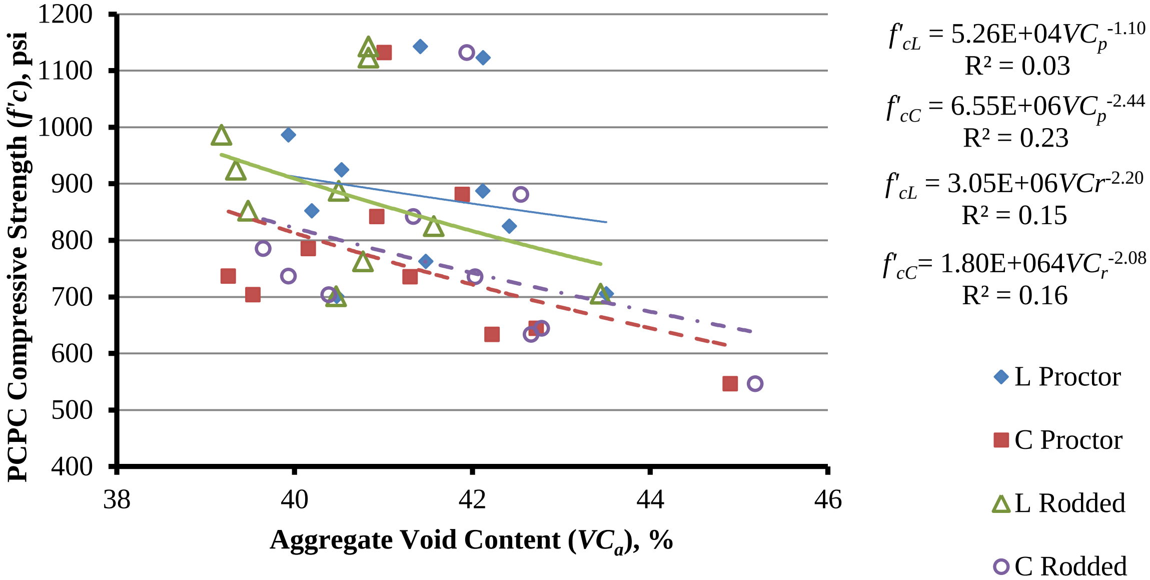

Figure 4.21 Relationship between PCPC compressive strength and the dry aggregate void content of aggregate L and C.

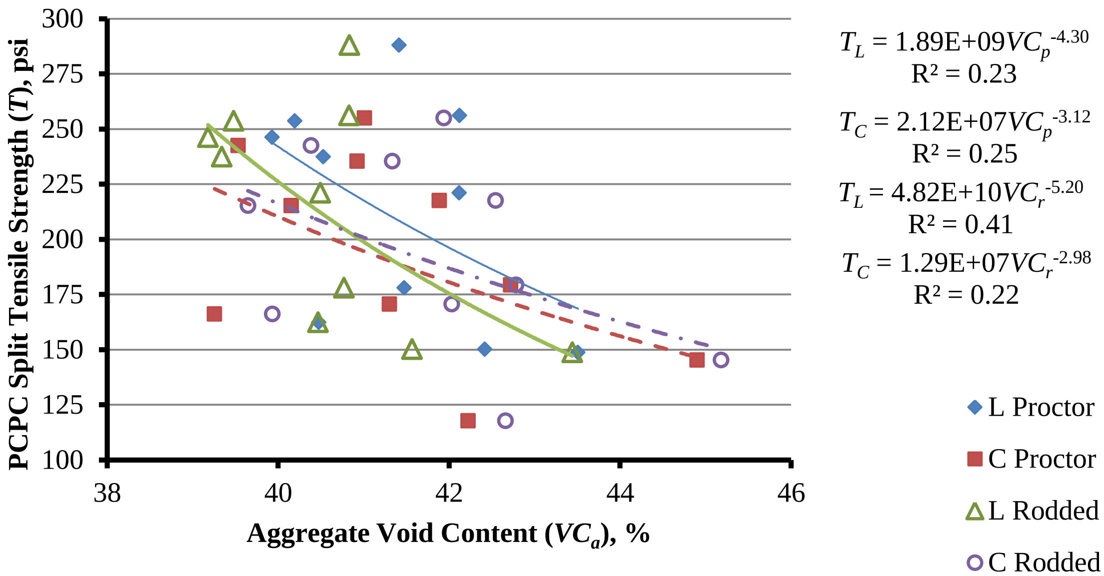

Figure 4.22 Relationship between PCPC split tensile strength and the dry aggregate void content of aggregate L and C.

Aggregate Void Content to PCPC Abrasion Loss

The pervious concrete abrasion loss, *AL*, to the aggregate void content, VC_a, relationship indicated an increase in VC_a led to an increase in *AL* (Figure 4.23). The void content function for rodded aggregate from source L explained the variability in abrasion loss better than the dry proctor void content. The linear functions showed that a 1% increase in aggregate void content results in approximately a 3% increase in abrasion loss as expressed by the equations in Figure 4.23, where AL_L is the abrasion loss for PCPC mixtures made from aggregate L and VC_r is the rodded aggregate voids content.

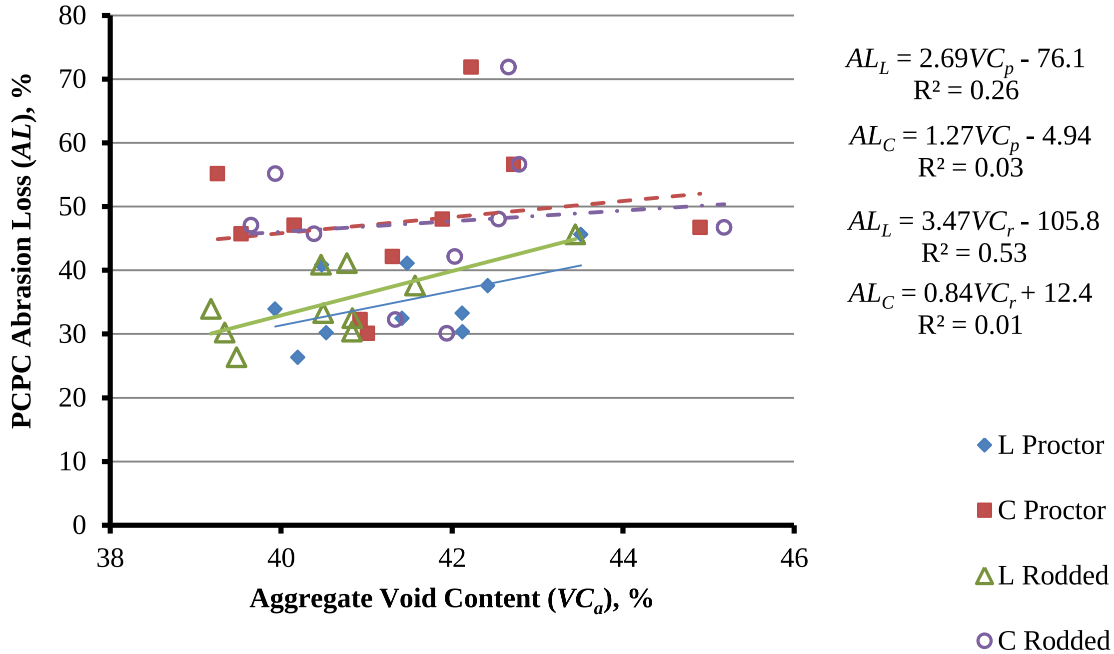

Figure 4.23 Relationship of the pervious concrete abrasion loss to the dry aggregate void content for aggregate L and C.

Uniformity Coefficient

The uniformity coefficient, C_u, is a numerical measure of the uniformity of the aggregate particles in the pervious concrete mixtures. It is calculated by the ratio D_{60} to D_{10}, obtained from the particle distribution curves of each aggregate gradation and listed in Table 4.1. The equations in the figures were listed in the same order as the legend.

Uniformity Coefficient and PCPC Unit Weight

The relationships between the aggregate uniformity coefficient, C_u, and the PCPC unit weight, γ, for aggregate source L and C mixtures are illustrated in Figure 4.24. The expected trend of unit weight increasing with increasing C_u values or with reducing uniformity was observed. Figure 4.24 shows the power functions for the relationships between the PCPC unit weight and the aggregate uniformity coefficient where γ_L and γ_C represent the pervious concrete unit weight for aggregate L and C, respectively. Source L pervious concrete mixtures had higher unit weights compared with source C mixtures. This was consistent with the dry density of source L aggregate generally having a higher density than source C.

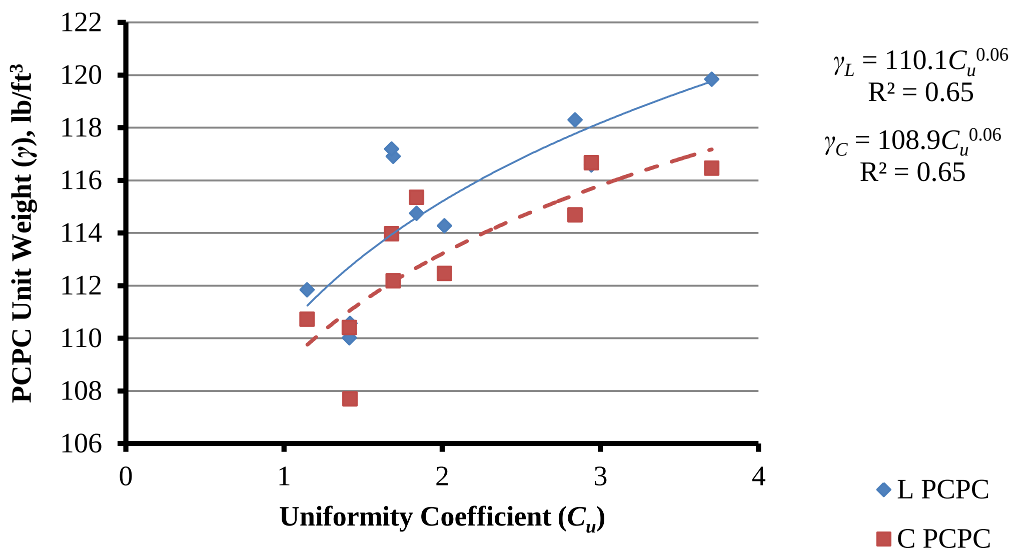

Figure 4.24 Relationships of PCPC unit weight and aggregate uniformity coefficient for aggregate sources L and C.

Uniformity Coefficient and Average Permeability

The relationships between the pervious concrete permeability, *k*, and the corresponding uniformity coefficient, C_u, values are shown in Figure 4.25. As the gradations became less uniform, the permeability decreased. Figure 4.25 shows the power functions that represent the relationship between the PCPC permeability and uniformity coefficient where k_L and k_C are the PCPC average permeability for source L and C mixtures, respectively. Between C_u values of 1 and 2, the permeability dropped by over 1100 in./hr. for source L mixtures and over 1000 in./hr. for source C mixtures. Thereafter, it was over 400 in./hr. for source L mixtures and just under 300 in./hr. for source C mixtures. The functions for both sources ran very close to each other, indicating that the differences in cement-aggregate ratios (c/a$_L$=0.23 and c/a$_C$=0.25) compensated for the difference in aggregate void content.

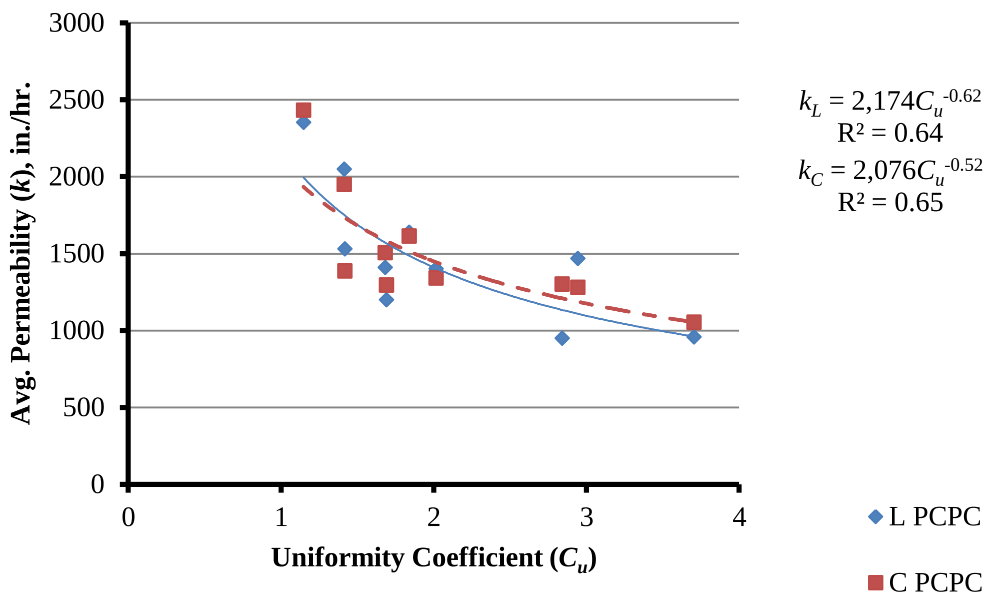

Figure 4.25 Relationship between PCPC average permeability and uniformity coefficient for aggregate L and C.

Uniformity Coefficient and Porosity

The effective porosity, *P*, to uniformity coefficient, C_u, relationship showed the typical trend of porosity decreasing as the C_u increased (Figure 4.26**)**. Uniformity coefficients between 1 and 2 generated steeper slopes reducing effective porosity in those blend at a higher rate compared to C_u values higher than 2. Figure 4.26 shows the equations that represent the power functions for effective porosity and uniformity coefficient, where P_L and P_C were the PCPC effective porosity for source L and C mixtures, respectively.

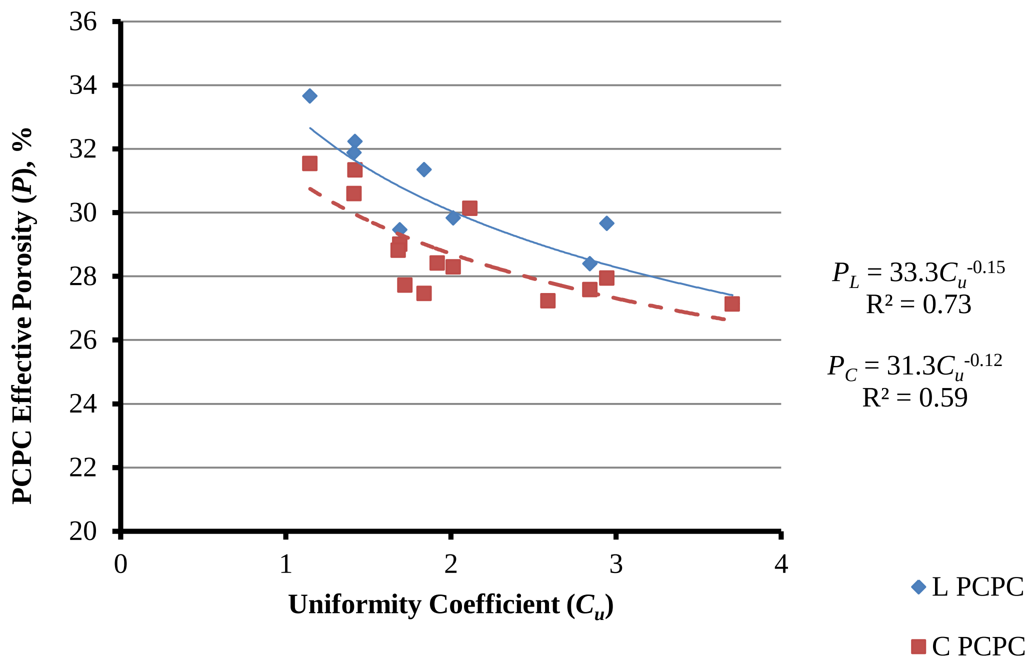

Figure 4.26 Relationship between effective porosity and uniformity coefficient for sources L and C.

Uniformity Coefficient, Compressive Strength and Split Tensile Strength

The relationships of compressive strength and split tensile strength to uniformity coefficient are shown in Figure 4.27 and 4.28, respectively. Both strength parameters gradually increased as the aggregate gradation became less uniform. But there was not a strong correlation evident for compressive strengths between the two parameters for both sources. Figure 4.27 shows the equations that represent the power functions for compressive strength and uniformity coefficient. The split tensile strengths showed a slight improvement in the relationships as variability of the results reduced. Figure 4.28 shows the equations that represent the power functions for split tensile strength and uniformity coefficient.

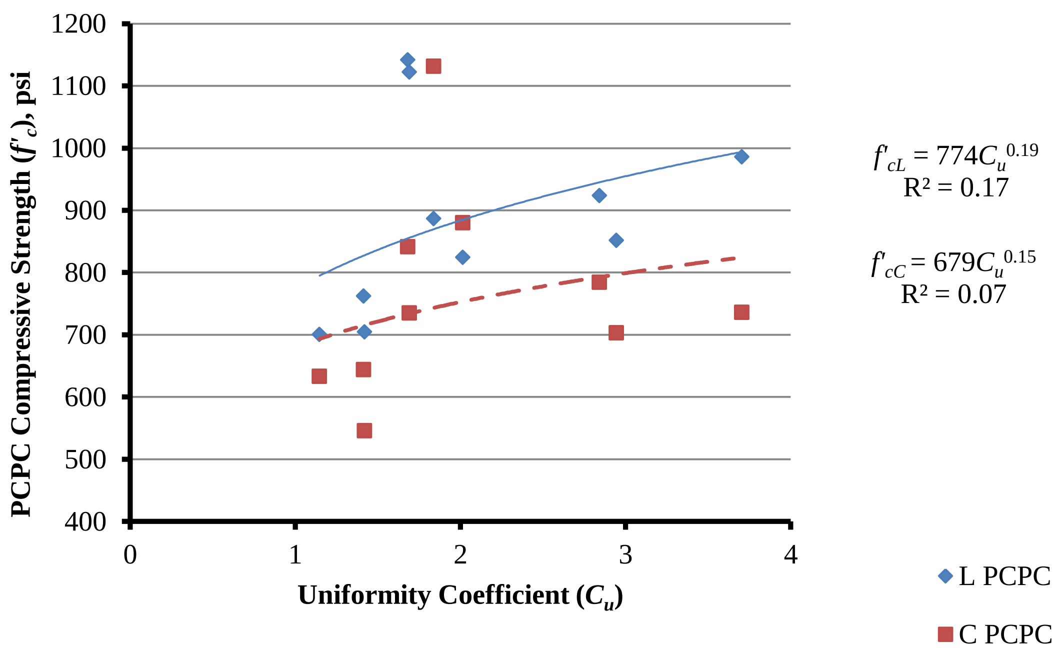

Figure 4.27 Relationship between compressive strength and uniformity coefficient for both source L and C mixtures.

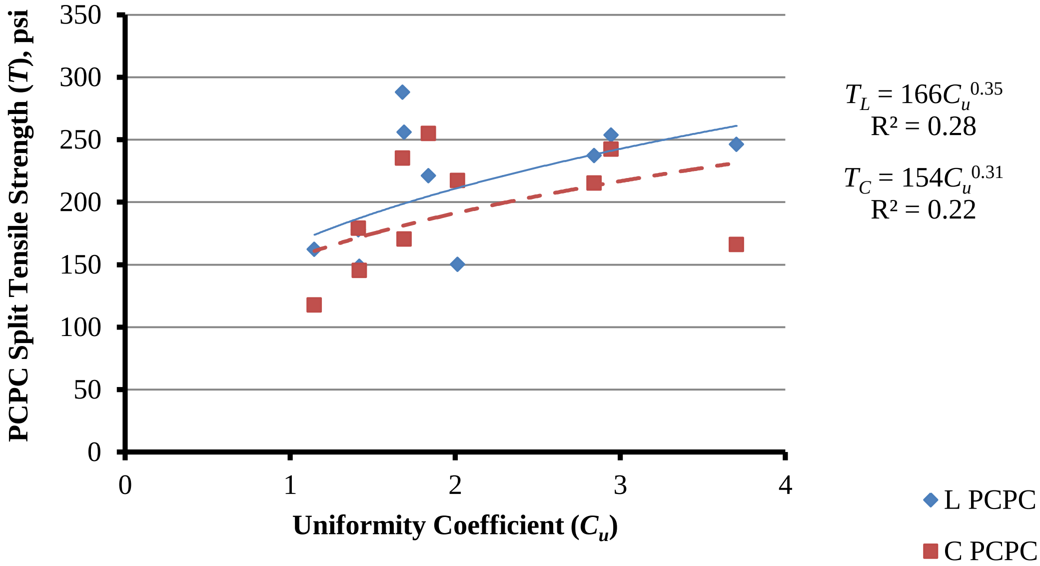

Figure 4.28 Relationship between split tensile strength and uniformity coefficient for source L and C mixtures.

Uniformity Coefficient and Abrasion Loss

The abrasion loss to uniformity coefficient relationship is shown in Figure 4.28. The functions showed some tendency towards abrasion loss being higher for gradations with a lower uniformity coefficient. The function for source L mixtures was able to better explain the variations in abrasion loss than the function for source C. Figure 4.29 shows the equations for the relationships between PCPC abrasion loss and the uniformity coefficient.

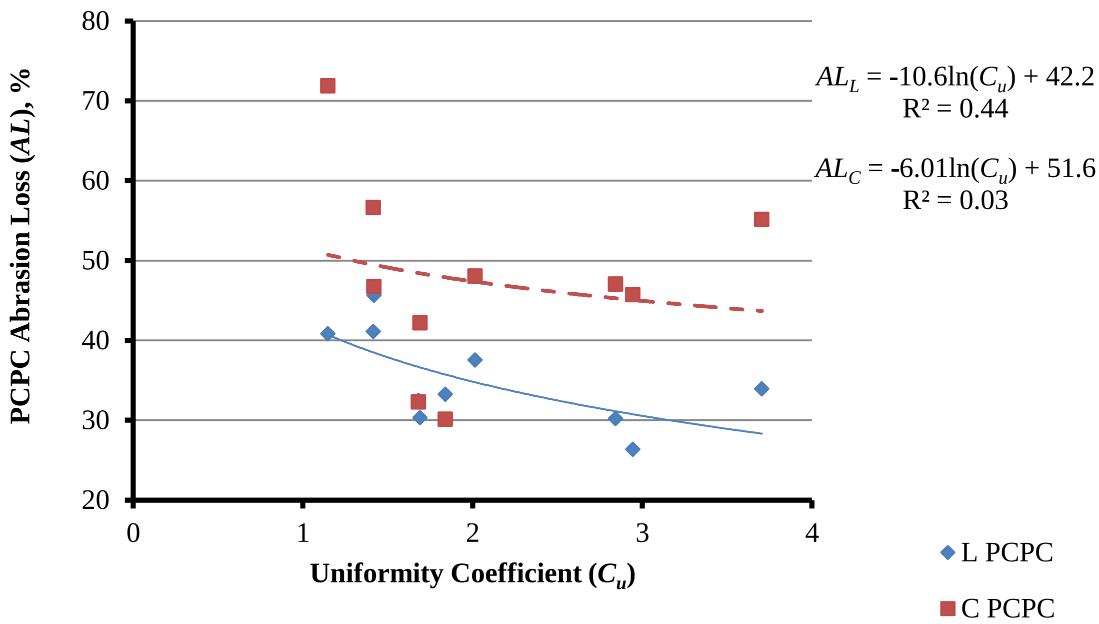

Figure 4.29 Relationship between abrasion loss and uniformity coefficient for sources L and C.

CBR Penetration Stress

The California Bearing Ratio, CBR, penetration stress, *PS*, was calculated at a penetration depth of 0.2 in. into the aggregate matrix. The only relationship between CBR penetration stress and any of the PCPC properties that gave a fair correlation was with permeability (Figure 4.30). As the penetration stress of the aggregate increased, the PCPC permeability increased. The larger aggregate had higher stress values that were likely linked to higher particle indices. The CBR penetration stress function for source C had a higher R^2 (0.45) than source L. Figure 4.30 shows the equations for the average permeability to the CBR penetration stress where k_L and k_C are the permeability for source L and C, respectively.

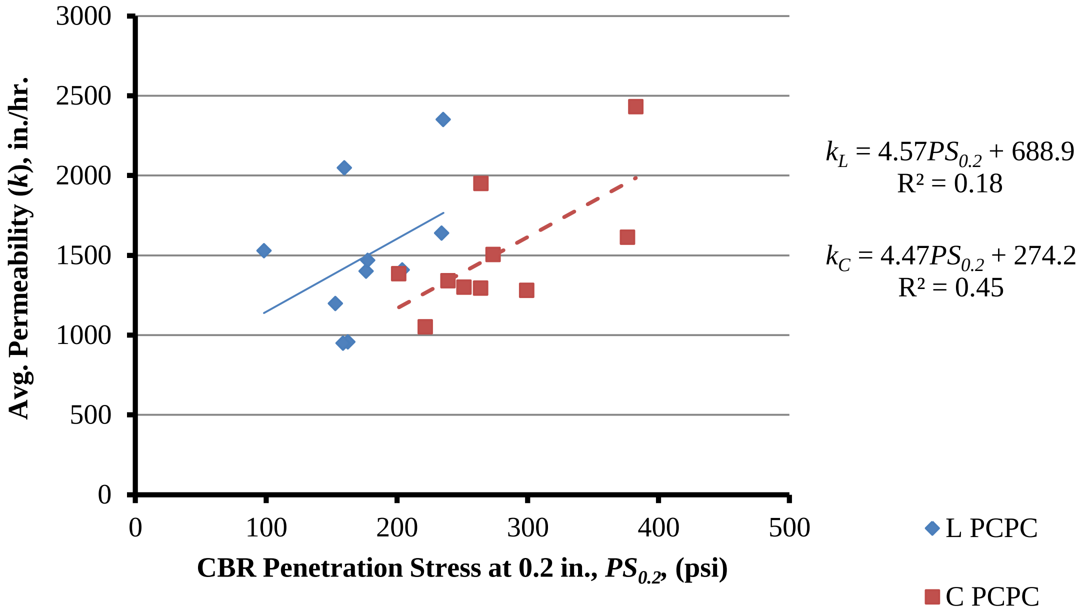

Figure 4.30 Relationship of PCPC permeability with CBR penetration stress at 0.2 in. for aggregate L and C.

Aggregate Compaction Index

The aggregate compaction index, C_a, showed fair relationships with only two (2) of the pervious concrete properties, porosity and split tensile strength of source C. The effects of the paste on the aggregate matrix were not only to fill some percentage of the voids but it also moves the aggregate apart leaving some elements to be examined further.

Aggregate Compaction Index and Effective Porosity

The relationship between the pervious concrete effective porosity and the aggregate compaction index, C_a, is shown in Figure 4.31. Source C mixture gave a fair correlation that showed a decrease in porosity with an increase in aggregate compaction index. These relationships showed some consistency with the general expectation that increased sensitivity of the aggregate to compaction could result in a decrease of PCPC effective porosity. Figure 4.31 shows the equations for the relationships between the effective porosity and aggregate compaction index.

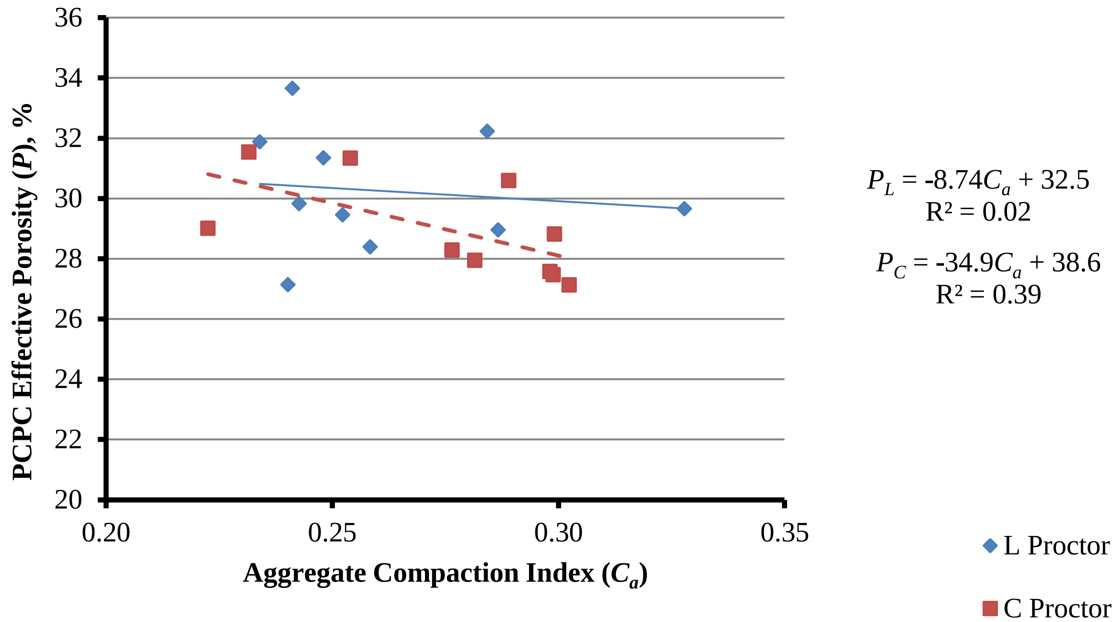

Figure 4.31 Relationship of PCPC effective porosity to the aggregate compaction index for L and C mixtures.

Aggregate Compaction Index and Split Tensile Strength

The relationship between the split tensile strength and aggregate compaction index for source C is shown in Figure 4.32. The split tensile strength increased as the aggregate compaction index increased. Figure 4.32 shows the equations for the relationships between the split tensile strength and aggregate compaction index, where T_C is the split tensile strength of source C mixtures.

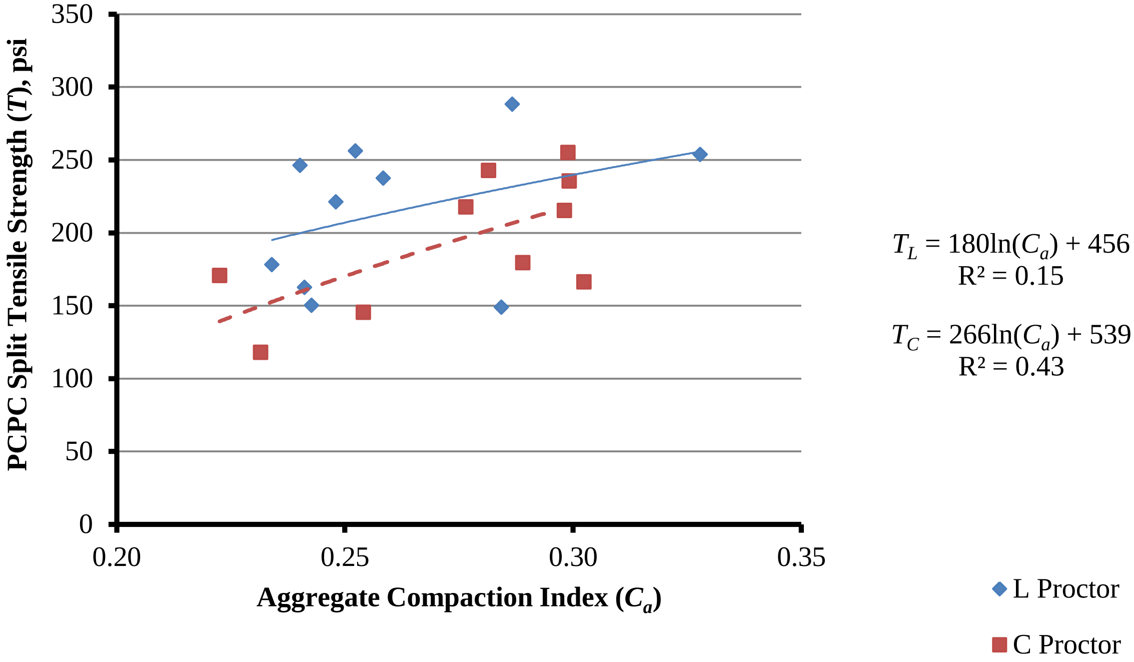

Figure 4.32 Relationship of PCPC split tensile effective porosity to the aggregate compaction index for L and C mixtures.

Aggregate Compaction Index and PCPC Compaction Index

The relationship between the aggregate compaction index, C_a, and the pervious concrete compaction index, C_c, is illustrated in Figure 4.33. Aggregate L mixtures followed a linear relationship that reduced C_c as C_a increased. The dry aggregate gradations from source L that were more sensitive to compaction were not as sensitive when in the pervious concrete mixture. These gradations did not consolidate as much when compacted. A greater portion of these gradations that had higher C_a values were made up of larger aggregates (4 and 38), and so the weight and smoothness of the aggregate particles and the lubricating property of the cement paste encouraged self-consolidation. Source C responded as expected with increasing C_a resulting in increasing C_c. Figure 4.33 shows the equations for the relationships between the PCPC compaction index and the aggregate compaction index.

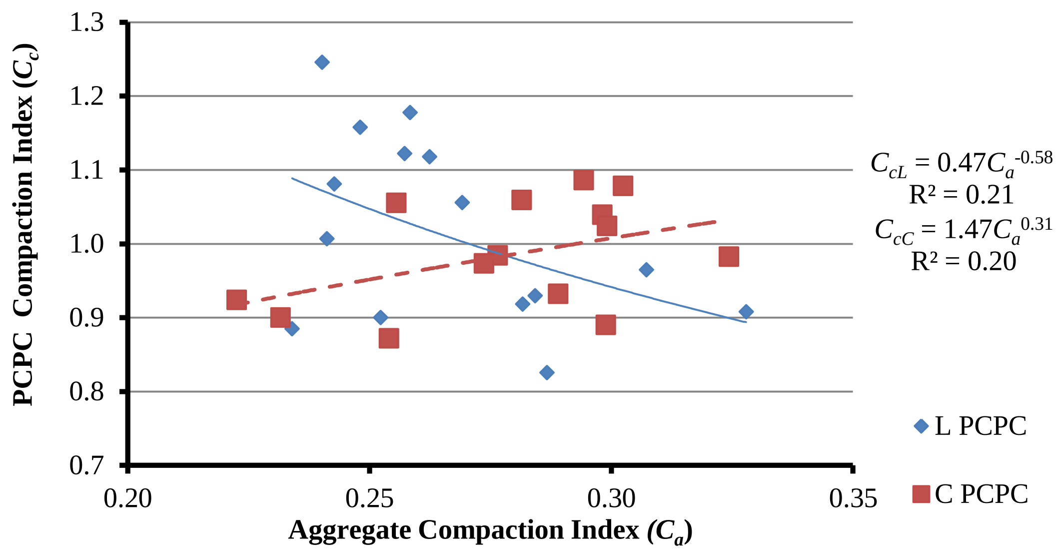

Figure 4.33 Relationship of PCPC compaction index to aggregate compaction index for sources L and C.

R^2 Values for PC Mixtures to Aggregate Properties

The R^2 values for the relationships between the pervious concrete properties to the aggregate properties are listed in Table 4.18. A comparison between the dry Proctor and dry rodded compaction methods for source L and C showed that the dry Proctor generated stronger relationships for source L and the dry rodded generated stronger relationships for source C. These effects are consistent with what was stated earlier about the reactions of the aggregate samples during compaction. Source L, having lower particle indices compared to source C aggregate, showed heaving of surrounding aggregate particles when compacted with the Proctor hammer but the rodding did not have that effect. From the R^2 values, the Proctor was more suitable for source C, which had a higher particle index and needed more impact force to overcome the frictional resistance between the aggregate particles.

Table 4.18 R^2 Values of the Relationships Between Aggregate and Pervious Concrete

Pervious Concrete Properties	Aggregate Properties		Void Content		Uniformity Coefficient		CBR Penetration Stress		Aggregate Compaction Index	
	Source		L	C	L	C	L	C	L	C
Unit Weight	L	Proctor	0.28		0.65		0.04		0.03	
	C			0.92		0.65		0.06		0.35
	L	Rodded	0.47							
	C			0.81						
Gravimetric Air Content	L	Proctor	0.28		0.66		0.04		0.03	
	C			0.92		0.69		0.05		0.35
	L	Rodded	0.81							
	C			0.47						
Porosity	L	Proctor	0.15		0.73		0.04		0.02	
	C			0.70		0.59		0.01		0.39
	L	Rodded	0.28							
	C			0.63						
Permeability	L	Proctor	0.04		0.64		0.18		0.04	
	C			0.22		0.65		0.45		0.12
	L	Rodded	0.13							
	C			0.19						
Compressive Strength	L	Proctor	0.03		0.17		0.03		0.01	
	C			0.23		0.07		0.18		0.24
	L	Rodded	0.15							
	C			0.16						
Split Tensile Strength	L	Proctor	0.23		0.28		0.06		0.15	
	C			0.25		0.22		0.03		0.43
	L	Rodded	0.41							
	C			0.22						
Abrasion Loss	L	Proctor	0.26		0.44		0.10		0.21	
	C			0.03		0.03		0.01		0.14
	L	Rodded	0.53							
	C			0.01						

* Dry Rodded compaction method was only done for the aggregate void content.

Relationships within Pervious Concrete Mixtures

The relationships between various pervious concrete mixture properties were examined in this section. The functions that gave the best fit to data points are the only ones presented in this discussion. These functions represent the relationships between permeability to effective porosity, alternative unit weight to effective porosity, compressive strength to split tensile strength and split tensile strength to abrasion loss.

Permeability and Effective Porosity

A typical relationship presented for pervious concrete mixtures is the PC permeability to the PC effective porosity as illustrated in Figure 4.37. The data points were not average permeability or average porosity values, but they were the measured values determined for each specimen. A total of 45 data points for source L and 42 for source C were used to develop the relationship. The exponential curve was the best fit for both sets of data points and showed that as the effective porosity, P, increased, the permeability, k, also increased. Based on this fit, the porosity relates to approximately 57% of the variation in permeability for source L pervious concrete mixtures. And for source C mixtures, porosity relates to 55% of the permeability. The equations for these relationships between the permeability and porosity for aggregate L and C are presented in Figure 4.34, where k_L and P_L, and k_C and P_C are the PC permeability and effective porosity for sources L and C, respectively. The functions showed that at a porosity of approximately 26.5%, the permeability of both source L and C mixtures had a very similar permeability of 1094 in./hr., which may be linked to the higher cement-aggregate ratio in source C mixes overpowering the frictional resistance of the finer particles, reducing the size of the voids. But as porosity increased from that point of equality, the permeability of source C mixtures were generally higher than source L mixes.

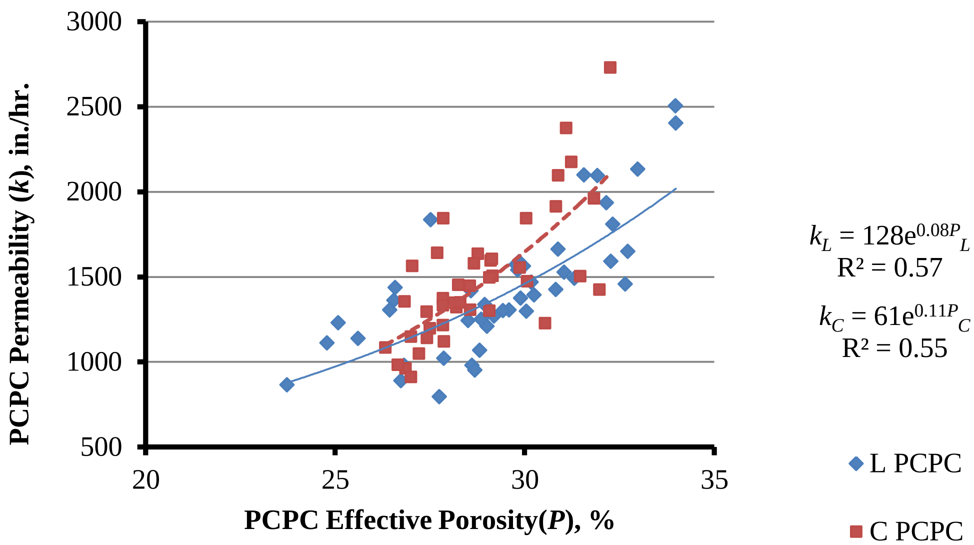

Figure 4.34 Relationship between PCPC permeability and effective porosity of aggregate L and C.

Alternative Unit Weight and Porosity

Unit weight influences the availability of voids that are accessible by water in the pervious concrete matrix, effective porosity. Figure 4.35 illustrates effective porosity as a function of unit weight for aggregates L and C pervious concrete mixtures. As expected, effective porosity decreases as unit weight increases, and the trends were depicted by linear functions that yielded R^2 values of 0.78 for source L mixtures, and 0.83 for source C mixtures. Figure 4.35 shows the equations for effective porosity as a function of the alternative unit weight and that the alternative unit weights had good correlation with porosity, where P_L and γ_L, and P_C and γ_C are the pervious concrete effective porosity and alternative unit weight for sources L and C, respectively.

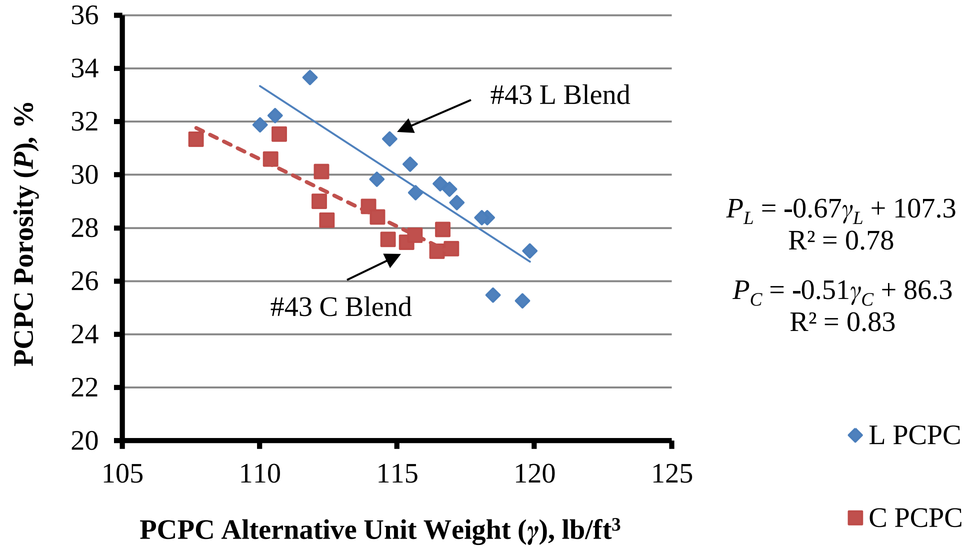

Figure 4.35 Relationship between the PCPC porosity and alternative unit weight of sources L and C pervious concrete mixtures.

It was observed that #43 binary blend had a high permeability that fell within the permeability range for pure blends (Table 4.15). Its porosity was either within (source L) or below (source C) the porosity range for the pure blends but it had higher unit weight, compressive and split tensile strength, and lower abrasion mass loss. Another blend that resembled the #43 was the #135 ternary blend but its pervious concrete mixture made from source C had a high abrasion loss.

Table 4.19 Properties of Blend 43

Aggregate Gradation ID	Alternative Unit Weight		Permeability		Porosity		Compressive Strength		Split Tensile Strength		Abrasion Loss	
	lb/ft^3		in./hr.		%		psi		psi		%	
	L	C	L	C	L	C	L	C	L	C	L	C
8	111	108	1528	1385	32.2	31.3	705	546	149	145	45.6	46.7
4	110	110	2047	1949	31.9	30.6	762	644	178	179	41.1	56.6
38	112	111	2351	2431	33.7	31.5	701	633	162	118	40.8	71.9
84	114	112	1400	1339	29.8	28.3	825	880	150	218	37.6	48.0
43	**115**	**115**	**1638**	**1613**	**31.3**	**27.5**	**887**	**1131**	**221**	**255**	**33.3**	**30.1**
83	120	116	957	1052	27.1	27.1	986	736	246	166	33.9	55.2
843	118	115	948	1300	28.4	27.6	924	785	237	215	30.2	47.1
135	118	117	1601	1299	28.4	27.2	1021	820	256	226	27.1	45.5

Compressive Strength and Split Tensile Strength

The relationship between the compressive strength and split tensile strength which indicates the shear resistance of the specimens is illustrated in Figure 4.36. As expected, the split tensile strength increased with increase in the compressive strength, but at a lower rate of approximately 20% of the compressive strength for both aggregate sources. The split tensile strength values had a narrow range from 122 psi to 333 psi for source L mixtures and 108 psi to 321 psi for source C. This increase of over 250% of the lowest strength indicated that the shear resistance of these samples was greatly impacted by the changes in mixture gradation. Figure 4.36 shows the equations represent the relationships of split tensile strength to compressive strength, where T_L and f'_{cL}, and T_C and f'_{cC} are the split tensile strength and compressive strength for sources L and C, respectively.

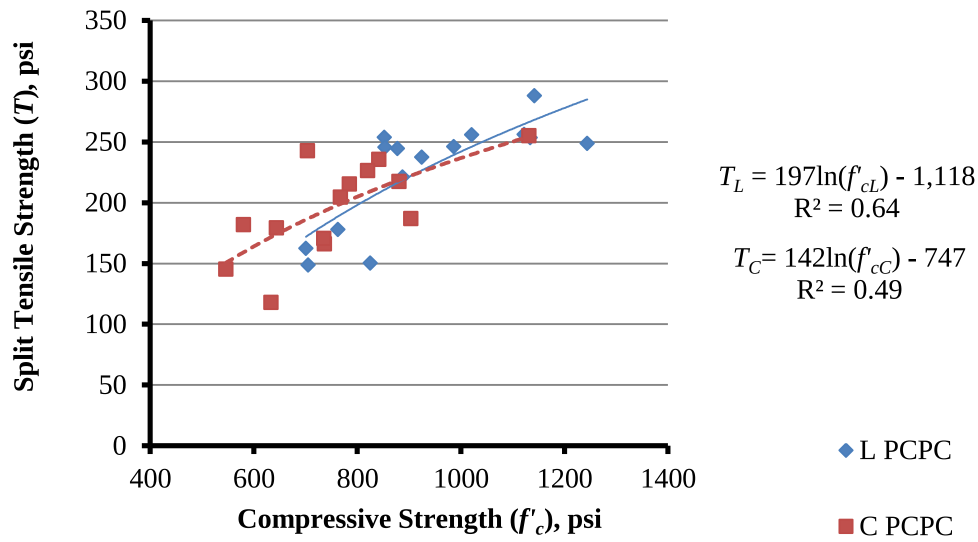

Figure 4.36 Relationship between average compressive strength and split tensile strength for sources L and C mixtures.

Abrasion Loss and Split Tensile Strength

The relationships between the abrasion loss, after 300 revolutions, and the split tensile strength are shown in Figure 4.37. The trends showed that an increase in split tensile strength resulted in a decrease in the abrasion loss. This is the case because the outer aggregate particles undergo shearing away from the surface as it impacts the rotating drum of the LA abrasion machine during the abrasion test. Source C mixtures were more susceptible to abrasion loss than source L mixtures. Figure 4.37 shows the equations that represented the abrasion loss as a function of split tensile strength, where AL_L and T_L, and AL_C and T_C are the abrasion loss and split tensile strength for sources L and C respectively.

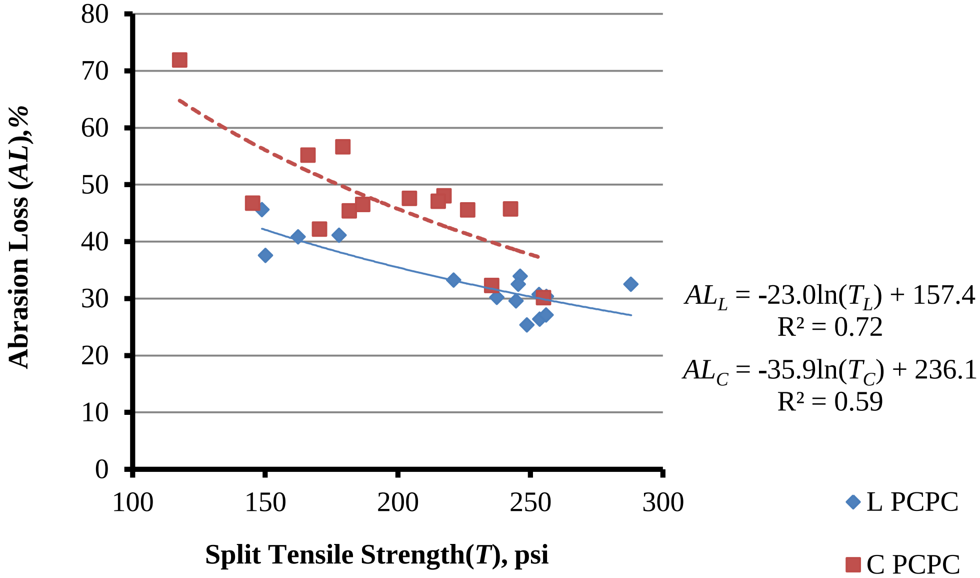

Figure 4.37 Relationship between abrasion loss and split tensile strength for mixtures from sources L and C.

CHAPTER 5 : STATISTICAL METHOD: SIMPLEX-CENTROID DESIGN

The objective of this study was to develop an optimization process for the preparation of porous pavement mixtures based on aggregate structure. The structure of the aggregate was analyzed in Chapter 4. In this chapter, the tools and methodology by which the optimization process was developed is discussed. The statistical tools used for this purpose were the regression analysis in combination with the design of experiment, DOE, simplex-centroid design in JMP Pro 10. These statistical tools were used to estimate the physical properties of aggregate gradations and performance properties of pervious concrete mixtures. The parameters involved in the estimation process will be described and illustrated. The aggregate parameters that gave evidence of better prediction power of the pervious concrete properties included density, void content, and uniformity coefficient

Regression analysis was first used to predict the required aggregate property from the desired pervious concrete property and then the simplex-centroid design was used to correlate the predicted aggregate property to suitable aggregate gradations. The simplex-centroid design was examined to develop a model that would best predict the aggregate properties and to explore its adequacy in also predicting pervious concrete properties. The models considered the most appropriate were the quadratic, special cubic and the special quartic. The augmented model that was best supported by the experimental design was the special quartic model.

The mixture design was focused on three (3) aggregate sizes #8 (2.36 in.), #4 (4.75 in.), and ⅜ in. (9.5 in.) used in preparing different aggregate gradations and pervious concrete mixtures. For aggregate source L, aggregate tests were conducted on three (3) single-sized aggregate fractions, nine (9) binary blends and nine (9) ternary blends. For aggregate source C, aggregate tests were conducted on three (3) single-sized aggregate fractions, four (4) binary blends and eight (8) ternary blends. Of those aggregate gradations, three (3) single-sized, three (3) binary and nine (9) ternary pervious concrete mixtures were made for source L, and the same was done for source C with the exception that eight (8) ternary mixtures were evaluated.

Simplex-Centroid Design

Special Quartic Model

The simplex-centroid design process was laid out by John Cornell, in his book *Experiments with Mixtures: Designs, Models, and the Analysis of Mixture Data* (2002). The general form of the polynomial function used in fitting the data, is referred to as the special quartic polynomial and it is expressed as

$$y_u = \beta_0 + \sum_{i=1}^{q} \beta_i x_i + \sum\sum_{i<j}^{q} \beta_{ij} x_i x_j + \sum\sum\sum_{i\leq j\leq k}^{q} \beta_{iijk} x_i^2 x_j x_k + \varepsilon_u$$

5.1

where y_u is the response value of the uth trial, β_0, β_i, β_{ij}, and β_{ijk} are the measured parameters for all i,j,k = 1,2,…q (q=3), x_i, x_j, and x_k are the aggregate proportions in the mixtures, $\sum_{i=1}^{q}\beta_i x_i$, $\sum\sum_{i<j}^{q}\beta_{ij}x_i x_j$ and $\sum\sum\sum_{i\le j\le k}^{q}\beta_{iijk}x_i^2 x_j x_k$ are the linear, quadratic and quartic effects, respectively of the aggregate blends, and ε_u is the experimental error. Because the mixture components are restricted to $x_1 + x_2 + x_3 = 1$, β_0 is omitted. The fitted model for the individual responses is expressed as

$$y_u = \beta_1 x_1 + \beta_2 x_2 + \beta_3 x_3 + \beta_{12}x_1x_2 + \beta_{13}x_1x_3 + \beta_{23}x_2x_3 + \beta_{1123}x_1^2x_2x_3 + \beta_{1223}x_1x_2^2x_3 + \beta_{1233}x_1x_2x_3^2 \quad 5.2$$

but for the estimated or averaged responses, it is expressed as

$$y_u = b_1 x_1 + b_2 x_2 + b_3 x_3 + b_{12}x_1x_2 + b_{13}x_1x_3 + b_{23}x_2x_3 + b_{1123}x_1^2x_2x_3 + b_{1223}x_1x_2^2x_3 + b_{1233}x_1x_2x_3^2 \quad 5.3$$

In this model, the ratio of mixture types, pure : binary : ternary, is 3 : 3 : 4. The model studies each component at 6 levels, x_i = 0, ⅙, ⅓, ½, ⅔, and 1. Within the simplex triangle there are three (3) augmented points besides the centroid. The augmented points generate the individual responses β_{1123}, β_{1223}, and β_{1233}. Because of these, this model gives more uniform information about the responses for ternary blends that are within the simplex triangle and can identify interior surface curvature (Cornell, 2002).

Interpreting the Simplex Triangle

When interpreting the simplex triangle, Figure 5.1 is a pictorial example that can aid this process. In this study, the vertices are the pure aggregate components (#8, #4 and #38). Reading the triangle counterclockwise, the aggregate components are followed by its corresponding axis which indicates the proportions of aggregate in the mixture. To the seven (7) points on the simplex-centroid design triangle, are the corresponding parameters or aggregate void contents placed within a coordinate system. In this coordinate system, the first number represents the proportion of the component to which the arrow points. These arrows indicate the direction of increasing component or aggregate proportions. The second number represents the aggregate void content. Through the point of interest (black dot), dashed lines are drawn parallel to each axis. Each vertex corresponds with the dashed line that is opposite to it. The point, at which each dashed line intersects the axis (at the x's) of its corresponding component, is the proportion of that component in the mixture. Therefore, the point of interest in this example would have proportions of approximately 0.26 for #8, 0.43 for #4 and 0.31 for ⅜ inch, all adding up to 1.

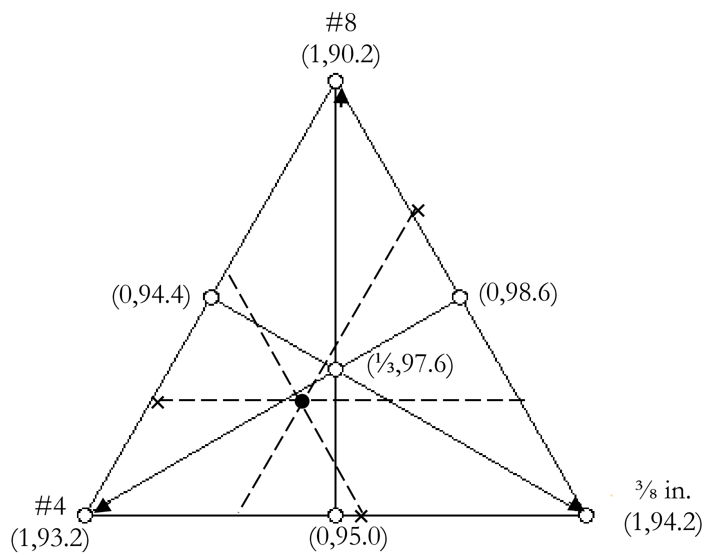

Figure 5.1 An example with arrows linking and showing the direction of each pure component proportion increase and the average aggregate densities (lb/ft^3) at the design points within a coordinate system.

Aggregate Density, Void Content and Uniformity Coefficient

The simplex-centroid design augmented with three interior points was used to predict aggregate properties for both aggregate sources L and C. The special quartic model was used to accomplish this goal. The measured aggregate densities, void content, and uniformity coefficient with the simplex-centroid predicted values from the augmented special quartic model are presented in Tables 5.1, 5.2 and 5.3, respectively. To verify the adequacy of the models, the lack of fit test was done for the special quartic model and for the relationships between the paired measured and predicted properties to the line of equality.

Aggregate Dry Proctor Density

Fitted to the 30 design points, the special quartic models for aggregate density of source L and C were

$$\begin{aligned} L: D_u &= \underset{(0.336)}{92.6x_1} + \underset{(0.336)}{95.9x_2} + \underset{(0.336)}{97.8x_3} + \underset{(1.65)}{0.366x_1x_2} + \underset{(1.65)}{13.4x_1x_3} - \underset{(1.65)}{7.57x_2x_3} - \underset{(34.44)}{57.3x_1^2x_2x_3} \\ &+ \underset{(34.44)}{73.2x_1x_2^2x_3} + \underset{(34.44)}{83.8x_1x_2x_3^2} \end{aligned} \quad 5.4$$

$$\begin{aligned} C: D_u &= \underset{(0.390)}{89.3x_1} + \underset{(0.390)}{93.1x_2} + \underset{(0.390)}{94.1x_3} + \underset{(1.91)}{12.6x_1x_2} + \underset{(1.91)}{28.0x_1x_3} + \underset{(1.91)}{9.57x_2x_3} - \underset{(40.0)}{53.6x_1^2x_2x_3} \\ &- \underset{(40.0)}{11.4x_1x_2^2x_3} + \underset{(40.0)}{50.4x_1x_2x_3^2} \end{aligned} \quad 5.5$$

The models, equations 5.4 and 5.5, comprised of the average responses or densities for each design point with its corresponding aggregate proportions and its estimated standard error in parentheses. From the model, the positive or negative values are associated with synergistic effects or antagonistic effects, respectively. The idea is that positive values mean that higher densities were achieved compared to the average density of the single-sized components within each blend and negative values convey the opposite (Cornell, 2002).

The augmented simplex-centroid design triangles with contour lines for the predicted aggregate densities based on the special quartic models are shown in Figure 5.2. Table 5.1 shows that the density residuals were small except for blend 8884 and

8883 for source L and blend 89 for source C. Besides examining the density residual, the adequacy of these special quartic models was checked by a lack of fit analysis. This analysis compares the *F*-ratio with the table *F*-distribution, $F_{\alpha,v1,v2}$, to check the adequacy of the model. The *v1* in the subscript represents the degrees of freedom for the pure-error (due to replicates) sum of squares, the *v2* represents the degrees of freedom for the lack-of-fit sum of squares and $\alpha = 0.01$ (Cornell, 2002). For $\alpha = 0.01$, the *F*-distribution values are higher than larger α values, which is better for pervious concrete mixtures as it compensates for the variability in the results. The lack-of-fit analysis for the complete set of data values showed the *F*-ratio for source L was 4.35, which exceeds the table value $F_{0.01,12,42} = 2.64$, but not by a large amount, but still showed the model as inadequate. For source C, $F_{0.01,6,30} = 1.67$, which did not exceed the table value of 3.47 and it was inferred that the model was adequate. Source C had five (5) validation points and source L had eleven (11), the removal of that additional six points from source L gave a $F_{0.01,6,30} = 1.72$ which is less than the tabled *F*-distribution of 3.47 and now would be considered adequate.

Figure 5.3 shows the relationship of the density predictions and measured densities for the validation points to the line of equality. The data points for source L with lower densities fell above the line of equality (dotted centerline) showing a tendency for the model to over predict, which could have resulted from the increased standard error for blends with lower densities. For higher densities, the model was much more accurate. A fit special done in JMP for source L measured and predicted densities to the line of equality gave a lack-of-fit *F*-ratio of 6.78 to a table value $F_{0.01,11,22} = 3.19$ with a *p*-value =

0.0001. Since the *F*-ratio exceeded the F-distribution value, the model is not adequate based on this test. For source C, the density points of correlation were mostly along the line of equality and gave a lack-of-fit *F*-ratio of 5.08 to a table value $F_{0.01,5,10} = 5.64$ and a *p*-value = 0.0141, showing adequacy of the model.

Table 5.1 Augmented Special Quartic Model: Measured, Predicted, and Residual Aggregate Dry Proctor Density

Aggregate Gradation		**Source L** Density			**Source C** Density		
		Measured	Predicted	Residuals	Measured	Predicted	Residuals
		lb/ft^3	lb/ft^3	lb/ft^3	lb/ft^3	lb/ft^3	lb/ft^3
Design Points	8	92.7	92.6	0.1	89.3	89.3	0.0
	4	95.9	95.9	0.0	93.0	93.1	0.0
	38	97.8	97.8	0.1	94.0	94.1	0.0
	84	94.4	94.3	0.1	94.3	94.3	-0.1
	43	95.0	94.9	0.1	95.9	95.9	0.0
	83	98.6	98.5	0.1	98.6	98.7	0.0
	843	97.6	97.2	0.4	97.2	97.4	-0.2
	8843	94.9	95.2	-0.2	95.2	95.1	0.2
	8443	96.0	96.3	-0.2	95.9	95.8	0.2
	8433	98.2	98.4	-0.2	98.3	98.2	0.2
Validation Points	8884	92.3	93.5	-1.1			
	8444	94.2	95.1	-0.9			
	4443	94.7	94.9	-0.2	94.9	95.1	-0.2
	4333	95.2	95.9	-0.6			
	8333	99.5	99.0	0.5			
	8883	94.5	96.4	-1.8			
	89	94.8	95.1	-0.3	95.9	94.5	1.4
	789	95.5	95.5	-0.1			
	613	96.7	96.6	0.1	96.7	96.9	-0.2
	341	94.8	95.9	-1.1	96.1	95.9	0.2
	135	97.6	97.7	-0.1	97.7	97.9	-0.1

*Aggregate proportions for #89: 0.2604 of (8), 0.7365 of (4), and 0.00311 of (38) and for #789: 0.2482 (8), 0.6932 (4), and 0.0586 (38). Darkened cells were additional aggregate blends that were not tested for source C.

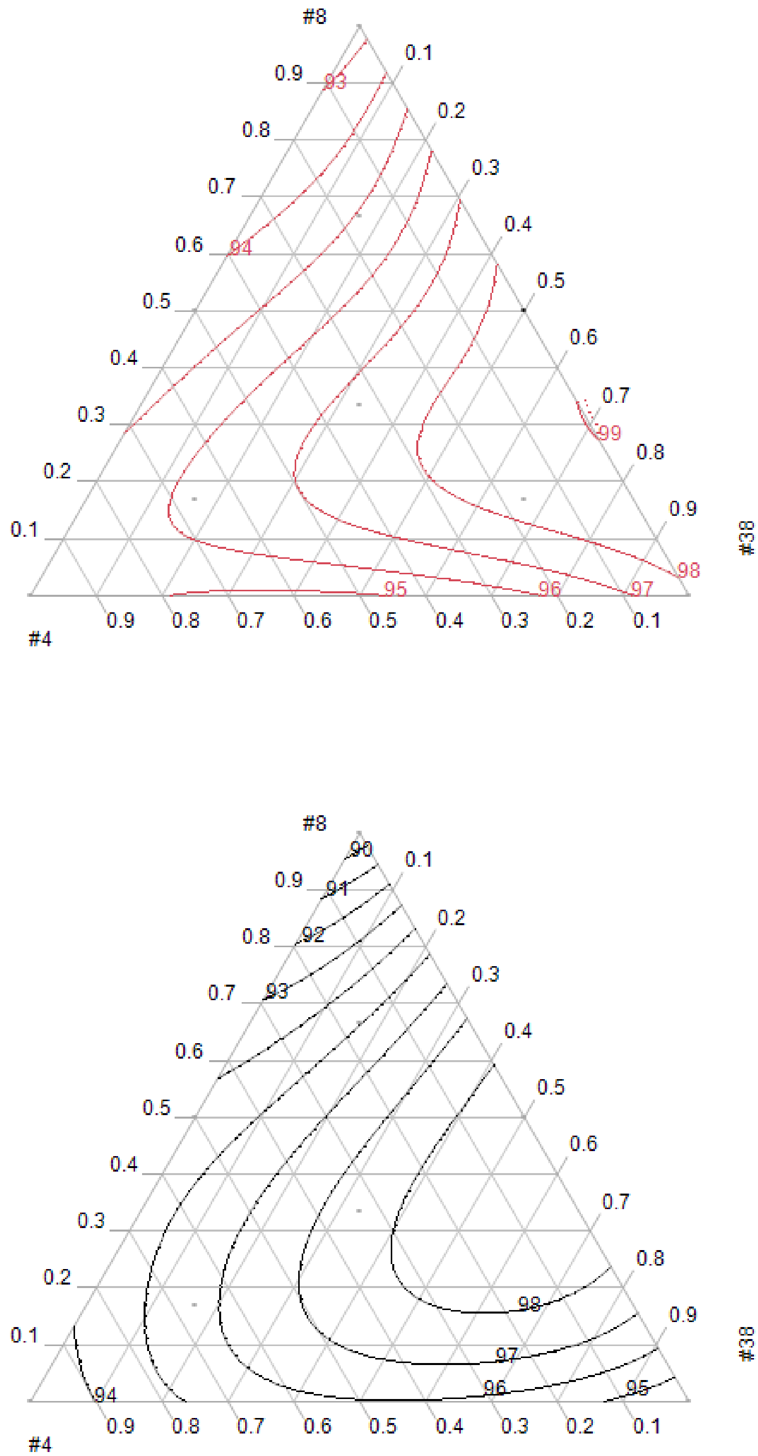

Figure 5.2 The augmented special quartic simplex triangle with contour lines for aggregate dry Proctor density (lb/ft^3)for source L (above) and C (below).

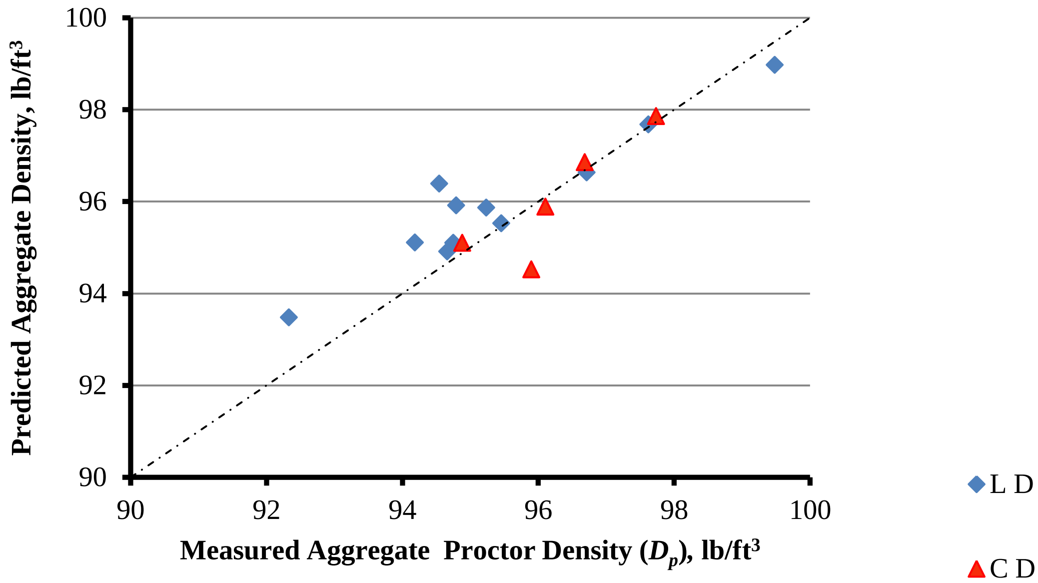

Figure 5.3 The relationship between the measured and predicted dry Proctor density of aggregate L and C using validation blends to the line of equality.

Aggregate Dry Proctor Void Content

The special quartic model for aggregate void content fitted to the 30 design points for sources L and C are expressed in the equation 5.6 and 5.7 repectively.

$$\begin{aligned} y_u = {} & \underset{(0.193)}{43.5x_1} + \underset{(0.193)}{41.5x_2} + \underset{(0.193)}{40.5x_3} - \underset{(0.948)}{0.290x_1x_2} - \underset{(0.948)}{8.16x_1x_3} + \underset{(0.948)}{4.58x_2x_3} + \underset{(19.82)}{38.0x_1^2x_2x_3} \\ & - \underset{(19.82)}{45.9x_1x_2^2x_3} - \underset{(19.82)}{50.5x_1x_2x_3^2} \end{aligned} \qquad 5.6$$

$$\begin{aligned} y_u = {} & \underset{(0.247)}{44.9x_1} + \underset{(0.247)}{42.6x_2} + \underset{(0.247)}{42.2x_3} - \underset{(1.21)}{7.84x_1x_2} - \underset{(1.21)}{17.3x_1x_3} - \underset{(1.21)}{5.97x_2x_3} + \underset{(25.32)}{31.1x_1^2x_2x_3} \\ & + \underset{(25.32)}{8.24x_1x_2^2x_3} - \underset{(25.32)}{28.6x_1x_2x_3^2} \end{aligned} \qquad 5.7$$

Table 5.2 presents the measured, predicted and residual aggregate void contents. Since the responses of the aggregate density and void content are quite similar to each other some of the values for the lack-of-fit test are similar. The void content residuals for source L were quite small with the exception of blend 8883. The simplex triangles with the contour lines that illustrate the change in level of void content are shown in Figure 5.4. For both sources, the contours showed that the aggregate void content was the highest for single-sized fraction 8. The correlation of the predicted aggregate void content to measured void content for validation blends is illustrated in Figure 5.5. The lack of fit analysis for the complete set of data values showed the *F*-distribution for source L was 4.35 which exceeds the table value $F_{0.01,12,42} = 2.64$ but not by a large amount, but showed the model as inadequate. For source C, $F_{0.01,6,30} = 2.04$, did not exceed the table value of 3.47 so the model was adequate. Again when source L had the same validation points as source C, the $F_{(6,30,0.01)} = 1.36$ which would be considered adequate. It must be noted that source C had fewer validation points which might be related to its passing the adequacy test. Since the aggregate void content and density were so closely related, the data points relative to the line of equality were quite similar to the density only flipped with the higher void contents under the line of equality showing a tendency of under prediction for source L. Source C was mostly along the line of equality. A fit special done in JMP for source L measured to predicted void contents in relation the line of equality gave a lack-of-fit *F*-ratio of 7.56 to a tabled value $F_{0.01,11,22} = 3.19$ and p-value = 0.0001. Since the *F*-ratio exceeded the *F*-distribution value, the model is not adequate based on this test. For source C, the void contents were mostly along the line of equality and gave a lack-of-fit F-ratio of 4.85 to a tabled value $F_{0.01,5,10}$ = 5.64 and p-value = 0.016, showing adequacy of the model.

Table 5.2 Augmented Special Quartic Model: Measured, Predicted and Residuals Aggregate Proctor Void Content for Sources L and C

Aggregate Gradation		Source L: Measured Void Content %	Source L: Predicted Void Content %	Source L: Void Content Residuals %	Source C: Measured Void Content %	Source C: Predicted Void Content %	Source C: Void Content Residuals %
Design Points	8	43.5	43.5	0.0	44.9	44.9	0.0
	4	41.5	41.5	0.0	42.7	42.7	0.0
	38	40.5	40.5	0.0	42.2	42.2	0.0
	84	42.4	42.4	0.0	41.9	41.8	0.1
	43	42.1	42.1	0.0	41.0	40.9	0.1
	83	39.9	40.0	0.0	39.3	39.2	0.0
	843	40.5	40.6	-0.1	40.2	39.9	0.3
	8843	42.1	42.1	0.1	41.3	41.5	-0.2
	8443	41.4	41.3	0.1	40.9	41.1	-0.2
	8433	40.2	40.1	0.1	39.5	39.7	-0.2
Validation Points	8884	43.7	42.9	0.7			
	8444	42.5	41.9	0.6			
	4443	42.3	42.1	0.2	41.6	41.4	0.2
	4333	42.0	41.6	0.4			
	8333	39.4	39.7	-0.3			
	8883	42.4	41.2	1.2			
	89	42.2	41.9	0.2	40.9	41.7	-0.8
	789	41.8	41.7	0.1			
	613	41.1	41.1	0.0	40.4	40.3	0.1
	341	42.2	41.5	0.7	40.8	40.9	-0.1
	135	40.5	40.5	0.1	39.9	39.8	0.1

*Aggregate proportions for #89: 0.2604 of (8), 0.7365 of (4), and 0.00311 of (38) and for #789: 0.2482 (8), 0.6932 (4), and 0.0586 (38). Darkened cells were additional aggregate blends that were not tested for source C.

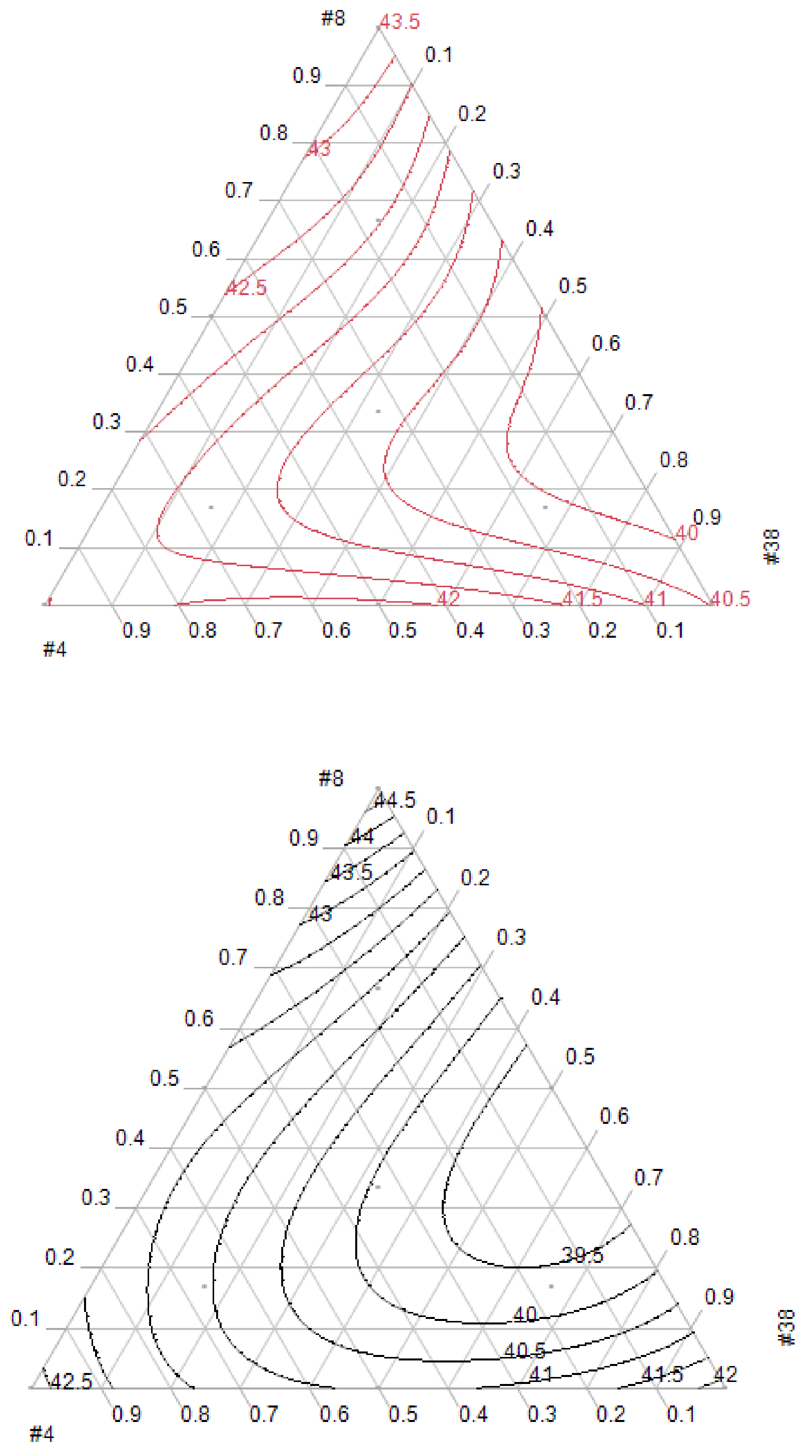

Figure 5.4 The aggregate Proctor void content (%) augmented special quartic simplex triangle with contour lines for source L (top) and C (below).

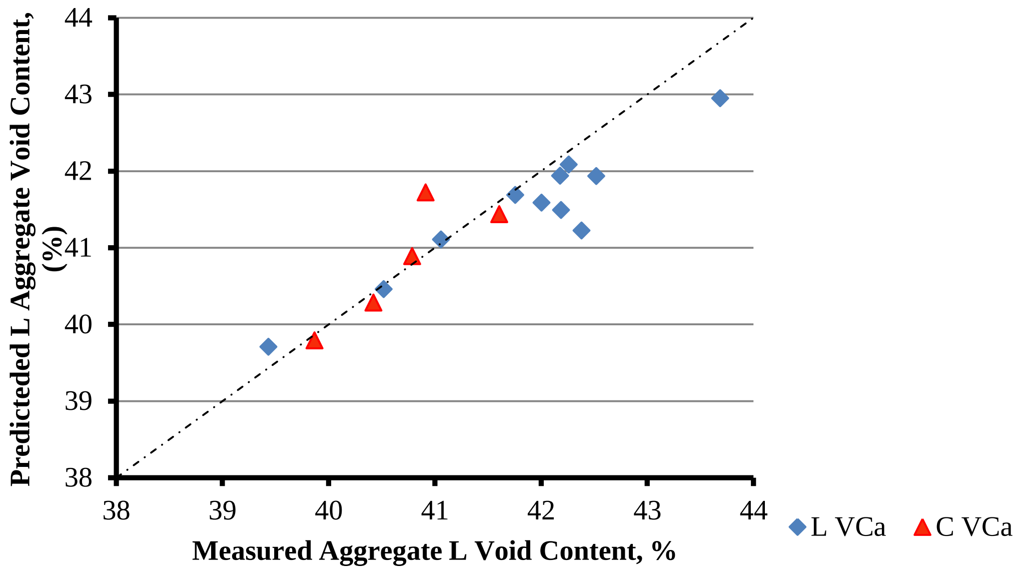

Figure 5.5 The relationship between the measured and predicted dry Proctor void content of aggregate L and C using validation blends to the line of equality.

Aggregate Uniformity Coefficient

Although the uniformity coefficient, C_u, is not a measured but calculated property, it was considered since it showed fairly good relationships between the aggregate and pervious concrete properties. The special quartic model for aggregate uniformity coefficient fitted to the 10 design points with 3 replicates each for sources L and C was

$$\begin{aligned} y_u =\ & 1.386x_1 + 1.382x_2 + 1.115x_3 + 2.259x_1x_2 + 9.553x_1x_3 + 2.097x_2x_{33} \\ & (0.105) \quad (0.105) \quad (0.105) \quad (0.513) \quad (0.513) \quad (0.513) \\ & -80.48x_1^2x_2x - 14.20x_1x_2^2x_3 + 70.36x_1x_2x_3^2 \\ & (10.73) \quad (10.73) \quad (10.73) \end{aligned} \qquad 5.8$$

Table 5.3 presents the measured, predicted and residuals for the aggregate uniformity coefficient. Figure 5.6 presents the contour lines for predicted uniformity coefficients which increased toward a 1:1 blend of #8 and #38. The correlation of the predicted aggregate uniformity coefficient to measured uniformity coefficient for validation blends is shown in Figure 5.7. There was no lack-of-fit analysis because the uniformity coefficient did not have replicated data points. Figure 5.7 showed both over and under predictions for lower C_u values but more over predictions for higher C_u values. The two validation points that where away from the line of equality were blends 8883 and 613 with the two highest residuals and had a larger proportion of finer aggregate sizes.

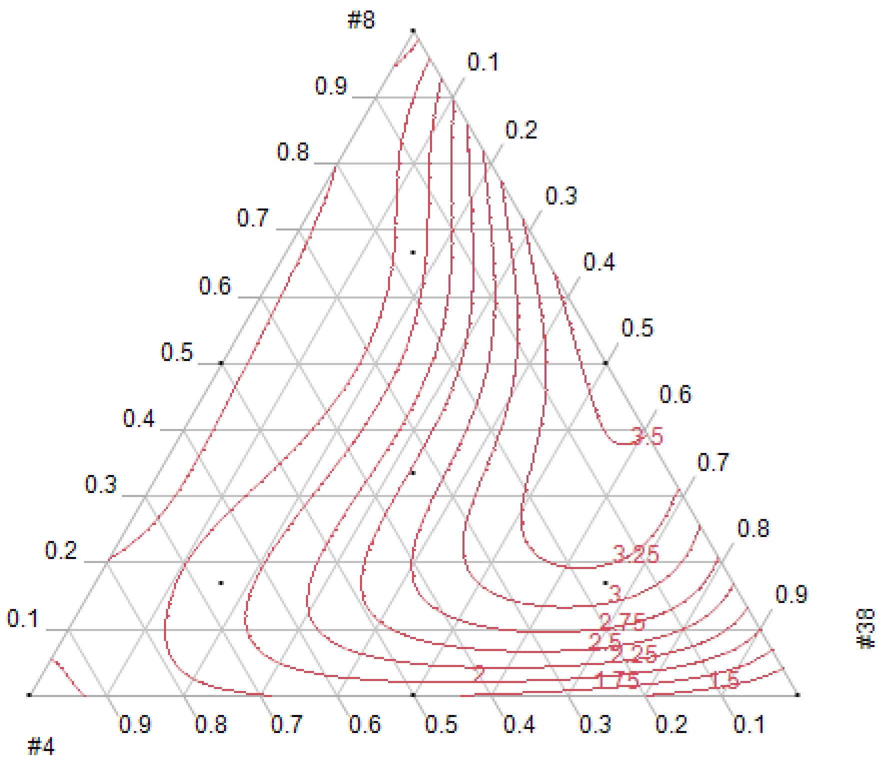

Figure 5.6 The aggregate uniformity coefficient augmented special quartic simplex triangle with contour lines. First contour line close to #38 vertex has a C_u of 1.5 and then increases with 0.25 increments up to 3.50

Table 5.3 Augmented Special Quartic Model: Measured, Predicted and Residual Aggregate Uniformity Coefficient

Aggregate Gradation ID		Measured Uniformity Coefficient	Predicted Uniformity Coefficient	Uniformity Coefficient Residuals
Design Points	8	1.419	1.386	0.033
	4	1.415	1.382	0.033
	38	1.148	1.115	0.033
	84	2.015	1.948	0.066
	43	1.839	1.772	0.066
	83	3.705	3.638	0.066
	843	2.842	2.537	0.305
	8843	1.691	1.892	-0.202
	8443	1.682	1.883	-0.202
	8433	2.944	3.145	-0.201
Validation Points	8884	1.595	1.808	-0.214
	8444	2.103	1.806	0.296
	4443	1.587	1.708	-0.121
	4333	1.722	1.575	0.148
	8333	3.462	2.974	0.488
	8883	1.595	3.109	-1.514
	89	2.117	1.809	0.307
	789	2.157	1.721	0.436
	613	1.722	2.708	-0.986
	341	1.917	1.740	0.177
	135	2.589	2.991	-0.401

*The aggregate proportions for #89: 0.2604 of (8), 0.7365 of (4), and 0.00311 of (38) and for #789: 0.2482 (8), 0.6932 (4), and 0.0586 (38).

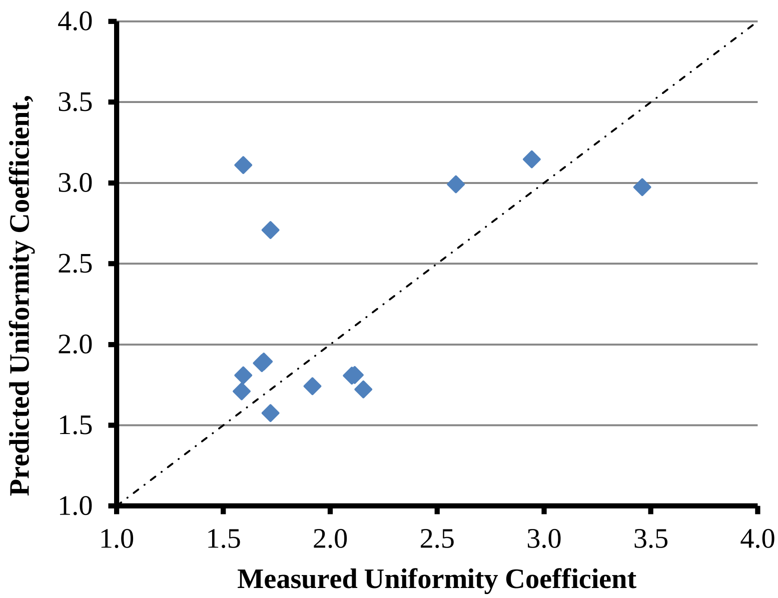

Figure 5.7 The relationship between the measured and predicted uniformity coefficient of aggregate L and C using validation blends to the line of equality.

Correlation of Pervious Concrete Parameters: Predicted to Measured

Alternative Unit Weight

The special quartic model that was used to estimate the aggregate parameters was also used to estimate the pervious concrete parameters. The actual models used to estimate the alternative unit weight, γ, of the validation points for the pervious concrete mixtures for sources L and C are equations 5.9 and 5.10, respectively.

$$L:\gamma_u = \underbrace{111x_1 + 110x_2 + 112x_3}_{(0.8)} + \underbrace{16x_1x_2 + 35x_1x_3 + 15x_2x_3}_{(4.0)} \underbrace{- 37x_1^2x_2x_3 + 185x_1x_2^2x_3 - 113x_1x_2x_3^2}_{(81)} \qquad 5.9$$

$$C:\gamma_u = \underbrace{108x_1 + 111x_2 + 111x_3}_{(0.5)} + \underbrace{13x_1x_2 + 29x_1x_3 + 20x_2x_3}_{(2.5)}$$

$$-\underbrace{151x_1^2x_2x_3 - 43x_1x_2^2x_3 + 82x_1x_2x_3^2}_{(51)} \qquad 5.10$$

The measured and predicted unit weight values and the residuals for the pervious concrete mixtures are shown in Table 5.4. Since the range of unit weights was relatively narrow, the residuals were small. The contour lines for the alternative unit weight are shown in Figure 5.8. The unit weight increases towards the center of the response surface for both sources but it was somewhat skewed towards the 38 mixture for source C. A lack of fit test for all the data points gave an *F*-ratio of 1.28 for source L with a table value $F_{0.01,6,25}$ = 3.63 and a *p*-value of 0.3 which is greater than the $\alpha = 0.01$ showing no significant lack-of-fit so the null hypothesis is not rejected (zero or no lack-of-fit) and the model is considered adequate. For source C mixtures, the *F*-ratio was 1.35 with a table value $F_{0.01,5,14}$ = 4.69 and a *p*-value of 0.3 giving evidence of the model being adequate.

The relationship of the predicted and measured alternative unit weight to the line of equality, LOE, is illustrated in Figure 5.9. A lack-of-fit test done for only the validation points to the linear LOE gave *F*-ratio of 4.59 for source L mixtures with a table value $F_{0.01,7,5}$ = 10.46 and a *p*-value of 0.056 which is greater than the $\alpha = 0.01$ showing no significant lack-of-fit therefore confirming adequacy of the model. For source C mixtures, the *F*-ratio was 14.36 with a table value $F_{0.01,5,3}$ = 28.24 and a *p*-value of 0.026 confirming the model as being adequate.

Table 5.4 Augmented Special Quartic Model: Measured, Predicted and Residual PCPC Alternative Unit Weight

		Source L			Source C		
Aggregate Gradation ID		Alternative Unit Weight			Alternative Unit Weight		
		Measured	Predicted	Residuals	Measured	Predicted	Residuals
		lb/ft^3	lb/ft^3	lb/ft^3	lb/ft^3	lb/ft^3	lb/ft^3
Design Points	8	111	111	-0.1	108	108	-0.3
	4	110	110	0.0	110	111	-0.1
	38	112	112	0.1	111	111	0.2
	84	114	114	-0.1	112	113	-0.1
	43	115	115	0.0	115	116	-0.2
	83	120	120	-0.2	116	117	-0.1
	843	118	119	-0.3	115	115	-0.4
	8843	117	117	0.1	112	112	-0.3
	8443	117	117	0.3	114	114	0.0
	8433	117	117	0.1	117	116	0.2
Validation Points	89	115	113	2.0	112	112	-0.1
	789	116	115	0.3			
	613	120	118	1.5	116	114	1.3
	341	118	118	0.4	114	113	1.0
	135	118	117	1.0	117	117	0.3

*Aggregate proportions for #89: 0.2604 of (8), 0.7365 of (4), and 0.00311 of (38) and for #789: 0.2482 (8), 0.6932 (4), and 0.0586 (38). Darkened cells were additional aggregate blends that were not tested for source C.

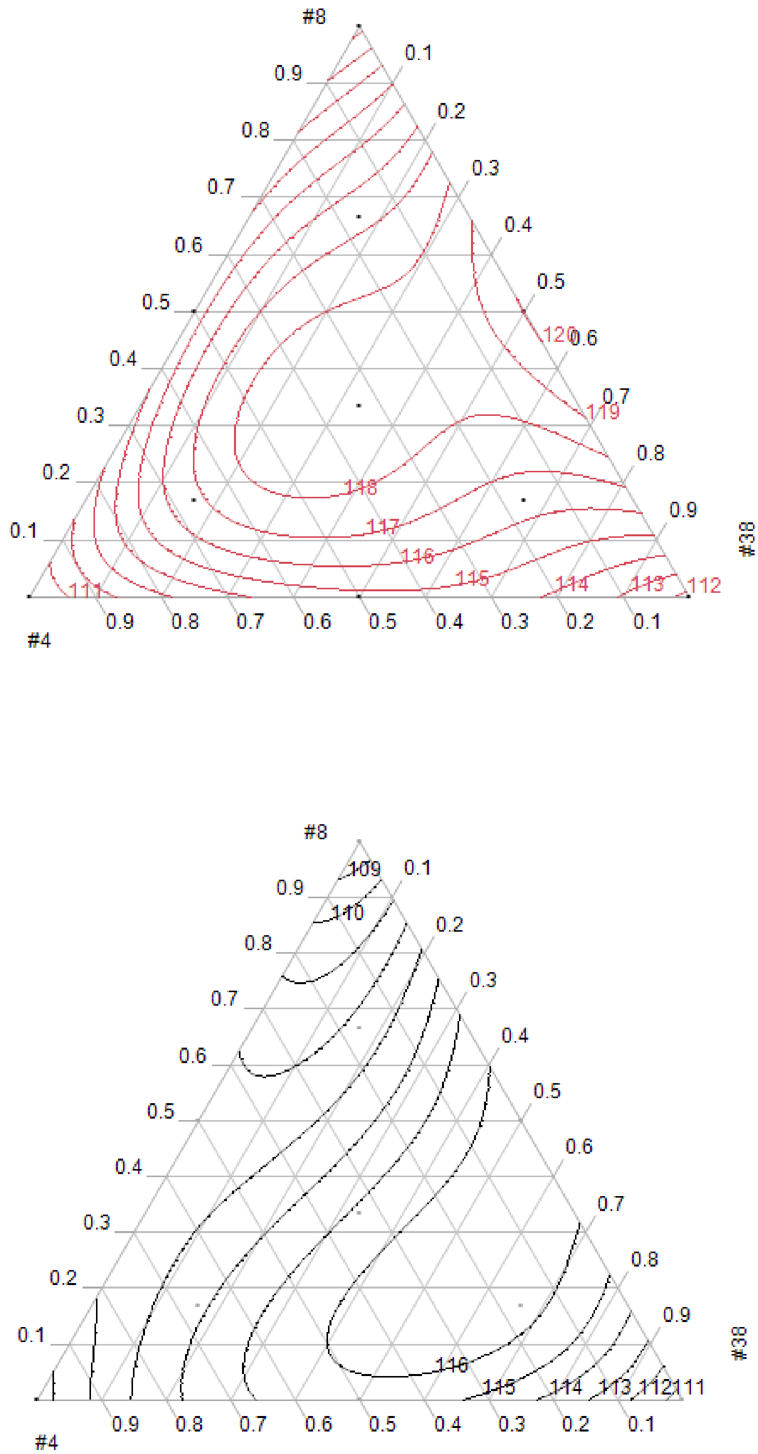

Figure 5.8 PC predicted alternative unit weight (lb/ft^3)special quartic triangle with contour lines for PCPC mixtures L (top) and C (bottom).

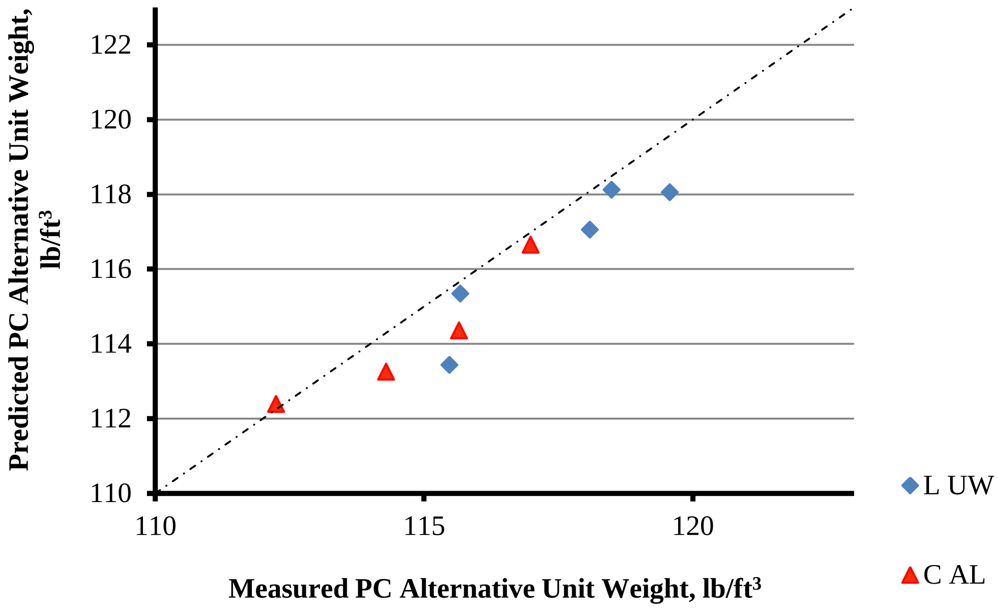

Figure 5.9 The relationship between the measured and predicted alternative unit weight of source L and C validation mixtures to the line of equality.

Permeability

The special quartic models that were used to estimate the permeability values of the validation points of the pervious concrete mixtures for sources L and C mixtures are given as equations 5.11 and 5.12, respectively.

$$L : k_u = \underbrace{1538x_1 + 2057x_2 + 2360x_3}_{(40)} \underbrace{-1511x_1x_2 - 3893x_1x_3 - 2205x_2x_3}_{(196)}$$

$$+ \underbrace{7067x_1^2x_2x_3 - 13412x_1x_2^2x_3 + 1982x_1x_2x_3^2}_{(4093)} \tag{5.11}$$

$$C: k_u = \underbrace{1380x_1 + 1944x_2 + 2426x_3}_{(36)} - \underbrace{1330x_1x_2 - 3444x_1x_3 - 2326x_2x_3}_{(176)}$$

$$+ \underbrace{25596x_1^2x_2x_3 + 7925x_1x_2^2x_3 + 23237x_1x_2x_3^2}_{(3672)} \qquad 5.12$$

The measured and predicted permeability values and the residuals for the pervious concrete mixtures are shown in Table 5.4. Higher residuals resulted from source L mixtures as compared to source C, giving a hint of source L model inadequacy. The simplex-triangle contour plots detected greater curvature within the response surface for source C mixtures compared with source L (Figure 5.10). Because the special quartic model has more design points within the triangle, it can detect more changes within the response surface but it is not as sensitive at the edges where it has fewer design points. With this, it is understandable that blend 89 which lies very close to the edge had high residuals for both sources. A lack-of-fit test gave the F-ratio of 15.42 for source L with a table value $F_{0.01,6,165}$ = 2.80 (p-value = 0.001) which it exceeded making the model inadequate. For source C mixtures, the F-ratio was 3.29 with a table value $F_{(5,154,0.01)}$ = 3.02 (p-value 0.0075) which is marginally exceeded but was also considered inadequate. Based on the contour plots, permeability estimates increased from the middle of the triangle (mix 843) toward mix 4 vertex and even more toward mix 38.

Figure 5.11 shows the relationship of the measured and predicted permeability to the line of equality. A lack-of-fit test done for the measured and predicted pair to the line of equality for the validation points gave a F-ratio of 31.5 for source L with a table value

$F_{0.01,5,55}$ = 3.38 (p-value = 0.0001) which it exceeded making the model inadequate. For source C mixtures, the F-ratio was 4.66 with a table value $F_{0.01,4,44}$ = 3.79 (p-value 0.0032) which is marginally exceeded but was also considered inadequate.

Table 5.5 Augmented Special Quartic Model: Measured, Predicted and Residual PCPC Permeability

Aggregate Gradation ID		Source L Permeability			Source C Permeability		
		Measured	Predicted	Residual	Measured	Predicted	Residual
		in./hr.	in./hr.	in./hr.	in./hr.	in./hr.	in./hr.
Design Points	8	1528	1538	-9.7	1385	1380	5.1
	4	2047	2057	-9.8	1949	1944	5.1
	38	2351	2361	-9.7	2431	2426	5.2
	84	1400	1420	-19.6	1339	1329	10.0
	43	1638	1658	-19.4	1613	1603	10.0
	83	957	976	-19.4	1052	1042	10.0
	843	948	1037	-88.6	1300	1254	46.2
	8843	1199	1140	58.6	1293	1323	-30.4
	8443	1408	1350	58.4	1504	1534	-30.4
	8433	1468	1409	58.4	1279	1309	-30.4
Validation Points	89	1392	1620	-227.5	1669	1543	126.2
	789	1334	1462	-128.4			
	613	1105	1021	84.3	1202	1146	55.9
	341	1239	1135	104.2	1413	1461	-48.2
	135	1601	1275	326.23	1299	1232	67.4

*Aggregate proportions for #89: 0.2604 of (8), 0.7365 of (4), and 0.00311 of (38) and for #789: 0.2482 (8), 0.6932 (4), and 0.0586 (38). Darkened cells were additional aggregate blends that were not tested for source C.

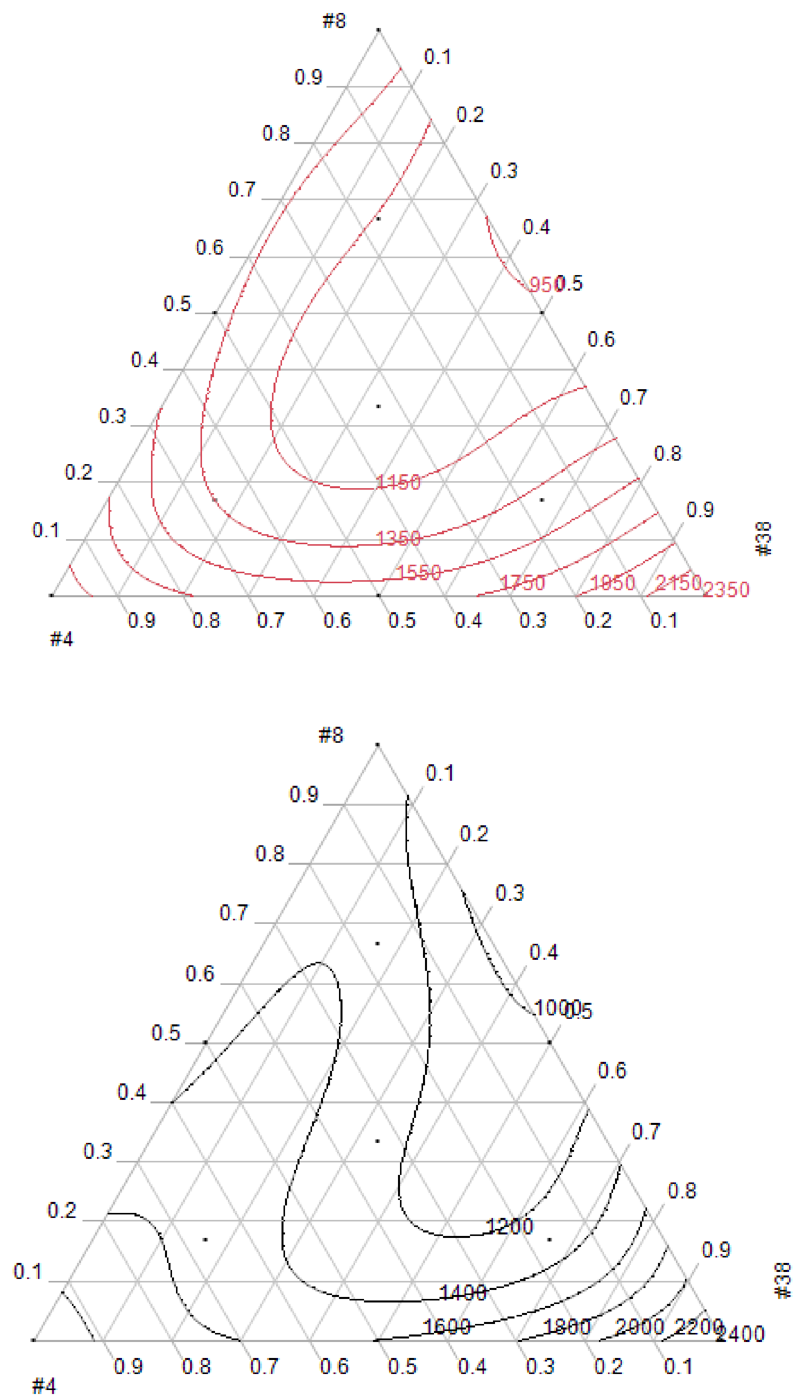

Figure 5.10 PC predicted permeability (in./hr.) special quartic triangle with contour lines for PCPC mixtures L (top) and C (bottom).

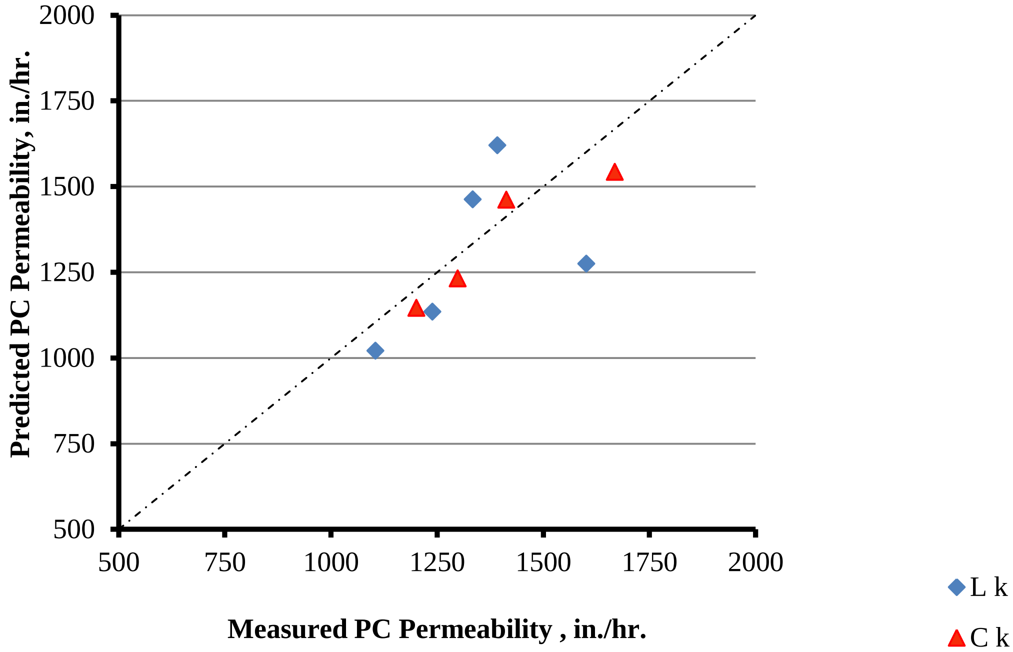

Figure 5.11 The relationship between the measured and predicted permeability of source L and C validation mixtures to the line of equality.

Porosity

The pervious concrete special quartic model for predicting effective porosity is given in equations 5.13 and 5.14 for source L and C, respectively.

$$L : P_u = \underbrace{32.2x_1 + 31.9x_2 + 33.7x_3}_{(0.35)} - \underbrace{9.1x_1x_2 - 23.3x_1x_3 - 5.8x_2x_3}_{(1.72)} \qquad 5.13$$

$$+ \underbrace{89.2x_1^2x_2x_3 - 99.9x_1x_2^2x_3 + 7.9x_1x_2x_3^2}_{(35.9)}$$

$$C : P_u = \underbrace{31.4x_1 + 30.6x_2 + 31.6x_3}_{(0.43)} - \underbrace{10.5x_1x_2 - 17.1x_1x_3 - 14.2x_2x_3}_{(2.11)}$$

$$+ \underbrace{70.4x_1^2x_2x_3 + 64.4x_1x_2^2x_3 - 25.1x_1x_2x_3^2}_{(44.19)} \qquad 5.14$$

The measured, predicted and residuals for porosity are presented in Table 5.6. The residuals were generally very small values except for mix 613 and 341 for source L mixtures. Contour lines show the rise and drop in porosity based on aggregate proportions in Figure 5.12. The check for the adequacy of the model for all the data points showed that the *F*-ratio was 5.61 for source L mixtures against the table $F_{0.01,6,30}$-distribution of 3.47 (*p*-value = 0.0005). Since the *F*-ratio exceeds the distribution value, the model shows inadequacy, especially with the two points that were the greatest distance from the line of equality. For source C, the *F*-ratio was 1.18 and it was less than the table $F_{0.01,5,28}$-distribution of 3.75 (*p*-value = 0.343) so the model was suitable. Porosity estimates increased as contours move toward the vertices.

Figure 5.13 presents the relationships of the predicted and measured porosities to the line of equality for both sources. A lack-of –fit test for the validation points for source L gave an *F*-ratio of 5.42 with a table $F_{0.01,5,10}$–distribution of 5.64 (*p*-value = 0.011) which showed that the porosity model for source L was adequate when only the validation points were used in the lack-of-fit. The source C lack-of-fit test gave an *F*-ratio of 1.35 with a table $F_{0.01,4,8}$ = 7.01 (*p*-value = 0.33) which is not exceeded, and so confirms the adequacy of the model.

Table 5.6 Augmented Special Quartic Model: Measured, Predicted and Residual PCPC Effective Porosity

Aggregate Gradation ID		Source L Porosity Measured %	Source L Porosity Predicted %	Source L Porosity Residuals %	Source C Porosity Measured %	Source C Porosity Predicted %	Source C Porosity Residuals %
Design Points	8	32.2	32.2	0.0	31.3	31.4	0.0
	4	31.9	31.9	0.0	30.6	30.6	0.0
	38	33.7	33.7	0.0	31.5	31.6	0.0
	84	29.8	29.8	0.0	28.3	28.4	-0.1
	43	31.3	31.3	0.0	27.5	27.5	-0.1
	83	27.1	27.1	0.0	27.1	27.2	-0.1
	843	28.4	28.3	0.1	27.6	27.9	-0.3
	8843	29.5	29.5	0.0	29.0	28.8	0.2
	8443	29.0	29.0	-0.1	28.8	28.6	0.2
	8433	29.7	29.7	-0.1	27.9	27.7	0.2
Validation Points	89	30.4	30.2	0.2	30.1	28.8	1.3
	789	29.3	29.5	-0.1			
	613	25.3	28.5	-3.3	27.7	28.0	-0.2
	341	25.5	28.6	-3.1	28.4	28.6	-0.2
	135	28.4	29.2	-0.85	27.2	27.4	-0.2

*Aggregate proportions for #89: 0.2604 of (8), 0.7365 of (4), and 0.00311 of (38) and for #789: 0.2482 (8), 0.6932 (4), and 0.0586 (38). Darkened cells were additional aggregate blends that were not tested for source C.

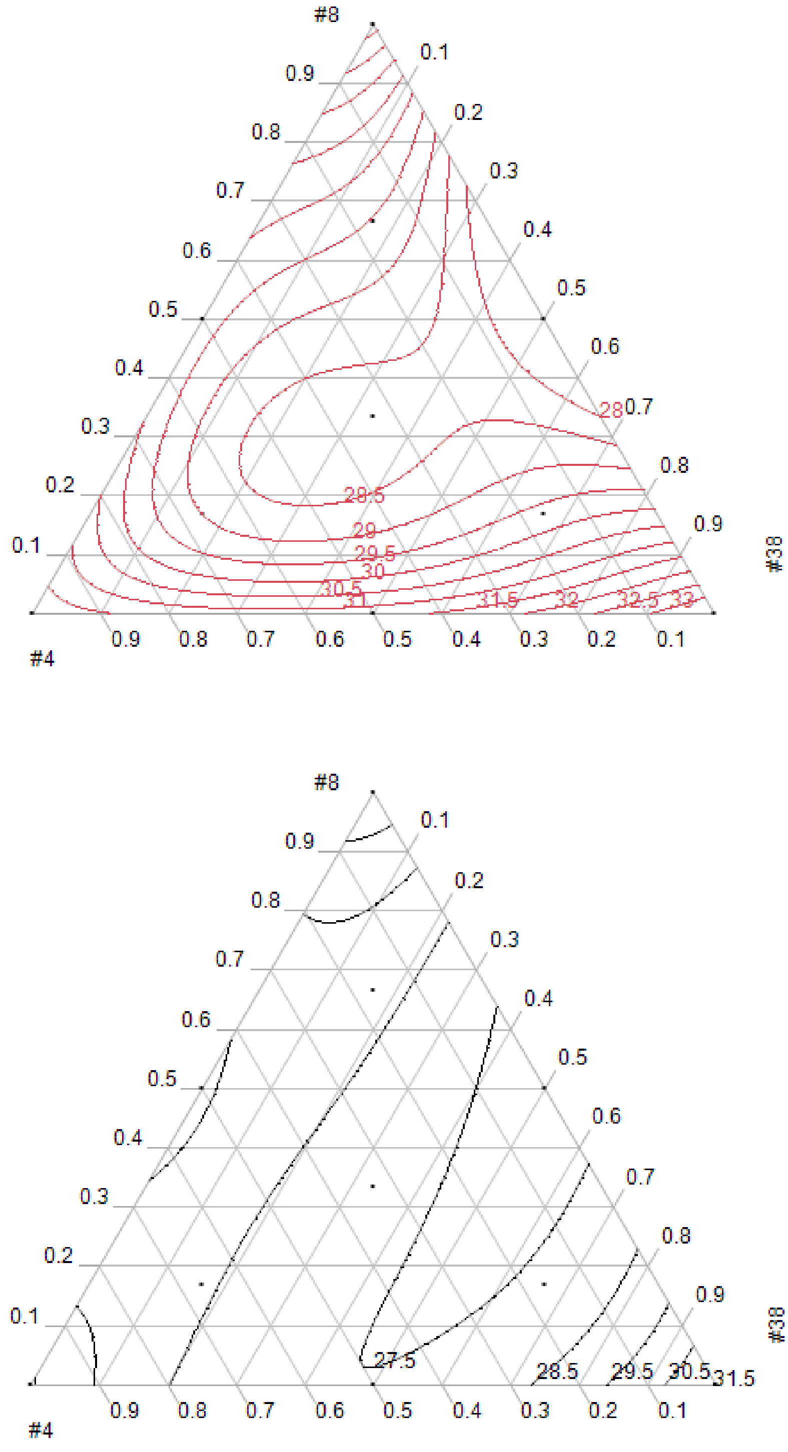

Figure 5.12 Special quartic model with contour lines of predicted porosity values (%) for aggregate L (top) and C (bottom).

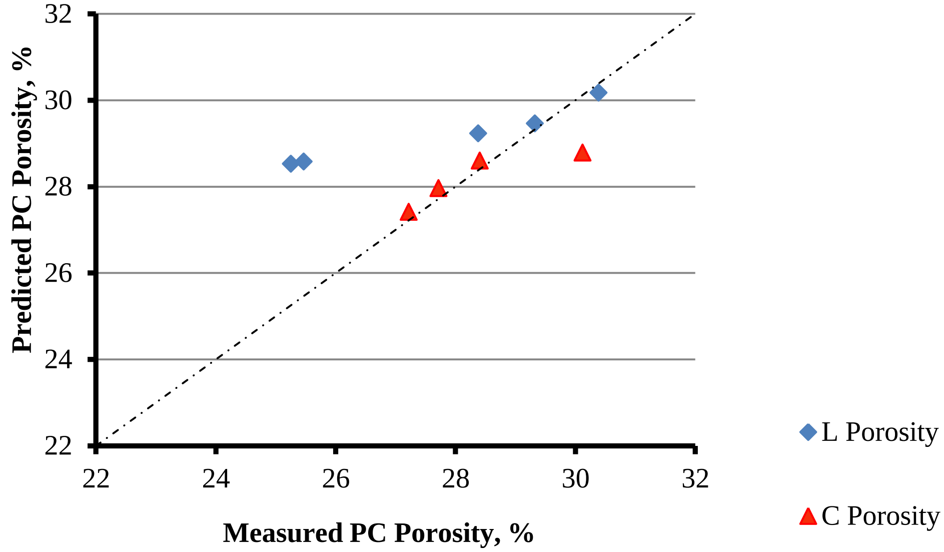

Figure 5.13 The relationship between the measured and predicted effective porosity of source L and C validation mixtures to the line of equality.

Compressive Strength

The compressive strength analysis with the augmented simplex-centroid design gave the special quartic models in equations 5.15 and 5.16 for source L mixtures and for source C, respectively.

$$L: f'_{cu} = \underbrace{718x_1 + 776x_2 + 714x_3}_{(107)} + \underbrace{418x_1x_2 + 1186x_1x_3 + 675x_2x_3}_{(523)} + \underbrace{10795x_1^2x_2x_3 + 14411x_1x_2^2x_3 - 20402x_1x_2x_3^2}_{(10923)} \qquad 5.15$$

$$C: f_{cu}^{'} = \underbrace{542x_1 + 641x_2 + 630x_3}_{(92)} + \underbrace{1128x_1x_2 + 574x_1x_3 + 1957x_2x_3}_{(449)}$$

$$+ \underbrace{299x_1^2x_2x_3 - 5938x_1x_2^2x_3 - 15210x_1x_2x_3^2}_{(9379)} \quad 5.16$$

The measured and predicted compressive strength values and residuals are shown in Table 5.7. The contour lines for sources L and C which show the change in compressive strengths relative to aggregate gradation are presented in Figure 5.14. The lack-of-fit test for all data points showed that the model for source L was adequate since the *F*-ratio of 1.40 was less than the $F_{0.01,6,30}$ -distribution of 3.47 with *p*-value 0.247. It was also adequate for source C with the *F*-ratio of 0.50 which was less than the $F_{0.01,5,28}$ -distribution of 3.75 with a *p*-value of 0.774. Compressive strength estimates decreased as contours moved toward the vertices.

Figure 5.15 shows the relationship of the predicted and the measured compressive strength values to the line of equality. Generally, the model underestimated the compressive strengths for source L mixtures but for source C mixtures, data points straddle the line of equality. A lack-of-fit test done for only the validation points showed the model for source L as adequate since the *F*-ratio of 1.34 was less than the $F_{0.01,5,10}$ -distribution of 5.64 with *p*-value 0.322. It was also adequate for source C with the *F*-ratio of 1.70 which was less than the $F_{0.01,4,8}$ -distribution of 7.01 with a *p*-value of 0.241.

Table 5.7 Augmented Special Quartic Model: Measured, Predicted and Residual PCPC Compressive Strength

		Source L			Source C		
Aggregate Gradation ID		Compressive Strength			Compressive Strength		
		Measured	Predicted	Residuals	Measured	Predicted	Residuals
		psi	psi	psi	psi	psi	psi
Design Points	8	705	718	-13.6	546	542	3.8
	4	762	776	-13.4	644	641	3.4
	38	701	714	-13.6	633	630	3.7
	84	825	852	-27.1	880	873	7.0
	43	887	914	-27.0	1131	1124	7.1
	83	986	1013	-26.9	736	729	6.8
	843	924	1047	-123.3	785	753	31.8
	8843	1122	1041	81.4	735	756	-20.9
	8443	1142	1061	81.4	842	863	-21.0
	8433	852	770	81.6	704	725	-21.1
Validation Points	89	877	851	26	903	834	70
	789	853	990	-137			
	613	1134	1014	120	580	718	-139
	341	1244	1148	96	768	835	-68
	135	1021	847	174	820	799	21

*Aggregate proportions for #89: 0.2604 of (8), 0.7365 of (4), and 0.00311 of (38) and for #789: 0.2482 (8), 0.6932 (4), and 0.0586 (38). Darkened cells were additional aggregate blends that were not tested for source C.

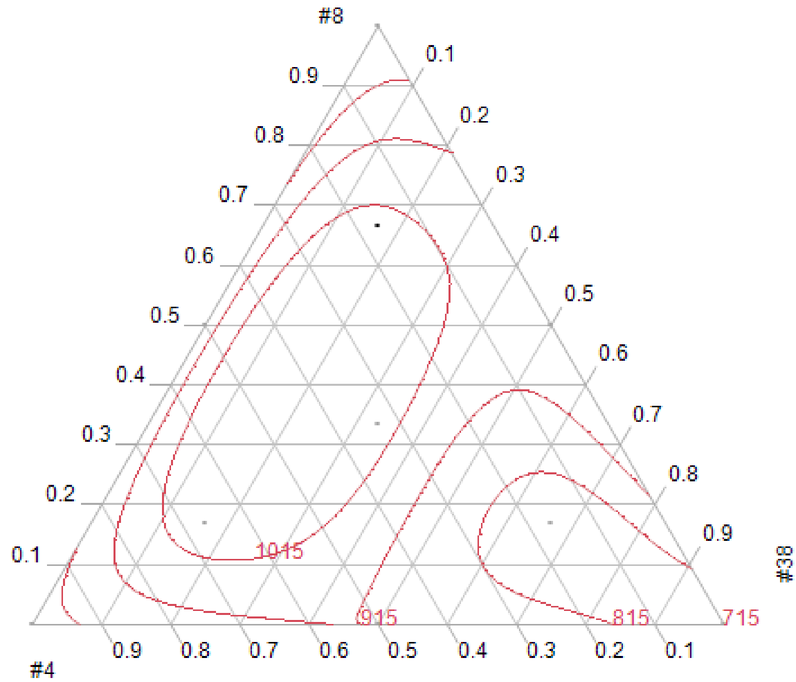

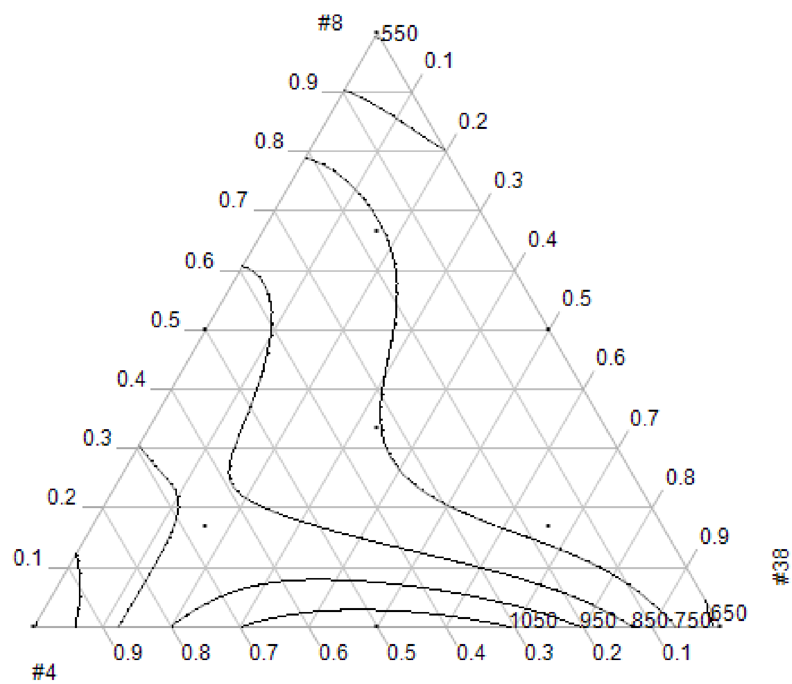

Figure 5.14 Augmented simple-centroid design triangle with contours representing compressive strength (psi) for aggregate source L (top) and C (bottom).

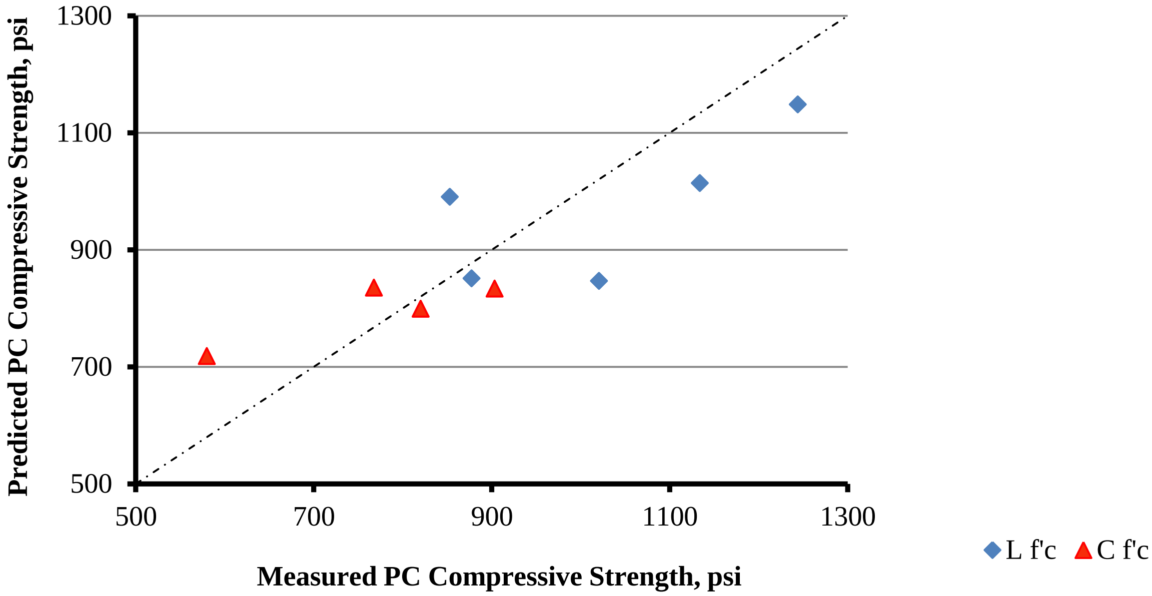

Figure 5.15 The relationship between the measured and predicted compressive strength of source L and C validation mixtures to the line of equality.

Split Tensile Strength

The special quartic polynomials produced by the augmented simplex-centroid design for the split tensile strength design points are given as equations 5.17 and 5.18 for sources L and C, respectively.

$$L: T_u = \underbrace{153x_1 + 182x_2 + 167x_3}_{(21)} - \underbrace{35x_1x_2 + 379x_1x_3 + 222x_2x_3}_{(105)} + \underbrace{1289x_1^2x_2x_3 + 4577x_1x_2^2x_3 - 1989x_1x_2x_3^2}_{(2192)} \quad 5.17$$

$$C : T_u = \underbrace{146x_1 + 180x_2 + 119x_3}_{(22)} + \underbrace{225x_1x_2 + 142x_1x_3 + 430x_2x_3}_{(109)}$$
$$- \underbrace{3588x_1^2x_2x_3 - 1085x_1x_2^2x_3 + 3717x_1x_2x_3^2}_{(2294)} \qquad 5.18$$

The measured and predicted values and the residuals of the split tensile strength are shown in Table 5.8. Generally, the split tensile strength residuals were larger for source L than for source C mixtures. The contour lines of the predicted split tensile strengths to the aggregate proportions in the mixtures are shown in Figure 5.16. Source L showed greater strength towards the centroid of the simplex triangle. Source C had a similar peak split tensile strength position only a little lower from the centroid and closer to the halfway point on the blend 4 axis or at blend 43 data point. The lack-of-fit test for source L showed that the split tensile strength model was marginally inadequate since its *F*-ratio of 3.52 was greater than the table value $F_{0,01,6,30}$ -distribution of 3.47 with a *p*-value = 0.009. But it was adequate for source C with a *F*-ratio of 0.58 which was less than the $F_{0.01,5,27}$ -distribution of 3.78 with a *p*-value = 0.714.

The relationships of the predicted and measured split tensile strengths to the line of equality were shown in Figure 5.17. The model underestimated the split tensile strengths for source L mixtures more than source C mixtures. The lack-of-fit test for the validation points for source L showed that the model was adequate since its *F*-ratio of 2.36 was less than the table value $F_{0,01,5,10}$ -distribution of 5.64 with a *p*-value = 0.116.

And it was adequate for source C with a *F*-ratio of 0.933 which was less than the $F_{0.01,4,8}$-distribution of 7.01 with a *p*-value = 0.491.

Table 5.8 Augmented Special Quartic Model: Measured, Predicted and Residual PCPC Split Tensile Strength

Aggregate Gradation ID		Source L Split Tensile Strength			Source C Split Tensile Strength		
		Measured	Predicted	Residuals	Measured	Predicted	Residuals
		psi	psi	psi	psi	psi	psi
Design Points	8	149	153	-4.7	145	146	-1.1
	4	178	182	-4.5	179	180	-1.1
	38	162	155	7.2	118	119	-1.4
	84	150	159	-9.1	218	220	-2.4
	43	221	230	-9.2	255	257	-2.2
	83	246	255	-8.8	166	168	-2.1
	843	237	278	-41.0	215	225	-9.9
	8843	256	229	27.2	171	164	6.3
	8443	288	261	27.1	235	229	6.8
	8433	254	227	27.1	243	236	6.9
Validation Points	89	245	171	73.4	187	215	-27.9
	789	245	216	29.3			
	613	253	245	8.0	182	173	8.8
	341	249	264	-15.2	204	200	3.9
	135	256	253	3.40	226	265	-39.0

*Aggregate proportions for #89: 0.2604 of (8), 0.7365 of (4), and 0.00311 of (38) and for #789: 0.2482 (8), 0.6932 (4), and 0.0586 (38). Darkened cells were additional aggregate blends that were not tested for source C.

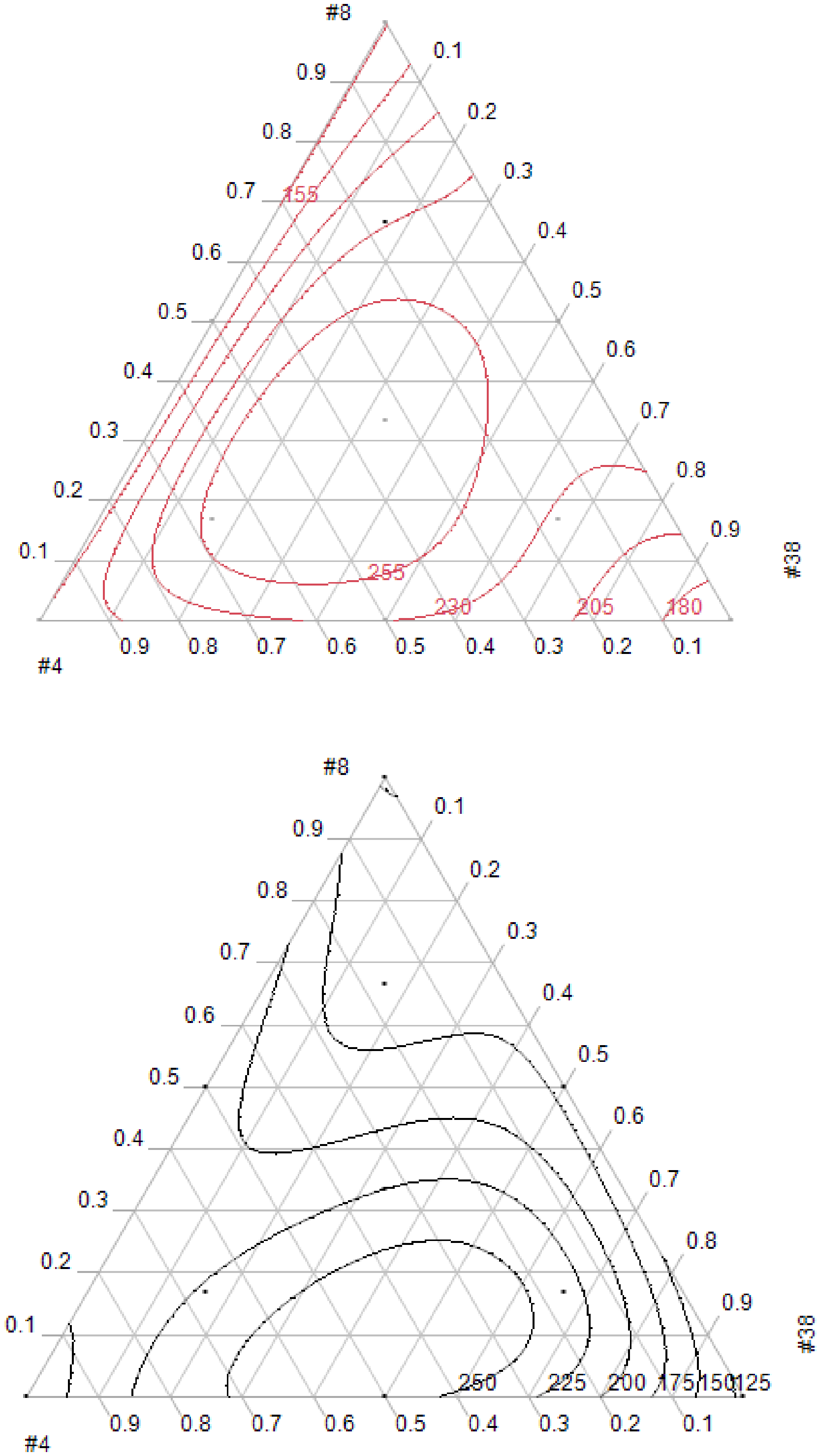

Figure 5.16 Augmented simple-centroid design triangle with contours of predicted split tensile strength (psi) for aggregate source L (top) and C (bottom).

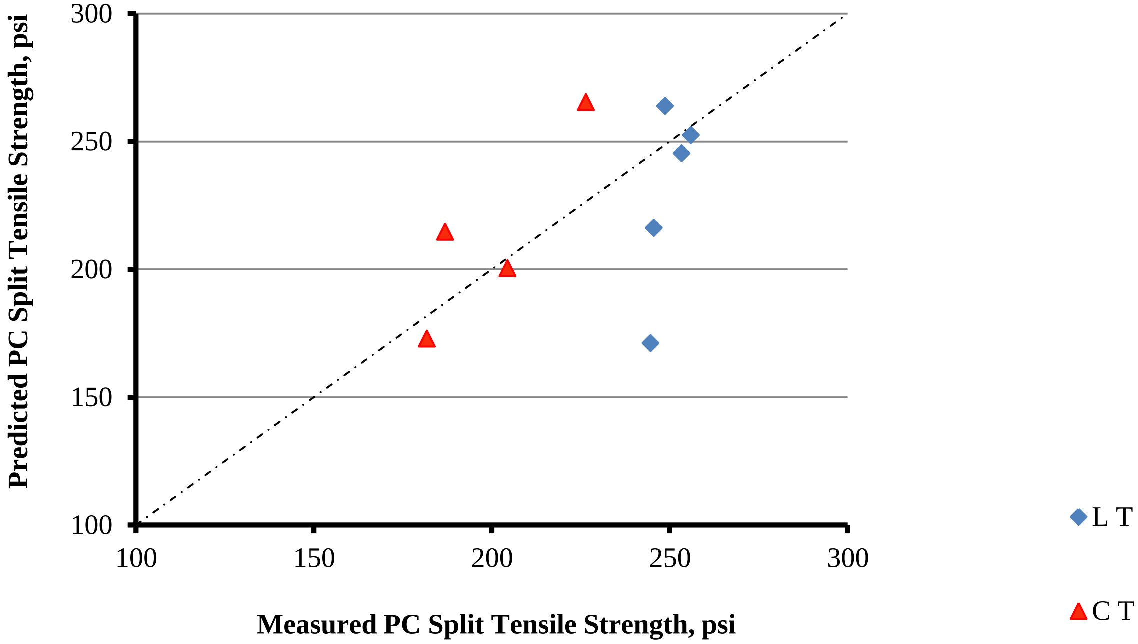

Figure 5.17 The relationship between the measured and predicted split tensile strength of source L and C validation mixtures to the line of equality.

Abrasion Loss

The special quartic models for predicting abrasion loss, *AL*, are given by equation 5.19 and 5.20 for sources L and C, respectively.

$$L: AL_u = \underbrace{45x_1 + 41x_2 + 40x_3}_{(2)} - \underbrace{25x_1x_2 - 39x_1x_3 - 32x_2x_3}_{(12)} \quad 5.19$$

$$- \underbrace{232x_1^2x_2x_3 + 187x_1x_2^2x_3 - 332x_1x_2x_3^2}_{(253)}$$

$$C : AL_u = \underbrace{46x_1 + 56x_2 + 71x_3}_{(3)} - \underbrace{17x_1x_2 - 19x_1x_3 - 139x_2x_3}_{(15)}$$

$$+ \underbrace{201x_1^2x_2x_3 - 325x_1x_2^2x_3 + 328x_1x_2x_3^2}_{(315)} \quad 5.20$$

The measured, predicted and residual values for abrasion loss are shown in Table 5.8. The abrasion loss residuals were comparable between the sources. Figure 5.18 shows the contour lines for source L with greater abrasion loss closer to the vertices or pure blends and reductions closer to the centroid. Source C had less loss closer to the central point between the 4 and 38 mixtures. The lack-of-fit analysis for all the data points showed that the model was adequate for source L with an *F*-ratio of 3.30 which was less than the table value $F_{0.01,6,30}$ -distribution of 3.47 with a *p*-value of 0.013. But for source C, the *F*-ratio of 6.44 exceeded the $F_{0.01,5,28}$ -distribution value of 3.75 with a *p*-value of 0.0004 and so was inadequate.

The relationships of the predicted and measured abrasion loss to the line of equality were shown in Figure 5.19. The model overestimated the abrasion loss for source L mixtures and had both over and under estimations for source C mixtures. The lack-of-fit test for only the validation points for source L showed that the model was inadequate since its *F*-ratio of 9.68 exceeded the table value $F_{0,01,5,10}$ -distribution of 5.64 with a *p*-value = 0.0014. This result differs from what was previously obtained when all the data points were included in the lack-of-fit test. More data points reduce the variance and may have helped in showing the model as adequate. For source C, the *F*-ratio of

4.22 was less than the $F_{0.01,4,8}$ -distribution of 7.01 with a *p*-value = 0.040 which gave evidence of the adequacy of the split tensile model.

Table 5.9 Augmented Special Quartic Model: Measured, Predicted and Residual PCPC Abrasion Loss

		Source L			Source C		
Aggregate Gradation ID		Abrasion Loss			Abrasion Loss		
		Measured	Predicted	Residuals	Measured	Predicted	Residuals
		%	%	%	%	%	%
Design Points	8	46	45	0.3	47	46	0.7
	4	41	41	0.4	57	56	0.7
	38	41	40	0.4	72	71	0.7
	84	38	37	0.7	48	47	1.4
	43	33	33	0.7	30	29	1.4
	83	34	33	0.7	55	54	1.4
	843	30	27	3.3	47	41	6.4
	8843	30	32	-2.2	42	46	-4.3
	8443	32	35	-2.2	32	36	-4.2
	8433	26	29	-2.2	46	50	-4.3
Validation Points	89	30	37	-7.5	47	50	-3.1
	789	32	36	-3.8			
	613	31	30	0.7	45	49	-3.8
	341	25	32	-6.4	48	40	7.8
	135	27	28	-0.62	46	39	6.5

*Aggregate proportions for #89: 0.2604 of (8), 0.7365 of (4), and 0.00311 of (38) and for #789: 0.2482 (8), 0.6932 (4), and 0.0586 (38). Darkened cells were additional aggregate blends that were not tested for source C.

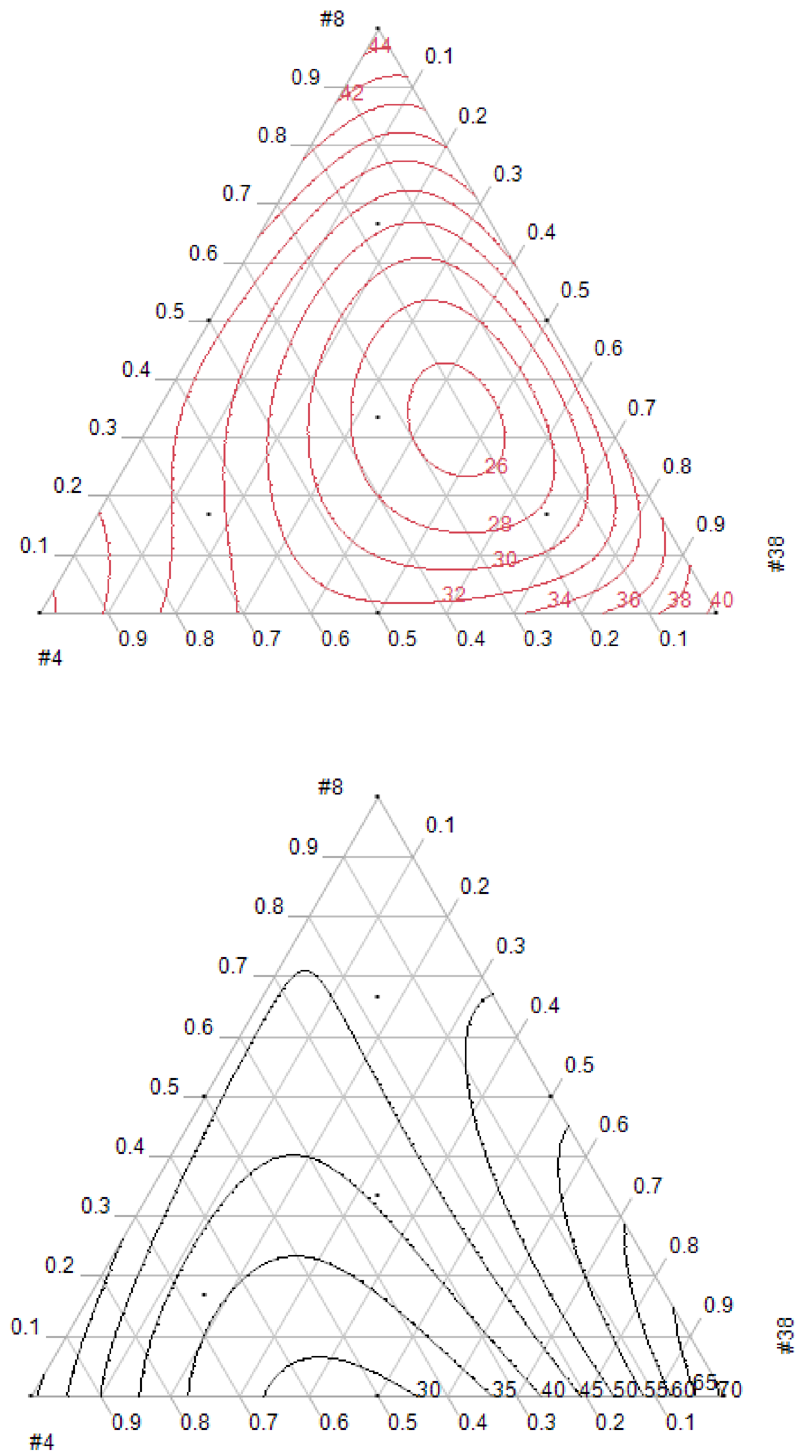

Figure 5.18 Augmented simple-centroid design triangle with contours of predicted abrasion loss (%) for aggregate source L (top) and C (bottom) mixtures.

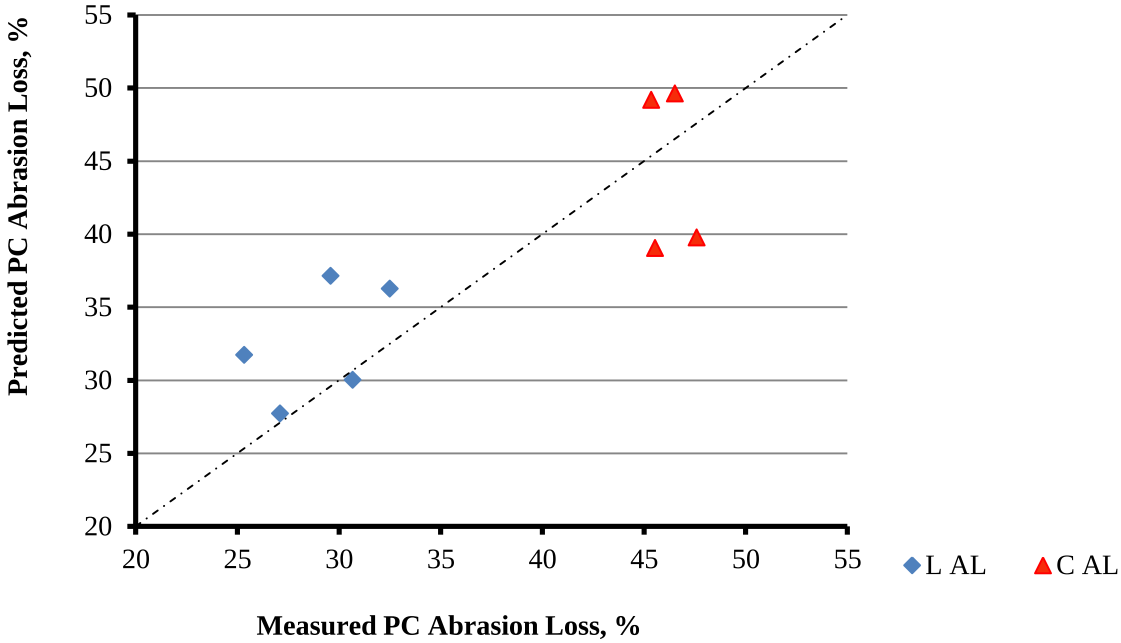

Figure 5.19 The relationship between the measured and predicted abrasion loss of source L and C validation mixtures to the line of equality.

A list of the lack-of-fit test results for the models are shown in Table 4.10. The first lack-of-fit results were done for all the data points using the special quartic model. The *F*-ratio and *F*-distribution were used to determine adequacy of the models, *p*-values could also be used. The second set of lack-of-fit results were done using the only the validation points, to the line of equality and the *p*-values. Since $\alpha = 0.01$, any *p*-value greater than 0.01 was considered adequate because there was no significant lack-of-fit. Some of the models such as porosity, split tensile strength and abrasion loss for source L had differing results when all points were tested as compared to when only the validation points were tested.

Table 5.10 Special Quartic Model Adequacy

		Source	F-Ratio	F-Distribution	α = 0.01	LOE *p*-value	α = 0.01
Aggregate Properties	Aggregate Density	L	4.35	2.64	Inadequate	0.0001	Inadequate
		C	1.67	3.47	Adequate	0.014	Adequate
		Adj. L	1.72	3.47	Adequate	0.175	Adequate
	Aggregate Void Content	L	4.35	2.64	Inadequate	0.0001	Inadequate
		C	2.04	3.47	Adequate	0.016	Adequate
		Adj. L	1.36	3.47	Adequate	0.151	Adequate
Pervious Concrete Properties	Unit Weight	L	1.28	3.63	Adequate	0.056	Adequate
		C	1.35	4.69	Adequate	0.026	Adequate
	Porosity	L	5.61	3.47	Inadequate	0.011	Adequate
		C	1.18	3.75	Adequate	0.33	Adequate
	Permeability	L	15.4	2.8	Inadequate	0.0001	Inadequate
		C	3.29	3.02	Inadequate	0.003	Inadequate
	Compressive Strength	L	1.4	3.47	Adequate	0.322	Adequate
		C	0.5	3.75	Adequate	0.241	Adequate
	Split Tensile Strength	L	3.52	3.47	Inadequate	0.116	Adequate
		C	0.58	3.78	Adequate	0.491	Adequate
	Abrasion Loss	L	3.3	3.47	Adequate	0.001	Inadequate
		C	3.75	6.44	Adequate	0.04	Adequate

The Research Product

The objective of this research was to investigate the correlations between the aggregate structure properties and the pervious concrete mixture properties for the purpose of optimizing a porous pavement mixture to meet desired performance criteria. This process of optimization can occur in two ways, (1) begin with a porous pavement property, for example permeability, use regression analysis to predict the aggregate property or other porous pavement or aggregate property that has a better relationship with the aggregate property. Then use the simplex-centroid design to link the aggregate property to the most suitable aggregate proportion for the porous mixture or (2) begin with a porous pavement property, and directly use the simplex-centroid design to link that property to the most suitable aggregate proportion for the porous mixture.

An example based on source L of what the final product of this study involves is illustrated in Figure 5.20. The pervious concrete property selected is a permeability of 1500 in./hr. and because the relationship to aggregate void content was weaker, the permeability to uniformity coefficient relationship is used. The predicted uniformity coefficient, C_u, is approximately 1.82. The C_u to aggregate void content relationship is used to predict the aggregate void content which was approximately 41.9%. This void content is taken to the augmented simplex-centroid design model (special quartic) and a possible aggregate proportion would be 30% of #8, 67% of #4, and 3% of #38. Suitable aggregate proportions could be found anywhere along the contour line that corresponded with the desired aggregate property. The other possible option is to link the permeability directly to the aggregate proportion from the simplex-centroid design as shown in Figure 5.21. Although the special quartic model did not test adequate from the lack-of-fit test, it was still capable of giving a contour line that permitted the same aggregate proportion as obtained in option (1). The proportion was again 30% of #8, 67% of #4, and 3% of #38. The other performance properties at the desired values are also available for consideration.

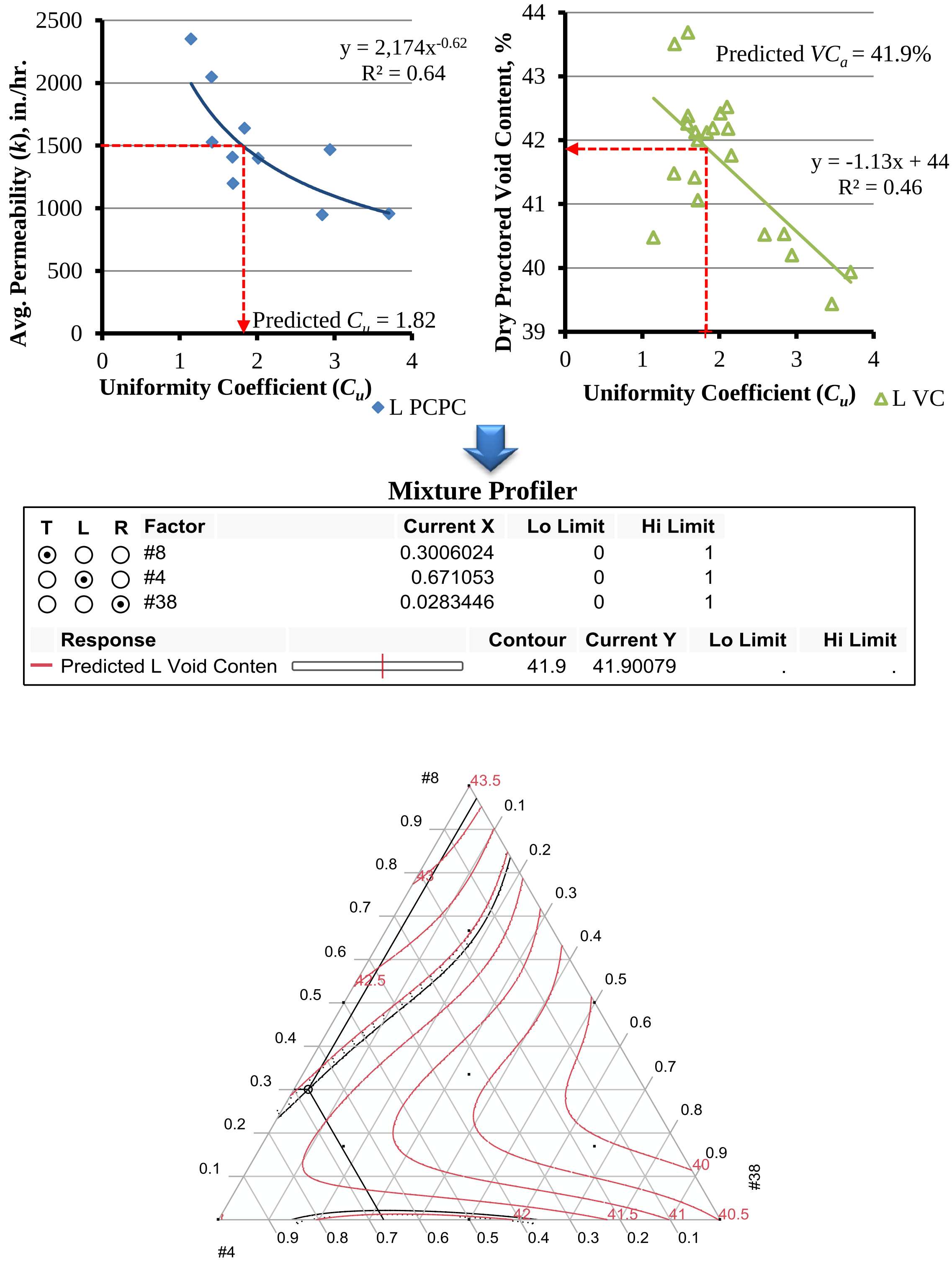

Figure 5.20 Option 1: Source L aggregate proportioning process from permeability, uniformity coefficient, and aggregate void content relationship to the aggregate proportion for the pervious concrete mixtures.

Mixture Profiler

T	L	R	Factor	Current X	Lo Limit	Hi Limit
⦿	○	○	#8	0.3006024	0	1
○	⦿	○	#4	0.671053	0	1
○	○	⦿	#38	0.0283446	0	1

Response	Contour	Current Y	Lo Limit	Hi Limit
Predicted L Perm	1500	1489.8483	.	.

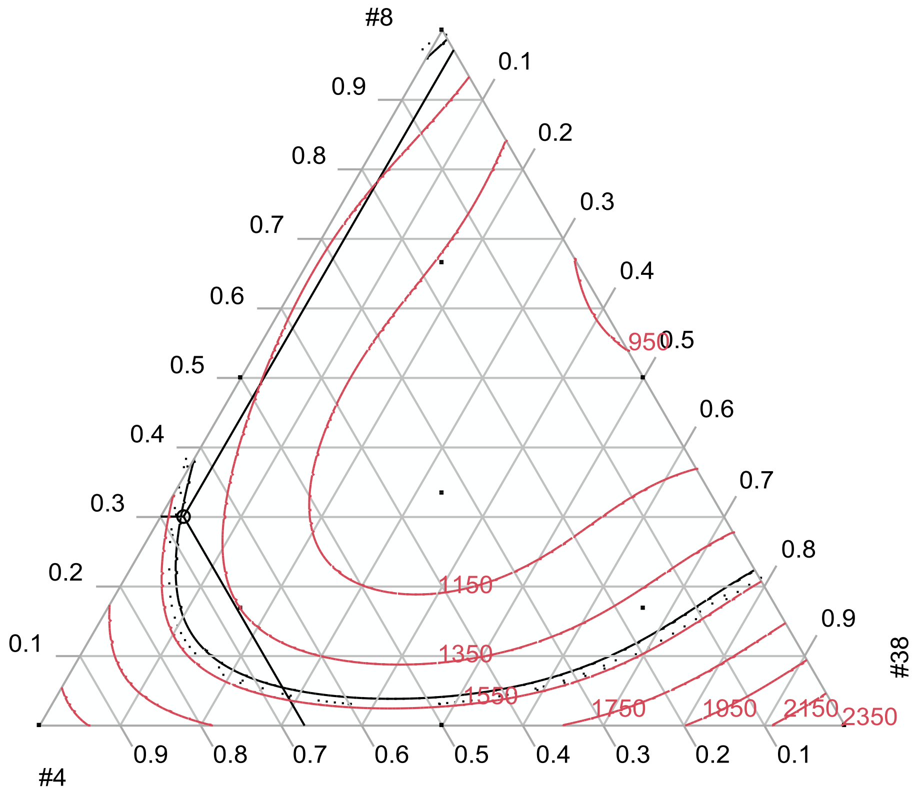

Figure 5.21 Option 2: Source L pervious concrete simplex-centroid triangle for with aggregate proportions at desired permeability of 1500 in./hr.

CHAPTER 6 : SUMMARY, CONCLUSIONS AND RECOMMENDATIONS

Summary

Pervious concrete has gained increasing attention because of its sustainable properties such as stormwater management, irrigating adjacent vegetation, and recharging aquifers. But along with these benefits are the concerns such as proper design, strength, maintenance and cost. These concerns create a need for an improved and in-depth understanding of the effects of the pervious concrete mixture components, namely aggregate gradation properties in meeting porous pavement performance requirements. The evaluation of an optimization process for the effective and efficient preparation of porous pavement mixtures based on aggregate structure will give versatility in presenting multiple aggregate gradations from which specifications can be met even when certain aggregate fractions might be scarce or unavailable.

In conducting this study, two (2) aggregate sources from South Carolina quarries were examined. It was beneficial to determine aggregate properties such as specific gravity, absorption, LA abrasion, shape, surface texture, uniformity coefficient, density, void content, CBR penetration stress, and compaction index. The experimental design was based on the augmented simplex-centroid design, SCD, therefore, three (3) aggregate sizes typical of pervious concrete mixtures were examined, the #8 (2.36 mm), the #4 (4.75 mm), and the ⅜ in. (9.5 mm). The aggregate gradations used were in accordance with the ten (10) design points of the augmented SCD along with 5 to 11 validation points for aggregate testing.

Pervious concrete mixtures were made with the same gradations as the ten design points along with an additional 4 to 5 validation points that had been used for aggregate testing. Fifteen sample groups of 12 pervious concrete specimens were made from aggregate source L, and fourteen sample groups were made from source C. The tests conducted on the fresh pervious concrete mixtures were unit weight and compaction index. The permeability test was conducted on all hardened specimens, to place them into subgroups of 3, with each group having permeability values that were not significantly different from the other subgroups. The other tests done on the hardened samples were effective porosity, compressive strength, split tensile strength and abrasion loss.

Regression analysis combined with the augmented simplex-centroid design was the statistical tools used to develop a methodology to optimize the preparation of pervious concrete mixtures based on aggregate properties. Pervious concrete properties were correlated to aggregate properties through regression analysis and the aggregate properties were linked to the aggregate proportions through the augmented simplex-centroid triangle. The other option examined used the augmented SCD to link the pervious concrete properties directly to the aggregate proportions. These methodologies have the potential of reducing the number of trial mixes necessary in choosing suitable gradations for porous paving mixtures. Therefore, time and effort can be saved and cost reduced with decisions based on data analysis rather than assumptions.

Conclusions

This laboratory investigation included a study of two (2) aggregate sources, L and C. These aggregate sources were tested and various properties were determined. Portland cement pervious concrete mixtures were prepared from these sources, and fresh and hardened samples were tested and various properties were determined. Relationships between the pervious concrete properties and the aggregate properties were examined. These properties were used in the development of the optimization process that incorporated both regression analyses and the augmented simplex-centroid design. Based on the results from this research to evaluate an optimization process for pervious concrete pavement mixtures based on aggregate structure, the following conclusions were made.

The shape, size and surface texture (particle index) were factors that gave evidence of controlling the pervious concrete results more so than properties like toughness determined by the LA abrasion procedure. Although source L had a lower aggregate LA abrasion value of 55% and a cement-aggregate ratio of 0.23 compared to the source C aggregate LA abrasion of 27% and cement-aggregate ratio of 0.25, source L generally had higher average compressive strengths and split tensile strengths, and lower abrasion loss values. Source L being the aggregate with a more rounded shape and lower particle index was more tightly packed thus reducing the voids. Source C with the higher LA abrasion value may transfer stresses more than absorbing it, leading to earlier failure.

Generally, aggregate source L had higher densities than source C because of its higher specific gravity. The density of the single-sized aggregates from both source L and C typically increased as the aggregate size increased whether compacted by the dry rodded or dry Proctor method. The same applied to the aggregate void content only that it decreased with the increase in aggregate size. Within the single-sized fractions, the dry rodded or dry Proctor compaction method did not generally produce significant differences between the densities and void contents for each aggregate source. This effect may relate to the uniformity of the aggregate gradation resisting compaction. But significant differences were evident in the binary and ternary blends. For these blends, source L had higher densities and lower void contents from dry rodding and source C had higher densities and lower void content from the dry Proctor. Since source L had a lower particle index, its surrounding particles were more inclined to heave with the impact from the Proctor hammer as compared to rodding, and because of the higher particle index of source C, it developed greater frictional resistance and needed more force, as provided by the Proctor hammer, to achieve compaction.

The compaction index which gave some indication of how sensitive a gradation was to compaction, showed source C increasing in pervious concrete compaction index as the aggregate compaction index increased. A different trend was observed for source L, where the pervious concrete compaction index decreased as the aggregate compaction increased. This may be linked to source L having a lower particle index, therefore being relatively smoother, and the cement paste acting more as a lubricating agent even in the unconsolidated state for the blends that were more sensitive to compaction, and so reducing the change in alternative unit weights based on equation 4.2. For source C, the higher particle index may have controlled the sensitivity to compaction over the lubricating properties of the cement paste.

The relationships of aggregate to aggregate properties showed very strong correlations between the aggregate void content and density for both dry rodded and dry Proctor. Generally, source L had better correlations when the dry aggregate was rodded and source C aggregate had better correlations when it was compacted using the dry Proctor method. Fair correlations existed between the uniformity coefficient to the aggregate rodded and Proctor density. The California Bearing Ratio penetration stress at 0.2 in. was greater for source C than source L for all blends because of the higher particle index and LA abrasion of source C.

The strength of the relationships between aggregate properties and pervious concrete properties depended on the aggregate source and the compaction technique used. Typically, the aggregate Proctor void content showed good to strong relationships with the pervious concrete alternative unit weight, gravimetric air content, and the effective porosity. The uniformity coefficient showed fairly good correlations with the pervious concrete alternative unit weight, average permeability, and effective porosity. Trends between these properties were as expected with increasing void content resulting in decreasing unit weight and increasing pervious concrete air content and porosity. Also, increasing uniformity coefficient resulted in increasing pervious concrete alternative unit weight, and decreasing permeability and porosity.

The relationships of pervious concrete to pervious concrete properties showed fair correlations between the pervious concrete permeability and porosity. Strong correlations existed between the effective porosity and the alternative unit weight. The relationship between the split tensile strength and the compressive strength was also fairly good; along with the relationship of the abrasion loss to the split tensile strength which relate to each other based on shear resistance.

The augmented simplex-centroid design was the statistical tool chosen because it gave more information on the responses within the triangle. Of the models tried, the special quartic was able to detect curvature with the response surface and, therefore gave the best fit for the points of interest within the triangle. Based on the lack-of-fit test, this model was over 50% adequate for source L and over 80% adequate for source C. This gave evidence that the augmented simplex-centroid special quartic model is a viable optimization process for pervious concrete pavement mixtures.

Recommendations

Based on this evaluation of an optimization process for the preparation of pervious concrete mixtures, the following recommendations are provided to generalize and to build upon the findings of this study.

Recommendation for Implementation

- The optimization process developed in this study could be used both in industry and academia to customize pervious concrete gradations to satisfy the needs of specified site conditions without having to produce large quantities of samples.

- An example of an aggregate gradation that may fit an application that required higher permeability and higher strength might be the binary pervious concrete mixture 43 made up of 50% #4 (4.75 mm) and 50% #38 (9.5 mm) from an aggregate source with a lower particle index. In this study, the 43 mixture generated average permeability results that was in the range of single-sized pervious concrete mixtures but had a higher average compressive and split tensile strength than the single-sized mixtures.

Recommendation for Future Research

- Examine the effects of adjusted cement-aggregate ratios with single-sized aggregate fractions that are typically used for pervious concrete mixtures to determine the best cement-aggregate ratios from which suitable ratios may be determined for additional gradations of these aggregate sizes.

- Examine the correlation between aggregate absorption and cement-aggregate ratio as a means of better understanding the effects of aggregate surface area. These two parameters should have a good correlation since surface area often explains the differences in absorption as aggregate size changes.

- Conduct this study with aggregate gradations all having a constant quantity of fines passing the #8 sieve (2.36 mm) that is typical of the gradations presently used for pervious concrete mixtures.

- Conduct a study similar to this for porous asphalt mixtures.

APPENDICES

APPENDIX A

Aggregate L: Loose Properties

Table A.1 Aggregate L: Loose Void Content Design Points

Aggregate Gradation		Aggregate L Loose Void Content (%) Individual	Average	Standard Deviation	Coefficient of Variation (%)
Design Blends	8	47.7	47.8	0.3	0.7
	8	48.2			
	8	47.7			
	4	45.2	45.0	0.5	1.1
	4	44.5			
	4	45.4			
	38	44.3	44.1	0.2	0.5
	38	44.3			
	38	43.9			
	84	46.2	46.1	0.1	0.2
	84	46.0			
	84	46.2			
	43	46.1	45.9	0.2	0.3
	43	45.8			
	43	45.8			
	83	44.1	43.6	0.4	0.9
	83	43.3			
	83	43.4			
	843	44.3	44.5	0.2	0.4
	843	44.7			
	843	44.4			
	8843	46.1	46.0	0.2	0.4
	8843	46.1			
	8843	45.8			
	8443	45.6	45.8	0.3	0.7
	8443	46.2			
	8443	45.6			
	8433	45.3	45.2	0.2	0.5
	8433	45.4			
	8433	44.9			

Table A.2 Aggregate L: Loose Void Content Validation Points

Aggregate Gradation		Aggregate L Loose Void Content (%)			
		Individual	Average	Standard Deviation	Coefficient of Variation (%)
Validation Points	8884	47.5	47.8	0.3	0.6
	8884	47.9			
	8884	48.0			
	8444	47.0	46.7	0.4	0.8
	8444	46.3			
	8444	46.9			
	4443	46.8	46.3	0.4	0.8
	4443	46.2			
	4443	46.0			
	4333	46.0	46.0	0.1	0.3
	4333	46.2			
	4333	45.9			
	8333	43.4	43.7	0.4	1.0
	8333	43.5			
	8333	44.2			
	8883	46.1	45.9	0.1	0.3
	8883	45.9			
	8883	45.8			
	89	46.3	46.1	0.2	0.4
	89	46.1			
	89	45.9			
	789	45.9	45.8	0.2	0.5
	789	45.9			
	789	45.5			
	613	45.3	45.2	0.2	0.5
	613	44.9			
	613	45.3			
	341	46.8	46.5	0.3	0.6
	341	46.4			
	341	46.2			
	135	45.4	45.2	0.3	0.8
	135	45.4			
	135	44.8			

Table A.3 Aggregate L: Loose Density Design Points

Aggregate Gradation		Aggregate L Loose Density (lb/ft^3) Individual	Average	Standard Deviation	Coefficient of Variation (%)
Design Points	8	85.8	85.5	0.51	0.6
	8	85.0			
	8	85.8			
	4	89.7	90.0	0.81	0.9
	4	90.9			
	4	89.4			
	38	91.6	91.8	0.34	0.4
	38	91.6			
	38	92.2			
	84	88.2	88.3	0.17	0.2
	84	88.5			
	84	88.2			
	43	88.5	88.8	0.25	0.3
	43	88.9			
	43	88.9			
	83	91.9	92.6	0.67	0.7
	83	93.1			
	83	92.9			
	843	91.3	91.1	0.28	0.3
	843	90.8			
	843	91.2			
	8843	88.5	88.6	0.31	0.3
	8843	88.4			
	8843	89.0			
	8443	89.2	88.9	0.54	0.6
	8443	88.2			
	8443	89.2			
	8433	89.8	90.0	0.41	0.5
	8433	89.7			
	8433	90.5			

Table A.4 Aggregate L: Loose Density Validation Point

Aggregate Gradation		Liberty Loose Density (lb/ft^3) Individual	Average	Standard Deviation	Coefficient of Variation (%)
Validation Points	8884	86.1	85.6	0.44	0.5
	8884	85.4			
	8884	85.3			
	8444	86.9	87.3	0.63	0.7
	8444	88.0			
	8444	87.0			
	4443	87.3	88.0	0.62	0.7
	4443	88.1			
	4443	88.5			
	4333	88.7	88.6	0.22	0.2
	4333	88.4			
	4333	88.8			
	8333	93.0	92.5	0.72	0.8
	8333	92.8			
	8333	91.6			
	8883	88.5	88.7	0.23	0.3
	8883	88.7			
	8883	89.0			
	89	88.0	88.3	0.34	0.4
	89	88.4			
	89	88.6			
	789	88.7	88.9	0.41	0.5
	789	88.6			
	789	89.4			
	613	89.8	90.0	0.36	0.4
	613	90.4			
	613	89.8			
	341	87.2	87.8	0.49	0.6
	341	87.9			
	341	88.2			
	135	89.6	89.9	0.56	0.6
	135	89.6			
	135	90.6			

Aggregate C: Loose Properties

Table A.5 Aggregate C: Loose Void Content Design Points

Aggregate Gradation		Aggregate C Void Content (%) Individual	Average	Standard Deviation	Coefficient of Variation (%)
Design Points	8	48.9	48.8	0.4	0.9
	8	49.2			
	8	48.3			
	4	47.6	47.2	0.4	0.7
	4	47.0			
	4	46.9			
	38	45.2	45.8	0.6	1.4
	38	46.5			
	38	45.6			
	84	45.8	46.1	0.4	0.8
	84	46.2			
	84	46.5			
	43	45.5	45.6	0.4	0.9
	43	46.0			
	43	45.3			
	83	44.7	43.9	0.7	1.6
	83	43.6			
	83	43.4			
	843	45.3	44.7	0.6	1.4
	843	44.9			
	843	44.1			
	8843	44.9	44.7	1.0	2.3
	8843	43.7			
	8843	45.7			
	8443	45.5	45.5	0.2	0.5
	8443	45.8			
	8443	45.3			
	8433	43.5	43.9	0.3	0.8
	8433	43.9			
	8433	44.2			

Table A.6 Aggregate C: Loose Void Content Validation Points

Aggregate Gradation		Aggregate C Void Content (%)			
		Individual	Average	Standard Deviation	Coefficient of Variation (%)
Validation Points	4443	45.9	46.2	0.675	1.5
	4443	47.0			
	4443	45.8			
	89	45.9	45.1	0.953	2.1
	89	45.4			
	89	44.1			
	613	45.7	45.4	0.514	1.1
	613	45.7			
	613	44.8			
	341	45.4	44.7	0.596	1.3
	341	44.6			
	341	44.2			
	135	43.8	44.4	0.598	1.3
	135	44.5			
	135	44.9			

Table A.7 Aggregate C: Loose Density Design Points

Aggregate Gradation		Aggregate C Loose Density (lb/ft^3)			
		Individual	Average	Standard Deviation	Coefficient of Variation (%)
Design Points	8	82.8	82.9	0.7	0.9
	8	82.3			
	8	83.7			
	4	85.1	85.8	0.6	0.7
	4	86.0			
	4	86.2			
	38	89.1	88.3	1.0	1.2
	38	87.1			
	38	88.5			
	84	88.0	87.4	0.6	0.7
	84	87.3			
	84	86.8			
	43	88.6	88.4	0.7	0.7
	43	87.7			
	43	89.0			
	83	89.8	91.1	1.2	1.3
	83	91.6			
	83	91.9			
	843	88.8	89.7	1.0	1.2
	843	89.6			
	843	90.8			
	8843	89.4	89.7	1.6	1.8
	8843	91.4			
	8843	88.2			
	8443	88.6	88.5	0.4	0.4
	8443	88.0			
	8443	88.8			
	8433	91.8	91.3	0.6	0.6
	8433	91.3			
	8433	90.7			

Table A.8 Aggregate C: Loose Density Validation Points

Aggregate Gradation		Aggregate C Loose Density (lb/ft^3) Individual	Average	Standard Deviation	Coefficient of Variation (%)
Validation Points	4443	87.9	87.4	1.1	1.3
	4443	86.1			
	4443	88.1			
	89	87.7	89.1	1.5	1.7
	89	88.7			
	89	90.8			
	613	88.1	88.6	0.8	0.9
	613	88.1			
	613	89.5			
	341	88.7	89.7	1.0	1.1
	341	89.9			
	341	90.6			
	135	91.4	90.4	1.0	1.1
	135	90.2			
	135	89.5			

APPENDIX B

Aggregate L: Dry Proctor Compaction

Table B.1 Aggregate L: Dry Proctor Void Content Design Points

Aggregate Gradation		Aggregate L Dry Proctor Void Content (%)			
		Individual	Average	Standard Deviation	Coefficient of Variation (%)
Design Points	8	43.7	43.5	0.4	0.8
	8	43.7			
	8	43.1			
	4	41.7	41.5	0.3	0.6
	4	41.2			
	4	41.5			
	38	40.7	40.5	0.2	0.6
	38	40.2			
	38	40.5			
	84	42.8	42.4	0.4	1.0
	84	42.5			
	84	41.9			
	43	41.9	42.1	0.3	0.7
	43	42.0			
	43	42.4			
	83	40.4	39.9	0.4	1.0
	83	39.8			
	83	39.6			
	843	40.6	40.5	0.2	0.4
	843	40.4			
	843	40.6			
	8843	41.8	42.1	0.3	0.8
	8843	42.5			
	8843	42.1			
	8443	41.6	41.4	0.5	1.1
	8443	41.7			
	8443	40.9			
	8433	40.4	40.2	0.3	0.8
	8433	40.4			
	8433	39.8			

Table B.2 Aggregate L: Dry Proctor Void Content Validation Points

Aggregate Gradation		Aggregate L Dry Proctor Void Content (%)			
		Individual	Average	Standard Deviation	Coefficient of Variation (%)
Validation Points	8884	44.1	43.7	0.4	0.8
	8884	43.5			
	8884	43.5			
	8444	42.7	42.5	0.2	0.4
	8444	42.5			
	8444	42.4			
	4443	42.8	42.3	0.6	1.5
	4443	41.5			
	4443	42.5			
	4333	42.4	42.0	0.4	0.9
	4333	42.1			
	4333	41.6			
	8333	39.7	39.4	0.2	0.6
	8333	39.2			
	8333	39.4			
	8883	42.3	42.4	0.1	0.3
	8883	42.4			
	8883	42.5			
	89	42.8	42.2	0.5	1.3
	89	41.9			
	89	41.9			
	789	41.9	41.8	0.2	0.4
	789	41.7			
	789	41.7			
	613	41.2	41.1	0.2	0.5
	613	40.9			
	613	41.1			
	341	42.2	42.2	0.0	0.1
	341	42.2			
	341	42.2			
	135	40.9	40.5	0.4	0.9
	135	40.3			
	135	40.3			

Table B.3 Aggregate L: Dry Proctor Density Design Points

Aggregate Gradation		Aggregate L Dry Proctor Density (lb/ft^3) Individual	Average	Standard Deviation	Coefficient of Variation (%)
Design Points	8	92.3	92.7	0.6	0.6
	8	92.3			
	8	93.3			
	4	95.5	95.9	0.4	0.5
	4	96.4			
	4	95.8			
	38	97.5	97.8	0.4	0.4
	38	98.2			
	38	97.7			
	84	93.8	94.4	0.7	0.7
	84	94.2			
	84	95.2			
	43	95.3	95.0	0.5	0.5
	43	95.2			
	43	94.5			
	83	97.9	98.6	0.6	0.6
	83	98.8			
	83	99.1			
	843	97.5	97.6	0.3	0.3
	843	97.9			
	843	97.4			
	8843	95.5	94.9	0.6	0.6
	8843	94.4			
	8843	94.9			
	8443	95.7	96.0	0.7	0.8
	8443	95.5			
	8443	96.9			
	8433	97.9	98.2	0.6	0.6
	8433	97.8			
	8433	98.8			

Table B.4 Aggregate L: Dry Proctor Density Validation Points

Aggregate Gradation		Aggregate L Dry Proctor Density (lb/ft^3) Individual	Average	Standard Deviation	Coefficient of Variation (%)
Validation Points	8884	91.6	92.3	0.6	0.6
	8884	92.6			
	8884	92.7			
	8444	93.9	94.2	0.3	0.3
	8444	94.3			
	8444	94.4			
	4443	93.8	94.7	1.1	1.1
	4443	95.8			
	4443	94.3			
	4333	94.6	95.2	0.6	0.7
	4333	95.2			
	4333	95.9			
	8333	99.1	99.5	0.4	0.4
	8333	99.8			
	8333	99.6			
	8883	94.7	94.5	0.2	0.2
	8883	94.6			
	8883	94.3			
	89	93.7	94.8	0.9	0.9
	89	95.2			
	89	95.3			
	789	95.2	95.5	0.3	0.3
	789	95.6			
	789	95.6			
	613	96.5	96.7	0.3	0.3
	613	97.1			
	613	96.6			
	341	94.7	94.8	0.1	0.1
	341	94.8			
	341	94.8			
	135	96.9	97.6	0.6	0.6
	135	98.0			
	135	98.0			

Aggregate L: Dry Rodded Compaction

Table B.5 Aggregate L: Dry Rodded Density Design Points

Aggregate Gradation		Aggregate L Dry Rodded Density (lb/ft^3) Individual	Average	Standard Deviation	Coefficient of Variation (%)
Design Points	8	92.6	92.8	0.3	0.4
	8	92.6			
	8	93.1			
	4	95.9	97.0	1.0	1.1
	4	97.3			
	4	97.9			
	38	97.8	97.8	0.3	0.3
	38	98.2			
	38	97.6			
	84	95.9	95.8	0.4	0.4
	84	96.1			
	84	95.3			
	43	97.7	97.6	0.2	0.2
	43	97.4			
	43	97.8			
	83	99.7	99.9	0.3	0.3
	83	100.1			
	83	99.7			
	843	99.2	99.5	0.3	0.3
	843	99.8			
	843	99.5			
	8843	97.1	97.1	0.1	0.1
	8843	97.1			
	8843	96.9			
	8443	97.0	97.0	0.0	0.0
	8443	97.0			
	8443	97.0			
	8433	99.6	99.4	0.2	0.2
	8433	99.3			
	8433	99.3			

Table B.6 Aggregate L: Dry Rodded Density Validation Points

Aggregate Gradation		Aggregate L Dry Rodded Density (lb/ft^3)			
		Individual	Average	Standard Deviation	Coefficient of Variation (%)
Validation Points	8884	92.9	93.7	0.9	1.0
	8884	93.5			
	8884	94.7			
	8444	96.0	95.8	0.2	0.2
	8444	95.6			
	8444	95.9			
	4443	96.2	97.0	0.7	0.7
	4443	97.4			
	4443	97.4			
	4333	99.5	99.5	0.2	0.2
	4333	99.3			
	4333	99.7			
	8333	100.4	100.4	0.0	0.0
	8333	100.4			
	8333	100.4			
	8883	96.4	96.7	0.3	0.3
	8883	97.0			
	8883	96.6			
	89	97.2	97.0	0.3	0.3
	89	97.1			
	89	96.6			
	789	97.3	98.0	0.7	0.8
	789	98.8			
	789	97.9			

Table B.7 Aggregate L: Dry Rodded Void Content Design Points

Aggregate Gradation		Aggregate L Dry Rodded Void Content (%) Individual	Average	Standard Deviation	Coefficient of Variation (%)
Design Points	8	43.5	43.4	0.2	0.5
	8	43.6			
	8	43.2			
	4	41.5	40.8	0.6	1.6
	4	40.6			
	4	40.2			
	38	40.5	40.5	0.2	0.5
	38	40.3			
	38	40.6			
	84	41.5	41.6	0.2	0.6
	84	41.4			
	84	41.8			
	43	40.4	40.5	0.1	0.3
	43	40.6			
	43	40.4			
	83	39.3	39.2	0.2	0.4
	83	39.0			
	83	39.2			
	843	39.6	39.3	0.2	0.5
	843	39.1			
	843	39.3			
	8843	40.8	40.8	0.1	0.1
	8843	40.8			
	8843	40.9			
	8443	40.8	40.8	0.0	0.0
	8443	40.8			
	8443	40.9			
	8433	39.4	39.5	0.1	0.2
	8433	39.6			
	8433	39.5			

Table B.8 Aggregate L: Dry Rodded Void Content Validation Points

Aggregate Gradation		Aggregate L Dry Rodded Void Content (%)			
		Individual	Average	Standard Deviation	Coefficient of Variation (%)
Validation Points	8884	43.4	42.9	0.6	1.3
	8884	43.0			
	8884	42.3			
	8444	41.4	41.5	0.1	0.3
	8444	41.6			
	8444	41.5			
	4443	41.3	40.8	0.4	1.0
	4443	40.6			
	4443	40.6			
	4333	39.4	39.4	0.1	0.3
	4333	39.5			
	4333	39.3			
	8333	38.9	38.9	0.0	0.0
	8333	38.9			
	8333	38.9			
	8883	41.2	41.1	0.2	0.4
	8883	40.9			
	8883	41.1			
	89	40.7	40.8	0.2	0.5
	89	40.7			
	89	41.1			
	789	40.7	40.2	0.5	1.1
	789	39.7			
	789	40.2			

Aggregate L: Compaction Index

Table B.9 Aggregate L: Compaction Index Design Points

Aggregate Gradation		Aggregate L Compaction index (%) Individual	Average	Standard Deviation	Coefficient of Variation (%)
Design Points	8	0.258	0.284	0.022	7.9
	8	0.295			
	8	0.299			
	4	0.231	0.234	0.019	8.3
	4	0.217			
	4	0.255			
	38	0.236	0.241	0.023	9.5
	38	0.266			
	38	0.221			
	84	0.223	0.243	0.030	12.5
	84	0.228			
	84	0.278			
	43	0.272	0.248	0.026	10.5
	43	0.252			
	43	0.220			
	83	0.243	0.240	0.012	4.9
	83	0.227			
	83	0.250			
	843	0.245	0.258	0.021	8.1
	843	0.283			
	843	0.248			
	8843	0.281	0.252	0.025	10.0
	8843	0.238			
	8843	0.238			
	8443	0.263	0.287	0.022	7.6
	8443	0.290			
	8443	0.307			
	8433	0.324	0.328	0.006	1.8
	8433	0.325			
	8433	0.335			

Table B.10 Aggregate L: Compaction Index Validation Points

Aggregate Gradation		Aggregate L Compaction index			
		Individual	Average	Standard Deviation	Coefficient of Variation (%)
Validation Points	8884	0.223	0.270	0.041	15.3
	8884	0.291			
	8884	0.297			
	8444	0.279	0.275	0.024	8.7
	8444	0.249			
	8444	0.297			
	4443	0.261	0.268	0.037	13.9
	4443	0.308			
	4443	0.235			
	4333	0.239	0.265	0.024	8.9
	4333	0.272			
	4333	0.285			
	8333	0.244	0.280	0.036	13.0
	8333	0.281			
	8333	0.316			
	8883	0.249	0.233	0.017	7.5
	8883	0.235			
	8883	0.214			
	89	0.231	0.257	0.023	8.8
	89	0.274			
	89	0.267			
	789	0.257	0.262	0.016	6.1
	789	0.281			
	789	0.250			
	613	0.268	0.269	0.004	1.4
	613	0.266			
	613	0.273			
	341	0.301	0.282	0.017	6.2
	341	0.278			
	341	0.266			
	135	0.294	0.307	0.022	7.2
	135	0.333			
	135	0.295			

Aggregate L: California Bearing Ratio Penetration Stress

Table B.11 Aggregate L: CBR Penetration Design Points

Aggregate Gradation		Aggregate L CBR Penetration Stress (psi) Individual	Average	Standard Deviation	Coefficient of Variation (%)
Design Points	8	92	98	6	5.8
	8	101			
	8	102			
	4	161	160	7	4.3
	4	152			
	4	166			
	38	231	236	12	5.0
	38	226			
	38	249			
	84	181	177	10	5.7
	84	183			
	84	165			
	43	241	234	18	7.7
	43	248			
	43	214			
	83	158	162	15	9.4
	83	150			
	83	179			
	843	159	159	14	8.6
	843	145			
	843	173			
	8843	159	153	7	4.3
	8843	154			
	8843	146			
	8443	194	204	27	13.1
	8443	234			
	8443	184			
	8433	214	178	37	20.9
	8433	180			
	8433	140			

Table B.12 Aggregate L: CBR Penetration Validation Points

Aggregate Gradation		Aggregate L CBR Penetration Stress psi Individual	Average	Standard Deviation	Coefficient of Variation (%)
Validation Points	89	179	177	16	9.3
	89	159			
	89	192			
	789	198	215	43	19.9
	789	184			
	789	264			
	613	158	162	15	9.4
	613	150			
	613	179			
	341	198	215	43	19.9
	341	184			
	341	264			
	135	171	161	17	10.8
	135	141			
	135	171			

Aggregate C: Dry Proctor Compaction

Table B.13 Aggregate C: Dry Proctor Void Content Design Points

Aggregate Gradation		Aggregate C Dry Proctor Void Content (%) Individual	Average	Standard Deviation	Coefficient of Variation (%)
Design Points	8	44.9	44.9	0.3	0.6
	8	45.2			
	8	44.6			
	4	43.3	42.7	0.5	1.2
	4	42.5			
	4	42.3			
	38	41.7	42.2	0.6	1.5
	38	42.1			
	38	42.9			
	84	42.1	41.9	0.4	1.1
	84	42.1			
	84	41.4			
	43	40.5	41.0	0.5	1.2
	43	41.1			
	43	41.4			
	83	39.6	39.3	0.3	0.8
	83	39.1			
	83	39.1			
	843	40.3	40.2	0.3	0.8
	843	40.3			
	843	39.8			
	8843	41.5	41.3	0.4	0.9
	8843	40.9			
	8843	41.5			
	8443	40.8	40.9	0.3	0.7
	8443	41.3			
	8443	40.7			
	8433	40.0	39.5	0.5	1.2
	8433	39.1			
	8433	39.6			

Table B.14 Aggregate C: Dry Proctor Void Content Validation Points

Aggregate Gradation		Aggregate C Dry Proctor Void Content (%)			
		Individual	Average	Standard Deviation	Coefficient of Variation (%)
Validation Points	4443	41.5	41.6	0.2	0.4
	4443	41.8			
	4443	41.5			
	89	40.9	40.9	0.0	0.1
	89	40.9			
	89	40.9			
	613	40.4	40.4	0.2	0.5
	613	40.7			
	613	40.2			
	341	41.0	40.8	0.4	1.1
	341	41.1			
	341	40.3			
	135	40.2	39.9	0.4	1.1
	135	40.0			
	135	39.4			

Table B.15 Aggregate C: Dry Proctor Density Design Points

Aggregate Gradation		Aggregate C Dry Proctor Density (lb/ft^3) Individual	Average	Standard Deviation	Coefficient of Variation (%)
Design Points	8	89.3	89.3	0.5	0.5
	8	88.8			
	8	89.7			
	4	92.1	93.0	0.8	0.9
	4	93.4			
	4	93.6			
	38	94.9	94.0	1.0	1.1
	38	94.2			
	38	93.0			
	84	93.9	94.3	0.7	0.8
	84	93.8			
	84	95.1			
	43	96.8	95.9	0.8	0.8
	43	95.7			
	43	95.2			
	83	98.1	98.6	0.5	0.5
	83	98.9			
	83	98.9			
	843	96.9	97.2	0.5	0.5
	843	96.9			
	843	97.8			
	8843	94.8	95.2	0.6	0.7
	8843	95.9			
	8843	94.9			
	8443	96.1	95.9	0.5	0.5
	8443	95.4			
	8443	96.3			
	8433	97.6	98.3	0.7	0.8
	8433	99.1			
	8433	98.2			

Table B.16 Aggregate C: Dry Proctor Density Validation Points

Aggregate Gradation		Aggregate C Dry Proctor Density (lb/ft^3) Individual	Average	Standard Deviation	Coefficient of Variation (%)
Validation Points	4443	95.1	94.9	0.3	0.3
	4443	94.6			
	4443	95.0			
	89	95.9	95.9	0.1	0.1
	89	95.8			
	89	95.9			
	613	96.7	96.7	0.4	0.4
	613	96.3			
	613	97.0			
	341	95.8	96.1	0.7	0.7
	341	95.6			
	341	96.9			
	135	97.2	97.7	0.7	0.7
	135	97.5			
	135	98.5			

Aggregate C: Dry Rodded Compaction

Table B.17 Aggregate C: Dry Rodded Density Design Points

Aggregate Gradation		Aggregate C Dry Rodded Density (lb/ft^3)			
		Individual	Average	Standard Deviation	Coefficient of Variation (%)
Design Points	8	88.7	88.8	0.3	0.3
	8	89.2			
	8	88.6			
	4	92.8	92.9	0.1	0.1
	4	93.1			
	4	92.9			
	38	93.6	93.3	0.4	0.4
	38	93.5			
	38	92.9			
	84	92.9	93.2	0.4	0.4
	84	93.1			
	84	93.7			
	43	95.3	94.4	0.8	0.9
	43	94.3			
	43	93.6			
	83	96.8	97.5	0.7	0.7
	83	98.2			
	83	97.7			
	843	96.1	98.0	2.4	2.4
	843	100.7			
	843	97.2			
	8843	94.1	94.0	0.3	0.3
	8843	94.3			
	8843	93.7			
	8443	95.1	95.3	0.2	0.2
	8443	95.5			
	8443	95.2			
	8433	96.6	96.9	0.3	0.3
	8433	96.9			
	8433	97.3			

Table B.18 Aggregate C: Dry Rodded Density Validation Points

Aggregate Gradation		Aggregate C Dry Rodded Density (lb/ft^3)			
		Individual	Average	Standard Deviation	Coefficient of Variation (%)
Validation Points	4443	94.3	94.1	0.2	0.2
	4443	93.9			
	4443	94.1			
	89	94.8	94.6	0.2	0.2
	89	94.4			
	89	94.6			
	613	95.8	95.8	0.1	0.1
	613	95.7			
	613	95.7			
	341	95.7	95.4	0.5	0.5
	341	94.9			
	341	95.7			
	135	97.4	97.1	0.4	0.4
	135	97.1			
	135	96.6			

Table B.19 Aggregate C: Dry Rodded Void Content Design Points

Aggregate Gradation		Aggregate C Dry Rodded Void Content (%)			
		Individual	Average	Standard Deviation	Coefficient of Variation (%)
Design Points	8	45.3	45.2	0.2	0.4
	8	45.0			
	8	45.3			
	4	42.9	42.8	0.1	0.2
	4	42.7			
	4	42.8			
	38	42.5	42.7	0.2	0.6
	38	42.5			
	38	42.9			
	84	42.8	42.5	0.3	0.6
	84	42.6			
	84	42.3			
	43	41.4	41.9	0.5	1.2
	43	42.0			
	43	42.4			
	83	40.4	39.9	0.4	1.1
	83	39.5			
	83	39.9			
	843	40.8	39.6	1.5	3.7
	843	38.0			
	843	40.2			
	8843	42.0	42.0	0.2	0.4
	8843	41.9			
	8843	42.2			
	8443	41.4	41.3	0.1	0.3
	8443	41.2			
	8443	41.4			
	8433	40.6	40.4	0.2	0.5
	8433	40.4			
	8433	40.2			

Table B.20 Aggregate C: Dry Rodded Void Content Validation Points

Aggregate Gradation		Aggregate C Dry Rodded Void Content (%)			
		Individual	Average	Standard Deviation	Coefficient of Variation (%)
Validation Points	4443	42.0	42.1	0.1	0.3
	4443	42.2			
	4443	42.1			
	89	41.6	41.7	0.1	0.3
	89	41.8			
	89	41.7			
	613	41.0	41.0	0.0	0.1
	613	41.0			
	613	41.0			
	341	41.0	41.2	0.3	0.7
	341	41.5			
	341	41.0			
	135	40.0	40.3	0.2	0.6
	135	40.3			
	135	40.5			

Aggregate C: Compaction Index

Table B.21 Aggregate C: Compaction Index Design Points

Aggregate Gradation		Aggregate C Compaction index: Individual	Average	Standard Deviation	Coefficient of Variation (%)
Design Points	8	0.261	0.254	0.012	4.7
	8	0.261			
	8	0.240			
	4	0.277	0.289	0.011	3.7
	4	0.294			
	4	0.296			
	38	0.233	0.232	0.054	23.3
	38	0.285			
	38	0.177			
	84	0.235	0.277	0.051	18.5
	84	0.261			
	84	0.334			
	43	0.327	0.299	0.043	14.4
	43	0.320			
	43	0.249			
	83	0.334	0.302	0.027	9.1
	83	0.292			
	83	0.282			
	843	0.323	0.298	0.023	7.8
	843	0.295			
	843	0.277			
	8843	0.217	0.223	0.044	19.8
	8843	0.182			
	8843	0.269			
	8443	0.302	0.299	0.004	1.4
	8443	0.294			
	8443	0.301			
	8433	0.230	0.282	0.045	15.9
	8433	0.313			
	8433	0.301			

Table B.22 Aggregate C: Compaction Index Validation Points

Aggregate Gradation		Aggregate C Compaction index			
		Individual	Average	Standard Deviation	Coefficient of Variation (%)
Validation Points	4443	0.286	0.299	0.034	11.3
	4443	0.338			
	4443	0.274			
	89	0.327	0.274	0.061	22.2
	89	0.287			
	89	0.207			
	613	0.345	0.324	0.024	7.3
	613	0.330			
	613	0.298			
	341	0.284	0.256	0.027	10.6
	341	0.230			
	341	0.252			
	135	0.233	0.294	0.064	21.7
	135	0.289			
	135	0.361			

Aggregate C: California Bearing Ratio Penetration Stress

Table B.23 Aggregate C: CBR Design Points

Aggregate Gradation		Aggregate C CBR Penetration Stress psi Individual	Average	Standard Deviation	Coefficient of Variation (%)
Design Points	8	279	201	76	37.7
	8	127			
	8	198			
	4	316	264	47	17.7
	4	252			
	4	225			
	38	498	383	100	26.2
	38	322			
	38	328			
	84	290	239	45	18.7
	84	220			
	84	208			
	43	338	376	83	22.2
	43	319			
	43	472			
	83	203	222	24	10.7
	83	248			
	83	214			
	843	261	251	22	8.8
	843	226			
	843	266			
	8843	231	264	37	14.0
	8843	258			
	8843	304			
	8443	229	274	46	16.9
	8443	271			
	8443	321			
	8433	371	299	79	26.5
	8433	214			
	8433	313			

Table B.24 Aggregate C: CBR Validation Points

Aggregate Gradation		Aggregate C CBR Penetration Stress psi Individual	Average	Standard Deviation	Coefficient of Variation (%)
Validation Points	4443	366	350	16	4.7
	4443	333			
	4443	350			
	89	272	227	45	19.6
	89	183			
	89	225			
	613	204	214	20	9.2
	613	237			
	613	201			
	341	226	258	59	22.9
	341	221			
	341	326			
	135	226	258	59	22.9
	135	221			
	135	326			

<u>APPENDIX C</u>

Source L: Loose Pervious Concrete Properties

Table C.1 Source L: Pervious Concrete Loose Unit Weight Design Points

Aggregate Gradation		L: Loose Pervious Concrete Unit Weight (lb/ft^3)			
		Individual	Average	Standard Deviation	Coefficient of Variation (%)
Design Points	8	85	87	3	2.9
	8	90			
	8	86			
	4	85	88	5	5.4
	4	91			
	4				
	38	85	87	4	4.1
	38	91			
	38	84			
	84	88	87	2	2.9
	84	89			
	84	85			
	43	87	86	1	0.9
	43	86			
	43	85			
	83	87	89	1	1.7
	83	89			
	83	90			
	843	89	89	0	0.2
	843	89			
	843	89			
	8843	94	94	0	0.2
	8843	95			
	8843				
	8443	97	97	4	4.1
	8443	92			
	8443	100			
	8433	93	94	1	1.3
	8433	94			
	8433	95			

Table C.2 Source L: Pervious Concrete Loose Unit Weight Validation Points

Aggregate Gradation		L: Loose Pervious Concrete Unit Weight (lb/ft^3)			
		Individual	Average	Standard Deviation	Coefficient of Variation (%)
Validation Points	89	87	87	1	0.7
	89	88			
	89	87			
	789	89	88	1	1.5
	789	87			
	789	87			
	613	94	93	1	1.0
	613	93			
	613				
	341	96	96	1	0.6
	341	95			
	341				
	135	94	94	1	0.6
	135	94			
	135				

Table C.3 Source C: Pervious Concrete Loose Unit Weight Design Points

Aggregate Gradation		C: Loose Pervious Concrete Unit Weight (lb/ft^3)			
		Individual	Average	Standard Deviation	Coefficient of Variation (%)
Design Points	8	85	86	1	0.9
	8	86			
	8				
	4	86	87	2	2.2
	4	88			
	4				
	38	88	88	0	0.3
	38	88			
	38				
	84	89	88	1	1.3
	84	87			
	84				
	43	93	93	1	0.8
	43	94			
	43				
	83	89	90	0	0.3
	83	90			
	83				
	843	89	89	1	0.7
	843	88			
	843				
	8843	89	89	0	0.5
	8843	89			
	8843				
	8443	87	88	1	1.6
	8443	89			
	8443				
	8433	90	90	0	0.3
	8433	90			
	8433				

Table C.4 Source C: Pervious Concrete Loose Unit Weight Validation Points

Aggregate Gradation		C: Loose Pervious Concrete Unit Weight (lb/ft^3)			
		Individual	**Average**	**Standard Deviation**	**Coefficient of Variation (%)**
Validation Points	89	89	88	1	1.1
	89	87			
	89				
	613	92	91	2	1.7
	613	90			
	613				
	341	88	88	1	0.6
	341	88			
	341				
	135	89	90	1	0.7
	135	90			
	135				

APPENDIX D

Source L: Pervious Concrete Compacted Properties

Table D.1 Source L: Pervious Concrete ASTM C1688 Unit Weight Design Points

Aggregate Gradation		L: Compacted PCPC ASTM C1688 Unit Weight (lb/ft^3) Individual	Average	Standard Deviation	Coefficient of Variation (%)
Design Points	8	112	113	1	0.68
	8	113			
	8	112			
	4	114	114	0	0.02
	4	114			
	4				
	38	115	116	1	0.78
	38	116			
	38	116			
	84	116	116	1	1.07
	84	114			
	84	116			
	43	117	117	2	1.53
	43	115			
	43	119			
	83	122	121	1	1.11
	83	122			
	83	120			
	843	122	121	1	0.96
	843	120			
	843	122			
	8843	117	118	2	1.62
	8843	120			
	8843				
	8443	119	119	2	1.45
	8443	118			
	8443	121			
	8433	119	120	1	0.77
	8433	120			
	8433				

Table D.2 Source L: Pervious Concrete ASTM C1688 Unit Weight Validation Points

Aggregate Gradation		L: Compacted PCPC ASTM C1688 Unit Weight (lb/ft^3)			
		Individual	Average	Standard Deviation	Coefficient of Variation (%)
Validation Points	89	119	118	2	1.40
	89	118			
	89	116			
	789	118	118	1	0.65
	789	117			
	789	119			
	613	124	124	1	0.40
	613	124			
	613				
	341	121	122	1	0.42
	341	122			
	341				
	135	122	122	1	0.64
	135	123			
	135				

Table D.3 Source L: Pervious Concrete Alternative Unit Weight Design Points

Aggregate Gradation		L: Compacted PCPC Alternative Unit Weight (lb/ft^3)			
		Individual	Average	Standard Deviation	Coefficient of Variation (%)
Design Points	8	109	111	1	1.33
	8	112			
	8	111			
	4	110	110	0	0.14
	4	110			
	4				
	38	112	112	1	0.60
	38	112			
	38	111			
	84	116	114	1	1.30
	84	113			
	84	114			
	43	115	115	0	0.39
	43	114			
	43	115			
	83	121	120	1	0.94
	83	120			
	83	119			
	843	118	118	2	1.93
	843	116			
	843	121			
	8843	116	117	2	1.56
	8843	118			
	8843				
	8443	118	117	1	0.95
	8443	116			
	8443	117			
	8433	115	117	1	1.02
	8433	117			
	8433	118			

Table D.4 Source L: Pervious Concrete Alternative Unit Weight Validation Points

Aggregate Gradation		L: Compacted PCPC Alternative Unit Weight (lb/ft^3)			
		Individual	**Average**	**Standard Deviation**	**Coefficient of Variation (%)**
Validation Points	89	116	115	1	0.72
	89	115			
	89	115			
	789	116	116	2	1.43
	789	114			
	789	117			
	613	120	120	0	0.06
	613	120			
	613				
	341	119	118	1	0.90
	341	118			
	341				
	135	117	118	1	0.85
	135	119			
	135				

Table D.5 Source L: Pervious Concrete Compaction Index Design Points

Aggregate Gradation		L: PCPC Compaction Index			
		Individual	Average	Standard Deviation	Coefficient of Variation (%)
Design Points	8	0.939	0.929	0.061	6.61
	8	0.864			
	8	0.986			
	4	1.014	0.885	0.183	20.64
	4	0.755			
	4				
	38	1.103	1.006	0.135	13.38
	38	0.853			
	38	1.063			
	84	1.118	1.080	0.138	12.76
	84	0.928			
	84	1.196			
	43	1.116	1.157	0.047	4.07
	43	1.147			
	43	1.209			
	83	1.344	1.245	0.104	8.31
	83	1.255			
	83	1.137			
	843	1.149	1.178	0.084	7.11
	843	1.112			
	843	1.272			
	8843	0.854	0.900	0.064	7.17
	8843	0.945			
	8843				
	8443	0.833	0.825	0.132	16.03
	8443	0.953			
	8443	0.689			
	8433	0.909	0.908	0.001	0.14
	8433	0.907			
	8433	0.907			

Table D.6 Source L: Pervious Concrete Compaction Index Validation Points

Aggregate Gradation		L: PCPC Compaction Index Individual	Average	Standard Deviation	Coefficient of Variation (%)
Validation Points	89	1.184	1.122	0.057	5.06
	89	1.073			
	89	1.108			
	789	1.081	1.117	0.064	5.76
	789	1.080			
	789	1.192			
	613	1.028	1.056	0.040	3.75
	613	1.084			
	613				
	341	0.932	0.918	0.019	2.12
	341	0.904			
	341				
	135	0.921	0.965	0.062	6.44
	135	1.008			
	135				

Table D.7 Source L: PC Permeability Design Points for Porosity Specimens

Aggregate Gradation		L Permeability for Porosity PCPC Specimens			
		Individual	Average	Standard Deviation	Coefficient of Variation (%)
Design Points	8	1648	1531	102	6.69
	8	1490			
	8	1456			
	4	2095	2042	93	4.57
	4	1935			
	4	2098			
	38	2505	2346	193	8.24
	38	2403			
	38	2131			
	84	1588	1396	166	11.87
	84	1297			
	84	1305			
	43	1426	1632	193	11.83
	43	1662			
	43	1808			
	83	979	963	67	7.00
	83	889			
	83	1021			
	843	796	947	139	14.62
	843	1068			
	843	979			
	8843	1301	1215	233	19.15
	8843	1392			
	8843	952			
	8443	1417	1410	165	11.72
	8443	1242			
	8443	1572			
	8433	1540	1457	163	11.16
	8433	1561			
	8433	1270			

Table D.8 Source L: PC Permeability Validation Points for Porosity Specimens

Aggregate Gradation		L PCPC Permeability for Porosity Specimens (in./hr.)			
		Individual	Average	Standard Deviation	Coefficient of Variation (%)
Validation Points	89	1373	1391	191	13.7
	89	1590			
	89	1209			
	789	1249	1352	111	8.2
	789	1469			
	789	1337			
	613	1305	1102	223	20.2
	613	864			
	613	1137			
	341	1230	1234	124	10.1
	341	1111			
	341	1360			
	135	1836	1599	209	13.1
	135	1526			
	135	1436			

Table D.9 Source L: PC Permeability Design Points for Compressive Strength Specimens

Aggregate Gradation		L PCPC Permeability for Compressive Strength Specimens (in./hr.)			
		Individual	Average	Standard Deviation	Coefficient of Variation (%)
Design Points	8	1588	1527	61	4.0
	8	1529			
	8	1465			
	4	2172	2044	111	5.4
	4	1989			
	4	1970			
	38	2471	2352	129	5.5
	38	2215			
	38	2369			
	84	1352	1400	47	3.3
	84	1405			
	84	1445			
	43	1663	1630	57	3.5
	43	1663			
	43	1565			
	83	976	955	77	8.1
	83	1020			
	83	870			
	843	1006	948	55	5.8
	843	896			
	843	943			
	8843	1444	1196	224	18.7
	8843	1137			
	8843	1007			
	8443	1285	1407	106	7.6
	8443	1457			
	8443	1479			
	8433	1454	1465	14	1.0
	8433	1461			
	8433	1481			

Table D.10 Source L: PC Permeability Validation Points for Compressive Strength Specimens

Aggregate Gradation		L PCPC Permeability for Compressive Strength Specimens (in./hr.)			
		Individual	Average	Standard Deviation	Coefficient of Variation (%)
Validation Points	89	1346	1387	142	10.2
	89	1270			
	89	1545			
	789	1238	1322	73	5.5
	789	1365			
	789	1363			
	613	1136	1096	78	7.1
	613	1147			
	613	1006			
	341	1329	1241	121	9.8
	341	1103			
	341	1290			
	135	1569	1601	64	4.0
	135	1674			
	135	1559			

Table D.11 Source L: PC Permeability Design Points for Split Tensile Strength Specimens

Aggregate Gradation		L: PCPC Permeability for Split Tensile Strength Specimens (in./hr.)			
		Individual	**Average**	**Standard Deviation**	**Coefficient of Variation (%)**
Design Points	8	1614	1527	122	8.0
	8	1580			
	8	1388			
	4	2205	2049	156	7.6
	4	2050			
	4	1893			
	38	2438	2352	244	10.4
	38	2077			
	38	2541			
	84	1541	1401	160	11.4
	84	1436			
	84	1227			
	43	1783	1659	199	12.0
	43	1429			
	43	1764			
	83	954	957	180	18.8
	83	778			
	83	1138			
	843	1036	948	82	8.7
	843	938			
	843	872			
	8843	1110	1198	221	18.4
	8843	1449			
	8843	1034			
	8443	1400	1407	120	8.6
	8443	1531			
	8443	1291			
	8433	1424	1462	303	20.7
	8433	1783			
	8433	1181			

Table D.12 Source L: PC Permeability Validation Points for Split Tensile Strength Specimens

Aggregate Gradation		L: PCPC Permeability for Split Tensile Strength Specimens (in./hr.)			
		Individual	Average	Standard Deviation	Coefficient of Variation (%)
Validation Points	89	1281	1389	97	7.0
	89	1467			
	89	1420			
	789	1136	1337	177	13.3
	789	1404			
	789	1471			
	613	1075	1107	28	2.5
	613	1126			
	613	1120			
	341	1308	1241	63	5.1
	341	1183			
	341	1231			
	135	1686	1604	152	9.5
	135	1429			
	135	1698			

Table D.13 Source L: PC Permeability Design Points for Abrasion Loss Specimens

Aggregate Gradation		L: PCPC Permeability for Abrasion Loss Specimens (in./hr.)			
		Individual	Average	Standard Deviation	Coefficient of Variation (%)
Design Points	8	1609	1528	71	4.7
	8	1498			
	8	1476			
	4	2137	2053	162	7.9
	4	1866			
	4	2155			
	38	2342	2354	72	3.1
	38	2289			
	38	2432			
	84	1610	1402	192	13.7
	84	1233			
	84	1364			
	43	1612	1632	22	1.3
	43	1627			
	43	1656			
	83	910	952	68	7.2
	83	1031			
	83	915			
	843	1028	949	70	7.3
	843	924			
	843	896			
	8843	1460	1185	238	20.1
	8843	1041			
	8843	1054			
	8443	1380	1408	41	2.9
	8443	1389			
	8443	1456			
	8433	1414	1486	295	19.9
	8433	1810			
	8433	1233			

Table D.14 Source L: PC Permeability Validation Points for Abrasion Loss Specimens

Aggregate Gradation		L: PCPC Permeability for Abrasion Loss Specimens (in./hr.)			
		Individual	Average	Standard Deviation	Coefficient of Variation (%)
Validation Points	89	1269	1402	124	8.9
	89	1422			
	89	1515			
	789	1243	1325	72	5.4
	789	1362			
	789	1372			
	613	1093	1114	148	13.2
	613	1271			
	613	979			
	341	1281	1242	71	5.7
	341	1286			
	341	1160			
	135	1916	1601	279	17.5
	135	1504			
	135	1383			

Table D.15 Source L: PC Overall Permeability Design Points

Aggregate Gradation		L: PCPC Overall Permeability (in./hr.) Individual	Average	Standard Deviation	Coefficient of Variation (%)
Design Points	8	1615	1528	79	5.2
	8	1524			
	8	1446			
	4	2152	2047	114	5.6
	4	1960			
	4	2029			
	38	2439	2351	147	6.2
	38	2246			
	38	2368			
	84	1523	1400	129	9.2
	84	1342			
	84	1335			
	43	1621	1638	122	7.4
	43	1595			
	43	1698			
	83	955	957	93	9.7
	83	929			
	83	986			
	843	966	948	78	8.3
	843	956			
	843	923			
	8843	1329	1199	196	16.3
	8843	1255			
	8843	1012			
	8443	1370	1408	100	7.1
	8443	1405			
	8443	1450			
	8433	1458	1468	194	13.2
	8433	1654			
	8433	1291			

Table D.16 Source L: PC Overall Permeability Validation Points

Aggregate Gradation		L: PCPC Overall Permeability (in./hr.)			
		Individual	Average	Standard Deviation	Coefficient of Variation (%)
Validation Points	89	1317	1392	122	8.8
	89	1437			
	89	1422			
	789	1216	1334	100	7.5
	789	1400			
	789	1386			
	613	1152	1105	119	10.8
	613	1102			
	613	1061			
	341	1287	1239	84	6.8
	341	1171			
	341	1260			
	135	1752	1601	165	10.3
	135	1533			
	135	1519			

Table D.17 Source L: PC Porosity Design Points

Aggregate Gradation		L: PCPC Porosity (%) Individual	Average	Standard Deviation	Coefficient of Variation (%)
Design Points	8	32.7	32.2	0.8	2.5
	8	31.3			
	8	32.7			
	4	31.9	31.9	0.3	0.9
	4	32.2			
	4	31.6			
	38	34.0	33.7	0.6	1.7
	38	34.0			
	38	33.0			
	84	29.8	29.8	0.2	0.8
	84	30.0			
	84	29.6			
	43	30.8	31.3	0.9	2.7
	43	30.9			
	43	32.3			
	83	26.8	27.1	0.6	2.3
	83	26.7			
	83	27.9			
	843	27.7	28.4	0.6	2.0
	843	28.8			
	843	28.6			
	8843	29.4	29.5	0.8	2.6
	8843	30.2			
	8843	28.7			
	8443	28.6	29.0	0.7	2.5
	8443	28.5			
	8443	29.8			
	8433	29.8	29.7	0.4	1.4
	8433	30.0			
	8433	29.2			

Table D.18 Source L: PC Porosity Validation Points

Aggregate Gradation		L: PCPC Porosity (%) Individual	Average	Standard Deviation	Coefficient of Variation (%)
Validation Points	89	29.9	30.4	1.7	5.6
	89	32.3			
	89	29.0			
	789	28.9	29.3	0.7	2.5
	789	30.2			
	789	28.9			
	613	26.4	25.3	1.4	5.5
	613	23.7			
	613	25.6			
	341	25.1	25.5	0.9	3.7
	341	24.8			
	341	26.6			
	135	27.5	28.4	2.3	8.3
	135	31.0			
	135	26.6			

Table D.19 Source L: PC Gravimetric Air Content Design Points

Aggregate Gradation		L: PCPC Gravimetric Air Content (%) Individual	Average	Standard Deviation	Coefficient of Variation (%)
Design Points	8	31.3	30.2	0.9	3.1
	8	29.5			
	8	30.0			
	4	30.5	30.5	0.1	0.3
	4	30.4			
	4				
	38	29.1	29.4	0.4	1.4
	38	29.2			
	38	29.9			
	84	27.0	27.8	0.9	3.4
	84	28.8			
	84	27.7			
	43	27.7	27.5	0.3	1.0
	43	27.7			
	43	27.2			
	83	23.7	24.4	0.7	2.9
	83	24.2			
	83	25.1			
	843	25.8	25.3	1.4	5.7
	843	26.4			
	843	23.7			
	8843	27.0	26.2	1.1	4.4
	8843	25.4			
	8843				
	8443	25.3	26.0	0.7	2.7
	8443	26.7			
	8443	25.9			
	8433	27.2	26.4	0.8	2.9
	8433	26.3			
	8433	25.7			

Table D.20 Source L: PC Gravimetric Validation Points

Aggregate Gradation		L: PCPC Gravimetric Air Content (%) Individual	Average	Standard Deviation	Coefficient of Variation (%)
Validation Points	89	26.4	27.0	0.5	1.9
	89	27.4			
	89	27.3			
	789	26.6	26.9	1.0	3.9
	789	28.1			
	789	26.1			
	613	24.5	24.5	0.0	0.2
	613	24.5			
	613				
	341	24.7	25.2	0.7	2.7
	341	25.6			
	341				
	135	25.9	25.4	0.6	2.5
	135	25.0			
	135				

Table D.21 Source L: PC Compressive Strength Design Points

Aggregate Gradation		L: PCPC Compressive Strength (psi) Individual	Average	Standard Deviation	Coefficient of Variation (%)
Design Points	8	532	705	229	32.5
	8	618			
	8	965			
	4	683	762	71	9.4
	4	784			
	4	820			
	38	703	701	102	14.5
	38	802			
	38	598			
	84	786	825	86	10.4
	84	923			
	84	765			
	43	843	887	72	8.1
	43	848			
	43	970			
	83	940	986	112	11.4
	83	1114			
	83	904			
	843	1082	924	267	28.9
	843	615			
	843	1075			
	8843	1210	1122	238	21.2
	8843	853			
	8843	1304			
	8443	1355	1142	195	17.1
	8443	1098			
	8443	973			
	8433	667	852	209	24.5
	8433	810			
	8433	1078			

Table D.22 Source L: PC Compressive Strength Validation Points

Aggregate Gradation		L: PCPC Compressive Strength (psi) Individual	Average	Standard Deviation	Coefficient of Variation (%)
Validation Points	89	918	877	233	26.5
	89	1087			
	89	627			
	789	753	853	159	18.6
	789	770			
	789	1036			
	613	1185	1134	58	5.1
	613	1071			
	613	1146			
	341	1288	1244	88	7.0
	341	1143			
	341	1300			
	135	1224	1021	270	26.4
	135	1124			
	135	714			

Table D.23 Source L: PC Split Tensile Strength Design Points

Aggregate Gradation		L: PCPC Split tensile Strength (psi)			
		Individual	Average	Standard Deviation	Coefficient of Variation (%)
Design Points	8	176	149	27	18.2
	8	122			
	8	149			
	4	164	178	16	9.2
	4	196			
	4	174			
	38	150	162	24	14.7
	38	147			
	38	190			
	84	123	150	29	19.4
	84	181			
	84	147			
	43	208	221	19	
	43	213			
	43	243			
	83	206	246	43	17.5
	83	292			
	83	240			
	843	200	237	33	13.8
	843	249			
	843	263			
	8843	260	256	4	1.5
	8843	255			
	8843	253			
	8443	333	288	39	13.6
	8443	263			
	8443	268			
	8433	217	254	33	12.9
	8433	265			
	8433	279			

Table D.24 Source L: PC Split Tensile Strength Validation Points

Aggregate Gradation		L: PCPC Split tensile Strength (psi) Individual	Average	Standard Deviation	Coefficient of Variation (%)
Validation Points	89	217	245	24	9.8
	89	257			
	89	260			
	789	248	245	23	9.4
	789	267			
	789	221			
	613	263	253	54	21.5
	613	195			
	613	302			
	341	254	249	17	6.7
	341	262			
	341	230			
	135	262	256	63	24.7
	135	190			
	135	316			

Table D.25 Source L: PC Abrasion Loss Design Points

Aggregate Gradation		L: PCPC Abrasion Loss (%) Individual	Average	Standard Deviation	Coefficient of Variation (%)
Design Points	8	52.2	45.6	6.1	13.3
	8	40.2			
	8	44.5			
	4	47.2	41.1	5.4	13.1
	4	39.0			
	4	37.1			
	38	40.0	40.8	0.9	2.2
	38	40.7			
	38	41.8			
	84	42.0	37.6	4.4	11.7
	84	37.5			
	84	33.2			
	43	33.9	33.3	1.7	5.2
	43	34.6			
	43	31.3			
	83	30.6	33.9	3.9	11.6
	83	38.3			
	83	32.9			
	843	33.2	30.2	2.6	8.6
	843	28.6			
	843	28.8			
	8843	33.9	30.3	5.2	17.0
	8843	24.4			
	8843	32.6			
	8443	32.7	32.5	2.2	6.7
	8443	34.5			
	8443	30.2			
	8433	25.7	26.3	3.0	11.4
	8433	29.6			
	8433	23.7			

Table D.26 Source L: PC Abrasion Loss Validation Points

Aggregate Gradation		L: PCPC Abrasion Loss (%) Individual	Average	Standard Deviation	Coefficient of Variation (%)
Validation Points	89	24.8	29.6	4.2	14.1
	89	32.0			
	89	32.0			
	789	32.7	32.5	2.2	6.7
	789	34.5			
	789	30.2			
	613	32.0	30.7	3.0	9.9
	613	32.8			
	613	27.2			
	341	23.3	25.3	1.9	7.6
	341	27.0			
	341	25.8			
	135	27.6	27.1	0.5	1.7
	135	26.7			
	135	27.1			

Table D.27 Source L: Pervious Concrete Compaction Validation Points

APPENDIX E

Source C: Pervious Concrete Compacted Properties

Table E.1 Source C: Pervious Concrete ASTM C1688 Unit Weight Design Points

Aggregate Gradation		C: Compacted PCPC ASTM C1688 Unit Weight (lb/ft^3)			
		Individual	Average	Standard Deviation	Coefficient of Variation (%)
Design Points	8	113	114	1	0.67
	8	114			
	8				
	4	114	114	0	0.00
	4	114			
	4				
	38	114	115	1	1.00
	38	115			
	38				
	84	117	117	0	0.09
	84	117			
	84				
	43	118	119	1	0.58
	43	119			
	43				
	83	123	123	0	0.14
	83	123			
	83				
	843	120	120	0	0.39
	843	121			
	843				
	8843	118	118	0	0.18
	8843	118			
	8843				
	8443	117	118	1	0.76
	8443	119			
	8443				
	8433	123	122	2	1.60
	8433	120			
	8433				

Table E.2 Source C: Pervious Concrete ASTM C1688 Unit Weight Validation Points

Aggregate Gradation		C: Compacted PCPC ASTM C1688 Unit Weight (lb/ft^3)			
		Individual	Average	Standard Deviation	Coefficient of Variation (%)
Validation Points	89	117	117	0.1	0.10
	89	117			
	89				
	613	120	120	0.2	0.17
	613	120			
	613				
	341	118	118	0.2	0.15
	341	118			
	341				
	135	121	121	0.6	0.47
	135	121			
	135				

Table E.3 Source C: Pervious Concrete Alternative Unit Weight Design Points

Aggregate Gradation		C: Compacted PCPC Alternative Unit Weight (lb/ft^3) Individual	Average	Standard Deviation	Coefficient of Variation (%)
Design Points	8	107	108	1	1.26
	8	109			
	8				
	4	110	110	1	0.46
	4	111			
	4				
	38	111	111	0	0.39
	38	110			
	38				
	84	112	112	0	0.19
	84	113			
	84				
	43	115	115	0	0.20
	43	116			
	43				
	83	117	116	1	0.53
	83	116			
	83				
	843	115	115	0	0.17
	843	115			
	843				
	8843	113	112	1	0.67
	8843	112			
	8843				
	8443	114	114	0	0.02
	8443	114			
	8443				
	8433	117	117	1	0.83
	8433	116			
	8433				

Table E.4 Source C: Pervious Concrete Alternative Unit Weight Validation Points

Aggregate Gradation		C: Compacted PCPC Alternative Unit Weight (lb/ft^3)			
		Individual	Average	Standard Deviation	Coefficient of Variation (%)
Validation Points	89	112	112	1	0.87
	89	113			
	89				
	613	116	116	0	0.00
	613	116			
	613				
	341	113	114	1	1.09
	341	115			
	341				
	135	117	117	0	0.08
	135	117			
	135				

Table E.5 Source C: Pervious Concrete Compaction Index Design Points

	Aggregate Gradation	C: PCPC Compaction Index			
		Individual	Average	Standard Deviation	Coefficient of Variation (%)
Design Points	8	0.856	0.872	0.022	2.53
	8	0.888			
	8				
	4	0.971	0.932	0.056	5.96
	4	0.893			
	4				
	38	0.905	0.900	0.008	0.87
	38	0.894			
	38				
	84	0.944	0.984	0.056	5.69
	84	1.023			
	84				
	43	0.904	0.890	0.019	2.19
	43	0.876			
	43				
	83	1.103	1.078	0.036	3.31
	83	1.053			
	83				
	843	1.017	1.039	0.032	3.03
	843	1.061			
	843				
	8843	0.933	0.924	0.013	1.44
	8843	0.914			
	8843				
	8443	1.063	1.024	0.055	5.34
	8443	0.985			
	8443				
	8433	1.095	1.059	0.051	4.77
	8433	1.023			
	8433				

Table E.6 Source C: Pervious Concrete Compaction Index Validation Points

Aggregate Gradation		C: PCPC Compaction Index			
		Individual	Average	Standard Deviation	Coefficient of Variation (%)
Validation Points	89	0.917	0.973	0.079	8.13
	89	1.029			
	89				
	613	0.939	0.982	0.061	6.16
	613	1.025			
	613				
	341	1.034	1.055	0.030	2.81
	341	1.076			
	341				
	135	1.101	1.086	0.022	2.01
	135	1.071			
	135				

Table E.7 Source C: PC Permeability Design Points for Porosity Specimens

Aggregate Gradation		C: PCPC Permeability for Porosity Specimens (in./hr.)			
		Individual	Average	Standard Deviation	Coefficient of Variation (%)
Design Points	8	1502	1384	143	10.3
	8	1225			
	8	1424			
	4	2094	1949	130	6.7
	4	1843			
	4	1911			
	38	2173	2424	281	11.6
	38	2727			
	38	2373			
	84	1505	1340	155	11.6
	84	1196			
	84	1320			
	43	1640	1612	246	15.2
	43	1843			
	43	1354			
	83	1215	1052	142	13.5
	83	960			
	83	981			
	843	1083	1293	190	14.7
	843	1451			
	843	1346			
	8843	1472	1296	177	13.6
	8843	1299			
	8843	1118			
	8443	1595	1511	180	11.9
	8443	1634			
	8443	1304			
	8433	1372	1319	161	12.2
	8433	1138			
	8433	1446			

Table E.8 Source C: PC Permeability Validation Points for Porosity Specimens

Aggregate Gradation		C: PCPC Permeability for Porosity Specimens (in./hr.)			
		Individual	Average	Standard Deviation	Coefficient of Variation (%)
Validation Points	89	1959	1697	228	13.4
	89	1577			
	89	1553			
	613	1348	1196	248	20.8
	613	1332			
	613	910			
	341	1603	1415	239	16.9
	341	1146			
	341	1495			
	135	1294	1301	258	19.8
	135	1046			
	135	1562			

Table E.9 Source C: PC Permeability Design Points for Compressive Strength Specimens

Aggregate Gradation		C: PCPC Permeability for Compressive Strength Specimens (in./hr.)			
		Individual	Average	Standard Deviation	Coefficient of Variation (%)
Design Points	8	1334	1386	57	4.1
	8	1446			
	8	1378			
	4	2155	1960	171	8.7
	4	1886			
	4	1838			
	38	2397	2432	127	5.2
	38	2573			
	38	2326			
	84	1489	1339	153	11.4
	84	1183			
	84	1346			
	43	1677	1613	56	3.5
	43	1589			
	43	1573			
	83	1154	1053	92	8.7
	83	975			
	83	1029			
	843	1288	1302	107	8.2
	843	1415			
	843	1203			
	8843	1388	1299	84	6.5
	8843	1287			
	8843	1222			
	8443	1474	1499	43	2.9
	8443	1473			
	8443	1548			
	8433	1189	1292	90	7.0
	8433	1351			
	8433	1336			

Table E.10 Source C: PC Permeability Validation Points for Compressive Strength Specimens

Aggregate Gradation		C: PCPC Permeability for Compressive Strength Specimens (in./hr.)			
		Individual	Average	Standard Deviation	Coefficient of Variation (%)
Validation Points	89	1677	1658	20	1.2
	89	1661			
	89	1637			
	613	1270	1208	55	4.5
	613	1169			
	613	1184			
	341	1306	1414	129	9.1
	341	1556			
	341	1378			
	135	1402	1301	95	7.3
	135	1288			
	135	1213			

Table E.11 Source C: PC Permeability Design Points for Split Tensile Strength Specimens

Aggregate Gradation		C: PCPC Permeability for Split Tensile Strength Specimens (in./hr.)			
		Individual	Average	Standard Deviation	Coefficient of Variation (%)
Design Points	8	1445	1385	96	7.0
	8	1274			
	8	1436			
	4	1795	1948	268	13.8
	4	1792			
	4	2258			
	38	2529	2438	126	5.2
	38	2294			
	38	2490			
	84	1458	1340	109	8.1
	84	1244			
	84	1320			
	43	1564	1608	43	2.7
	43	1650			
	43	1611			
	83	987	1049	70	6.6
	83	1124			
	83	1037			
	843	1226	1299	112	8.6
	843	1428			
	843	1243			
	8843	1243	1286	42	3.3
	8843	1288			
	8843	1327			
	8443	1625	1504	106	7.0
	8443	1450			
	8443	1436			
	8433	1082	1141	54	4.8
	8433	1152			
	8433	1189			

Table E.12 Source C: PC Permeability Validation Points for Split Tensile Strength Specimens

Aggregate Gradation		C: PCPC Permeability for Split Tensile Strength Specimens (in./hr.)			
		Individual	Average	Standard Deviation	Coefficient of Variation (%)
Validation Points	89	1707	1654	46	2.8
	89	1626			
	89	1628			
	613	1238	1200	41	3.4
	613	1157			
	613	1207			
	341	1438	1414	28	2.0
	341	1419			
	341	1384			
	135	1381	1301	109	8.4
	135	1178			
	135	1345			

Table E.13 Source C: PC Permeability Design Points for Abrasion Loss Specimens

Aggregate Gradation		C: PCPC Permeability for Abrasion Loss Specimens (in./hr.) Individual	Average	Standard Deviation	Coefficient of Variation (%)
Design Points	8	1465	1385	90	6.5
	8	1402			
	8	1287			
	4	1969	1937	34	1.7
	4	1902			
	4	1941			
	38	2698	2431	232	9.5
	38	2288			
	38	2307			
	84	1413	1337	151	11.3
	84	1435			
	84	1163			
	43	1519	1620	131	8.1
	43	1768			
	43	1574			
	83	1099	1054	82	7.8
	83	1105			
	83	959			
	843	1335	1305	138	10.6
	843	1426			
	843	1155			
	8843	1249	1291	152	11.8
	8843	1164			
	8843	1459			
	8443	1533	1503	119	7.9
	8443	1371			
	8443	1604			
	8433	1216	1364	128	9.4
	8433	1449			
	8433	1426			

Table E.14 Source C: PC Permeability Validation Points for Abrasion Loss Specimens

Aggregate Gradation		C: PCPC Permeability for Abrasion Loss Specimens (in./hr.) Individual	Average	Standard Deviation	Coefficient of Variation (%)
Validation Points	89	1598	1667	122	7.3
	89	1807			
	89	1595			
	613	1287	1203	157	13.1
	613	1299			
	613	1021			
	341	1415	1410	168	11.9
	341	1575			
	341	1240			
	135	1188	1293	126	9.7
	135	1432			
	135	1259			

Table E.15 Source C: PC Overall Permeability Design Points

Aggregate Gradation		C: PCPC Overall Permeability (in./hr.) Individual	Average	Standard Deviation	Coefficient of Variation (%)
Design Points	8	1437	1385	86	6.2
	8	1337			
	8	1381			
	4	2003	1949	147	7.6
	4	1856			
	4	1987			
	38	2450	2431	173	7.1
	38	2470			
	38	2374			
	84	1466	1339	122	9.1
	84	1265			
	84	1287			
	43	1600	1613	123	7.6
	43	1712			
	43	1528			
	83	1114	1052	85	8.1
	83	1041			
	83	1001			
	843	1233	1300	120	9.2
	843	1430			
	843	1237			
	8843	1338	1293	107	8.3
	8843	1259			
	8843	1282			
	8443	1557	1504	104	6.9
	8443	1482			
	8443	1473			
	8433	1215	1279	132	10.3
	8433	1273			
	8433	1349			

Table E.16 Source C: PC Overall Permeability Validation Points

Aggregate Gradation		C: PCPC Overall Permeability (in./hr.) Individual	Average	Standard Deviation	Coefficient of Variation (%)
Validation Points	89	1735	1669	114	6.8
	89	1668			
	89	1603			
	613	1286	1202	129	10.7
	613	1239			
	613	1080			
	341	1440	1413	136	9.7
	341	1424			
	341	1374			
	135	1316	1299	137	10.5
	135	1236			
	135	1345			

Table E.17 Source C: PC Porosity Design Points

Aggregate Gradation		C: PCPC Porosity (%) Individual	Average	Standard Deviation	Coefficient of Variation (%)
Design Points	8	31.5	31.3	0.7	2.3
	8	30.5			
	8	32.0			
	4	30.9	30.6	0.5	1.5
	4	30.0			
	4	30.8			
	38	31.2	31.5	0.6	2.0
	38	32.3			
	38	31.1			
	84	29.2	28.3	0.8	2.9
	84	27.5			
	84	28.2			
	43	27.7	27.5	0.5	2.0
	43	27.9			
	43	26.8			
	83	27.8	27.1	0.6	2.3
	83	26.9			
	83	26.7			
	843	26.3	27.6	1.1	3.9
	843	28.3			
	843	28.1			
	8843	30.1	29.0	1.1	3.8
	8843	29.1			
	8843	27.9			
	8443	29.1	28.8	0.3	1.0
	8443	28.8			
	8443	28.6			
	8433	27.8	27.9	0.6	2.0
	8433	27.4			
	8433	28.6			

Table E.18 Source C: PC Porosity Validation Points

Aggregate Gradation		C: PCPC Porosity (%) Individual	Average	Standard Deviation	Coefficient of Variation (%)
Validation Points	89	31.8	30.1	1.6	5.3
	89	28.7			
	89	29.9			
	613	28.3	27.7	0.7	2.4
	613	27.8			
	613	27.0			
	341	29.1	28.4	1.2	4.3
	341	27.0			
	341	29.1			
	135	27.4	27.2	0.2	0.7
	135	27.2			
	135	27.0			

Table E.19 Source C: PC Gravimetric Air Content Design Points

	Aggregate Gradation	C: PCPC Gravimetric Air Content (%) Individual	Average	Standard Deviation	Coefficient of Variation (%)
Design Points	8	31.7	31.1	0.9	2.8
	8	30.5			
	8				
	4	29.7	29.4	0.3	1.1
	4	29.2			
	4				
	38	29.1	29.3	0.3	0.9
	38	29.5			
	38				
	84	28.2	28.1	0.1	0.5
	84	28.0			
	84				
	43	26.4	26.3	0.2	0.6
	43	26.2			
	43				
	83	25.3	25.6	0.4	1.6
	83	25.9			
	83				
	843	26.8	26.7	0.1	0.5
	843	26.6			
	843				
	8843	27.9	28.3	0.5	1.7
	8843	28.6			
	8843				
	8443	27.2	27.2	0.0	0.1
	8443	27.2			
	8443				
	8433	25.0	25.5	0.6	2.4
	8433	25.9			
	8433				

Table E.20 Source C: PC Gravimetric Air Content Validation Points

Aggregate Gradation		C: PCPC Gravimetric Air Content (%)			
		Individual	Average	Standard Deviation	Coefficient of Variation (%)
Validation Points	89	28.7	28.2	0.6	2.2
	89	27.8			
	89				
	613	26.1	26.1	0.0	0.0
	613	26.1			
	613				
	341	27.5	26.9	0.8	3.0
	341	26.4			
	341				
	135	25.3	25.3	0.1	0.3
	135	25.2			
	135				

Table E.21 Source C: PC Compressive Strength Design Points

Aggregate Gradation		C: PCPC Compressive Strength (psi) Individual	Average	Standard Deviation	Coefficient of Variation (%)
Design Points	8	433	546	110	20.2
	8	551			
	8	653			
	4	685	644	42	6.5
	4	602			
	4	645			
	38	602	633	67	10.6
	38	710			
	38	587			
	84	907	880	33	3.7
	84	844			
	84	890			
	43	1258	1131	138	12.2
	43	985			
	43	1151			
	83	462	736	365	49.6
	83	596			
	83	1151			
	843	986	785	175	22.3
	843	703			
	843	665			
	8843	915	735	187	25.4
	8843	542			
	8843	748			
	8443	769	842	66	7.8
	8443	860			
	8443	896			
	8433	707	704	140	19.9
	8433	562			
	8433	842			

Table E.22 Source C: PC Compressive Strength Validation Points

Aggregate Gradation		C: PCPC Compressive Strength (psi) Individual	Average	Standard Deviation	Coefficient of Variation (%)
Validation Points	89	880	903	23	2.6
	89	903			
	89	927			
	613	583	580	48	8.2
	613	626			
	613	531			
	341	877	768	101	13.2
	341	678			
	341	747			
	135	662	820	195	23.8
	135	1038			
	135	760			

Table E.23 Source C: PC Split Tensile Strength Design Points

Aggregate Gradation		C: PCPC Split Tensile Strength (psi) Individual	Average	Standard Deviation	Coefficient of Variation (%)
Design Points	8	173	145	24	16.7
	8	126			
	8	137			
	4	167	179	19	10.7
	4	201			
	4	170			
	38	127	118	13	11.4
	38	108			
	38				
	84	186	218	36	16.7
	84	210			
	84	257			
	43	321	255	74	28.9
	43	175			
	43	269			
	83	167	166	39	23.2
	83	127			
	83	204			
	843	251	215	33	15.2
	843	188			
	843	206			
	8843	187	171	14	8.2
	8843	162			
	8843	164			
	8443	191	235	46	19.5
	8443	283			
	8443	232			
	8433	224	243	44	18.0
	8433	292			
	8433	211			

Table E.24 Source C: PC Split Tensile Strength Validation Points

ggregate Gradation		C: PCPC Split Tensile Strength (psi)			
		Individual	Average	Standard Deviation	Coefficient of Variation (%)
Validation Points	89	148	187	40	21.2
	89	227			
	89	185			
	613	168	182	50	27.3
	613	237			
	613	141			
	341	187	204	36	17.7
	341	246			
	341	181			
	135	206	226	50	22.1
	135	190			
	135	283			

Table E.25 Source C: PC Abrasion Loss Design Points

Aggregate Gradation		C: PCPC Abrasion Loss (%) Individual	Average	Standard Deviation	Coefficient of Variation (%)
Design Points	8	46.9	46.7	1.9	4.2
	8	48.6			
	8	44.7			
	4	58.8	56.6	2.6	4.6
	4	57.4			
	4	53.8			
	38	71.0	71.9	7.2	10.1
	38	65.1			
	38	79.5			
	84	49.0	48.0	0.9	1.8
	84	47.4			
	84	47.7			
	43	30.6	30.1	3.9	13.1
	43	33.8			
	43	26.0			
	83	57.4	55.2	2.4	4.3
	83	55.4			
	83	52.6			
	843	48.8	47.1	5.6	12.0
	843	51.6			
	843	40.8			
	8843	43.7	42.2	3.7	8.7
	8843	38.0			
	8843	44.8			
	8443	32.0	32.3	2.2	6.7
	8443	34.5			
	8443	30.2			
	8433	42.1	45.7	3.1	6.9
	8433	47.4			
	8433	47.7			

Table E.26 Source C: PC Abrasion Loss Validation Points

Aggregate Gradation		C: PCPC Abrasion Loss (%)			
		Individual	Average	Standard Deviation	Coefficient of Variation (%)
Validation Points	89	41.4	46.5	4.5	9.7
	89	49.9			
	89	48.3			
	613	39.6	45.4	5.2	11.5
	613	46.6			
	613	49.8			
	341	48.4	47.6	6.9	14.4
	341	54.0			
	341	40.4			
	135	44.9	45.5	1.0	2.1
	135	46.2			
	135				

APPENDIX F

Example of Optimization Process for Pervious Concrete Mixtures

A scenario of the optimization process evaluated in the study is presented in Figure F.1 and Figure F.2. The aggregate source used for this example was source C. The pervious concrete mix design requires a permeability of approximately 1500 in./hr., a compressive strength of approximately 800 psi and an abrasion loss of a maximum value of 40%. Based on regression analyses that gave stronger relationships, it was more suitable to use these relationships:

1. Permeability to porosity,
2. Compressive strength to split tensile strength,
3. Abrasion loss to split tensile strength,
4. Split tensile strength to porosity,
5. Averaged porosity to aggregate void content.

The values obtained from the regression analyses are listed in the plots in Figure F.1. The predicted porosity based on the permeability of 1500 in./hr. was 28.9%. The split tensile strength based on the compressive strength of 800 psi was 202 psi. To be conservative, an abrasion value of 35% loss was used instead of 40% and this predicted a split tensile strength of 266 psi. From these split tensile strengths, porosity values were estimated to be 28.4% and 25.6%. An average of the three porosity values gave 27.6% as the desired porosity. The porosity relationship to aggregate void content was used and it estimated an aggregate void content of 39.7%. The augmented simplex-centroid design was used based on the special quartic model to give a suitable aggregate proportion of 23% of #8, 34% of #4, and 43% of #38. Other suitable aggregate proportions could be found anywhere along the contour line that corresponds with the aggregate void content of 39.7%.

The other possible option is to link the pervious concrete properties directly to the aggregate proportions, skipping the use of regression analyses. The augmented simplex-centroid design in Figure F.2 is used. A suitable aggregate proportion that can be used to prepare a pervious concrete mix could be 16% of #8, 64% of #4, and 20% of #38. When this proportion was used in option (1) simplex triangle, it gave a void content of 40.9%.

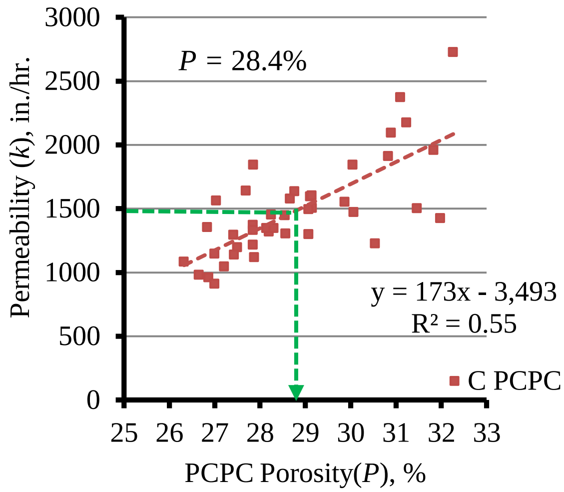

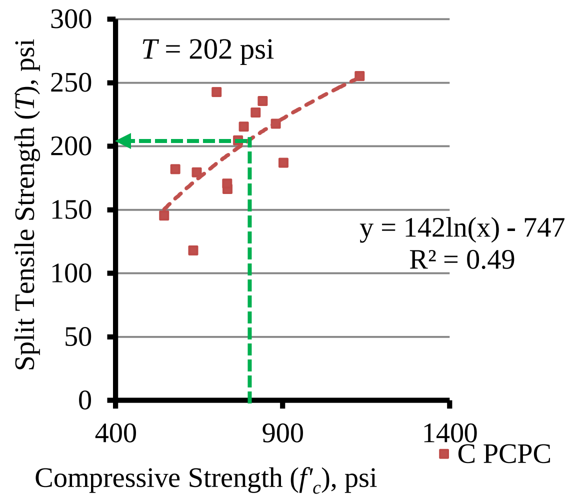

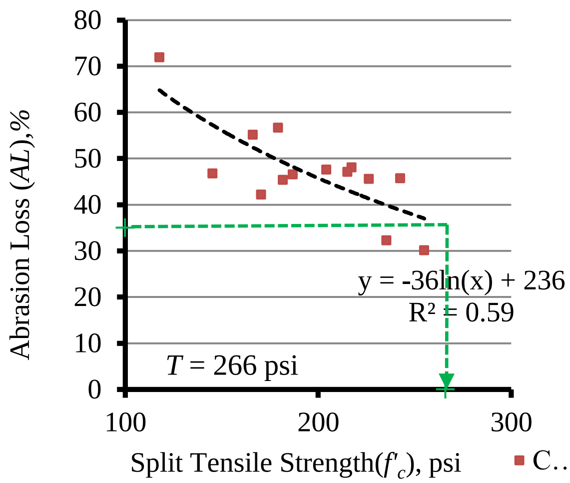

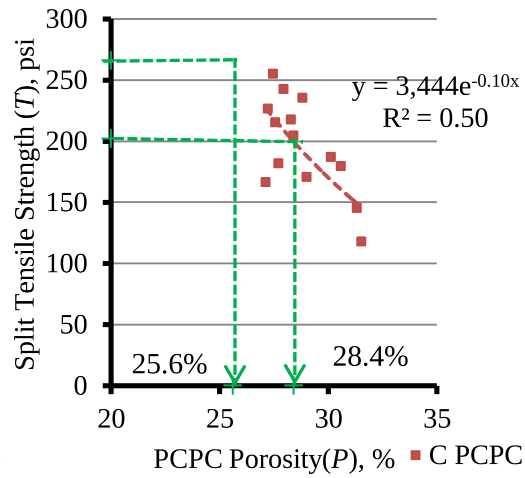

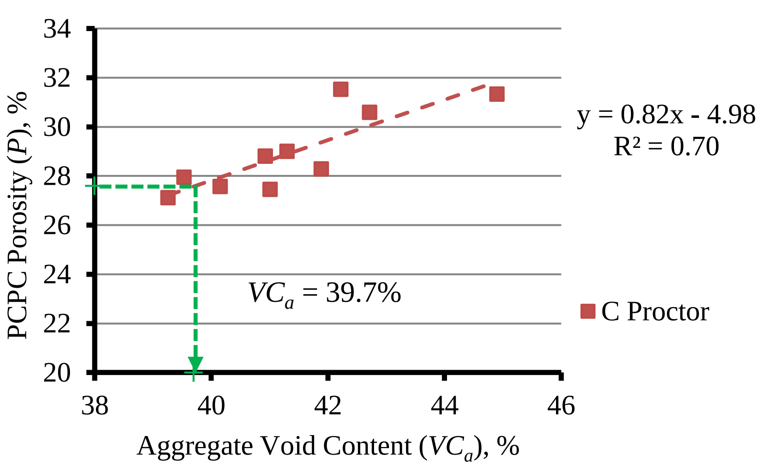

Figure F.1(a)
continued on the
following page.

Mixture Profiler

T	L	R	Factor	Current X	Lo Limit	Hi Limit
⦿	○	○	#8	0.2283133	0	1
○	⦿	○	#4	0.34001	0	1
○	○	⦿	#38	0.4316767	0	1

Response	Contour	Current Y	Lo Limit	Hi Limit
Predicted C Void Conten	39.7	39.701434	39.7	.

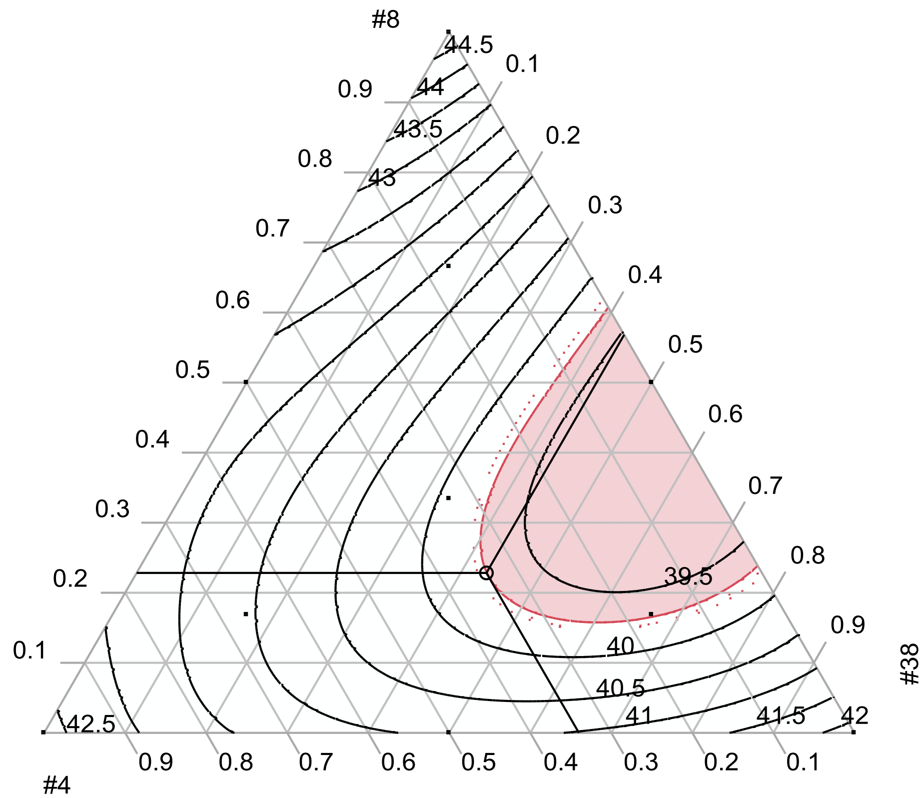

(b)

Figure F.1 Option 1: Optimization process using regression analyses and the augmented simplex-centroid design based on the special quartic model to predict aggregate proportions.

Mixture Profiler

T	L	R	Factor	Current X	Lo Limit	Hi Limit
⦿	○	○	#8	0.1650602	0	1
○	⦿	○	#4	0.6398657	0	1
○	○	⦿	#38	0.195074	0	1

Response	Contour	Current Y	Lo Limit	Hi Limit
Predicted C Perm	1500	1501.1447	1500	.
Predicted C Abr. Los	35	35.136582	35	.
Predicted C Comp.	800	865.72276	800	.

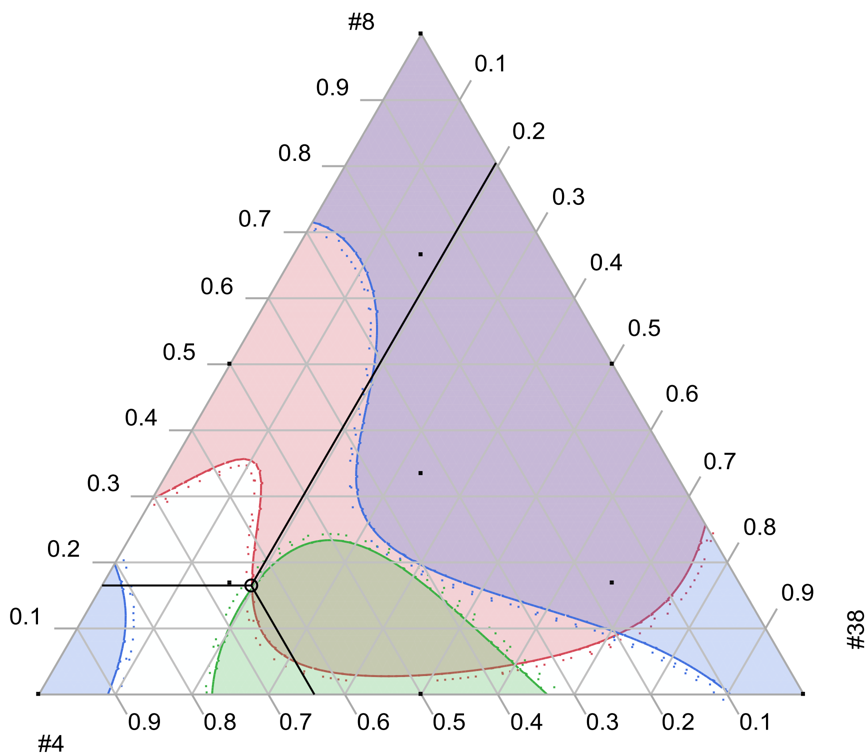

Figure F.2 Option 2: Optimization process using the simplex-centroid design to predict aggregate proportions from pervious concrete properties.

REFERENCES

A.K. Jain, S. G. (2011, October). Effects of Shape and Size of Aggregate on Permeability of Pervious Concrete. *Journal of Engineering Research and Studies*, 4.

ACI Committee E-701. (2007). *Aggregate for Concrete.* American Concrete Institute. Farmington Hills: American Concrete Institute.

American Society for Testing and Materials. (2004). *ASTM Standards.* West Conshohocken: ASTM International.

Bedient, P. H. (2002). *Hydrology and Floodplain Analysis.* Upper Saddle River, New Jersey, USA: Prentice Hall, Inc.

Cornell, J. A. (2002). *Experiments with Mixtures: Designs, Models, and the Analysis of Mixture Data* (3rd ed.). New York, NY, USA: John Wiley & Sons, Inc.

Das, B. M. (2006). *Principles of Geotechnical Engineering.* Toronto, Canada: Thomson Canada Limited.

Garboczi, E. J. (1990, July). Permeability, Diffusivity and Microstructural Parameters: A critical review. *Cement and Concrete Research, 20*(4), 591-601.

Hardiman, M. (2004, September). Application of Packing Theory on Grading Design for Porous Asphalt Mixtures. *Civil Engineer Dimension, 6*(No. 2), 57-63.

Kevern, J. S. (2009, May). The Effect of Curing Regime on Pervious Concrete Abrasion Resistance. *ASTM Journal of Testing and Evaluation, 37*(4), 6.

Larrard, F. d. (2009). Concrete Optimisation with Regard to Packing Density and Rheology. *Rheology of Cement Suspensions Such as Fresh Concrete* (pp. 1-8). France: Rilem International Symposium.

Latham, J. P. (2002). On the Prediction of Void Porosity and Packing of Rock Particulates. *Elsevier Science B.V.*, 18.

Manoj Chopra, M. W. (2006). *Compressive Strength of Pervious Concrete Pavement.* Orlando: Stormwater Management Academy.

Montes F., V. S. (2005, January). A New Test Method for Porosity Measurements of Portland Cement Pervious Concrete. *Journal of ASTM International, 2*(1), 13.

National Stone Association. (1993). *The Aggregate Handbook.* (R. Barksdale, Ed.) Rockville, MD: Mercury Publishing Services.

Neithalath, N. S. (2010, August 31). Characterizing Pore Volume, Sizes, and Connectivity in Pervious Concrete for Permeability Prediction. *Materials Characterization, 61*(8), 802-813.

Neithalath, N. W. (2006). Predicting the Permeability of Pervious Concrete (Enhanced Porosity Concrete) from Non-Destructive Electrical Measurements. *Purdue University*, 14.

Omkar Deo, M. S. (2010, July). Permeability Reduction in Pervious Concretes Due to Clogging: Experiments and Modeling. *Journal of Material in Civil Engineering*, 11.

Paul W.J. Glover, M. J. (2000, May 18). A Modified Archie's Law for Two Conductive Phases. *Elsevier: Earth and Planetary Science Letters*, 369-383.

Roberts, F. K.-Y. (1996). *Hot Mix Asphalt Materials, Mixture Design, and Construction* (2nd ed.). Lanham, Maryland: NAPA Research and Educational Foundation.

Schaefer et al. (2006). *Mix Design Development for Pervious Concrete in Cold Climates.* Iowa State University, Center for Transportation Research and Education,. Ames: Iowa State University.

Scheffe, H. (1958). Experiments with Mixtures. *Royal Statistical Society, 20*(2), 344-360. Retrieved 02 25, 2013, from http://www.jstor.org/stable/2983895

Scheffe, H. (1963). The Simplex-Centroid Design for Experiments with Mixtures. *Royal Statistical Society, 25*(2), 235-263. Retrieved 2 25, 2013, from http://www.jstor.org/stable/2984294

Schokker, A. J. (2010). *The Sustainable Concrete Guide - Strategies and Examples.* Farmington Hills, Michigan: US Green Concrete Council.

Simon, M. L. (1997). Concrete Mixture Optimization Using Statistical Mixture Design Methods. *International Symposium on High Performance Concrete* (pp. 230-244). New Orleans: ResearchBib.

Singer, D. (2012). *An Examination of the Influence of Cement Paste on Pervious Concrete Mixtures.* Clemson: Clemson University.

South Carolina Department of Transportation. (2007). *Standard Specifications for Highway Construction.* Columbia: SCDOT.

Steven H. Kosmatka, B. K. (2002). *Design and Control of Concrete Mixtures* (14 ed.). Skokie, Illinois: Portland Cement Association.

Tennis, P.D., Leming, M.L., Akers, D.J. (2004). *Pervious Concrete Pavements.* Skokie, Illinois: Portland Cement Association.

USEPA. (1996). *Overview of the Stormwater Program.* Washington D.C.: EPA 833-R-96-008.

USEPA. (2000). *Stormwater Phase II Final Rule: Small MS4 Stormwater Program Overview. Factsheet 2.0.* Washington D.C.: EPA 833/F-00-002.

Yeh, I.-C. (2008). Optimization of Concrete Mix Proportioning Using A Flattened Simplex-Centroid Design and Neural Networks. *Engineering with Computers*, 179-190.

Youd, T. (1973). Factors Controlling Maximum and Minimum Densities of Sands. *ASTM Special Technical Publications*(523), 98-112.